University of Alberta

OPTICAL DETECTION METHODS FOR LAB ON A CHIP SYSTEMS

by

Christopher Layne Bliss

A thesis submitted to the Faculty of Graduate Studies and Research in partial fulfillment of the requirements for the degree of **Master of Science**.

in

Micro-Electro-Mechanical Systems (MEMS) and Nanosystems

Department of Electrical & Computer Engineering

Edmonton, Alberta
Fall 2007

Your file Votre référence
ISBN: 978-0-494-33203-0
Our file Notre référence
ISBN: 978-0-494-33203-0

For Charlotte.
Thank you for your love and encouragement.

Abstract

Optical detection methods, such as laser induced fluorescence, are well suited for high-sensitivity biochemical analysis on miniaturised platforms. While instrumentation for fluorescence sensing is well-established for conventional systems, the application of these technologies to lab on a chip (LOC) platforms prohibit the use of these systems as portable, point-of-care (POC) medical diagnostics due to the size and cost of these components. In this work we have developed several novel methods to eliminate the requirement for conventional bulk optics. This is accomplished through the direct replacement of these components with integrated optics and through the use of non-imaging optics by instead relying on the proximity between components to achieve high optical efficiencies. We demonstrate methods for on-chip light delivery using integrated optical waveguides with comparable sensitivity to conventional detection systems. In an extension to this work, dye-doped waveguides are fabricated which act as integrated optical filters, removing the need for external dielectric interference filters. Finally, we report the development of a novel hybrid fluorescence-based capillary electrophoresis (CE) system. This system consists of a polymer microfluidic chip and a high-voltage CMOS microchip capable of providing optical detection as well as supplying the high-voltage required for CE. This system has the capability of being integrated into a portable "USB-key" style platform.

Acknowledgements

I would like to thank my supervisors Dr. Chris Backhouse and Dr. Jim McMullin for their guidance and wisdom over the course of my program. Most of all, I am grateful for their time and patience. It often seemed that quick questions turned into lengthy discussions. However, it tended to be during these casual chats when moments of insight occurred and I learned the greatest lessons.

Special thanks go out to Dr. Duncan Elliott and Dr. Lorenz Sigurdson, my other examining committee members, for taking time to read and improve my thesis. In an extension to his duties as my committee member, an academic collaboration with Dr. Elliott and his lab resulted in an exciting research direction with many promising results (reported on in the latter part of Chapter 4).

It was a great pleasure to be a member of the Applied Miniaturisation Laboratory. I greatly appreciate the support, advice and friendship from all of the students and staff at the AML. Additionally, I am grateful for the staff at the University of Alberta Nanofab who shared their expertise and assisted with process troubleshooting.

Thank you to the Natural Sciences and Engineering Research Council of Canada (NSERC), Alberta Ingenuity and the Informatics Circle of Research Excellence (iCORE) for financial support.

Lastly and most importantly, my deepest thanks go to my fiancée Charlotte for her love and support during my graduate studies. I would also like to offer my most sincere thanks to my parents and family for their support and encouragement during this time.

Table of Contents

List of Tables

List of Figures

List of Symbols

^{o}C	degrees Celsius
α	propagation loss
ϵ	extinction coefficient
μ_{EOF}	electro-osmotic mobility
μ_{EP}	electrophoretic mobility
μAPD	micro avalanche photodiode
μL	microliter
μm	micrometer
μTAS	micro-total-analysis system
μTK	Microfluidic Toolkit (Micralyne, AB, Canada)
Ω	solid angle
A	ampere
ADC	analog-to-digital converter
BKV	BK virus
c	concentration
CE	capillary electrophoresis
cm	centimeter
CMOS	complementary metal-oxide-semiconductor
CVD	chemical vapour deposition
dB	decibel
DNA	deoxyribonucleic acid
E	electric field
FWHM	full width at half maximum
GRIN	graded index

HV	high voltage
Hz	hertz
I	optical intensity
IR	infrared
kHz	kilohertz
l	length (absorption length)
L	optical loss
LCD	liquid crystal display
LCE	light collection efficiency
LED	light-emitting diode
LIF	laser-induced fluorescence
LOC	lab-on-a-chip
LOD	limit of detection
LPA	linear polyacrylamide
MEMS	micro-electro-mechanical systems
mm	millimeter
mW	milliwatt
n	index of refraction
N	theoretical number of plates
NA	numerical aperture
nA	nanoampere
nL	nanoliter
nm	nanometer
nW	nanowatt
OD	optical density
OLED	organic light-emitting diode
PC	personal computer
PCR	polymerase chain reaction
PDMS	polydimethylsiloxane
pL	picoliter
PMT	photomultiplier tube

POC	point of care
pW	picowatt
s	second
SNR	signal-to-noise ratio
TIR	total internal reflection
t_m	retention time
TTE	tris- taurine- ethylenediaminetetraacetic acid
USB	universal serial bus
UV	ultraviolet
v	velocity
V	volts
VCSEL	vertical-cavity surface-emitting laser
W	watt
W_t	FWHM (full width at half maximum)

Chapter 1

Introduction

1.1 Lab on a Chip

The miniaturisation of biochemical assays onto microfluidic platforms has the potential to revolutionize health care. These devices, interchangeably termed *Lab on a Chip* (LOC) or *Micro Total Analysis Systems* (μTAS), are cited as providing advantages in terms of low cost, reduced size, rapid analysis and reduced sample and reagent requirements as compared to conventional techniques. The potential to provide point-of-care (POC) diagnosis and to reduce the cost of drug development has attracted a large amount of research attention in recent years [1–5].

While a few demonstrations of innovative miniaturised chemical analysis systems were reported prior to 1990 [6], the establishment of the vision and motivation behind μTAS is attributed to the paper published by Manz *et al.* in 1990 [7]. Manz describes the effects in scaling chemical analysis systems. As the dimension of the system is decreased (channel length / cross-sectional area) chromatographic and electrophoretic separations become quicker and more efficient. While higher pressures are required for hydrodynamic fluid flow, electroosmotic transport becomes more advantageous since the flow rate remains constant for a constant field strength. Additionally, larger electric fields can be used in miniaturized systems since the effects of Joule heating are reduced as the larger surface-to-volume ratio increases the heat dissipation.

The rapid advancement of LOC-based technologies since this seminal paper appeared stems from the transfer of fabrication techniques from the microelectronics

industry to the development of microfluidic-based microelectromechanical systems (MEMS), which is the backbone of nearly all LOC platforms. Currently, commercial LOC platforms are available from companies such as Agilent, Caliper, Micralyne and Cepheid, along with several others. However, these commercial systems remain quite large. Instead of the portable, hand-held systems initially envisioned, these devices tend to be restricted to the laboratory bench. While porting conventional assays onto microfluidic platforms is still an issue, an additional challenge is the miniaturisation of the external equipment required to interface to the microchip. For instance, the optical detection equipment often makes up the majority of the total system size, as is the case with the Microfluidic Toolkit marketed by Micralyne.

The work reported in this thesis addresses this problem through the development of methods to integrate the components required for optical detection directly onto the LOC system. The goal of this work is to reduce the size and decrease the cost of LOC systems while maintaining high sensitivity to allow for clinical diagnostics. While the integrated optical components developed in this work could be used for several different applications, the performance of the components was determined by performing laser induced fluorescence detection on electrophoretically separated DNA samples. A brief introduction to laser induced fluorescence, electrophoresis and integrated optics follows this section. This introductory chapter is concluded with a definition of the scope of the thesis.

Further information on the latest advances in LOC and μTAS technology can be found in scientific journals such as *Lab on a Chip*, *Analytical Chemistry*, *Electrophoresis*, *Journal of Micromechanics and Microengineering* and *Sensors and Actuators*.

1.2 Laser Induced Fluorescence

While numerous advantages become apparent as the dimensions of the analysis system are scaled down, detection becomes more challenging since the sample volume is reduced from μL to nL or pL. Increased sensitivity is required since fewer molecules are present in the detection region. For this reason, fluorescence sensing has

become extremely popular.

Laser induced fluorescence (LIF) is a detection technique that involves the excitation of a fluorescent molecule, or fluorophore, with a beam of light (typically from a laser). The fluorophore absorbs the light energy and is brought to an excited state. The fluorophore releases energy as light, but at a lower energy (longer wavelength).

Numerous fluorescent molecules have been isolated or synthesized for various applications and a fluorophore can be found with an excitation or emission spectrum for any region within the visible spectrum. Labelling kits are commercially available to bind fluorophores to nearly any biomolecule (i.e. amino acids, proteins, DNA, cells) and thus fluorescence sensing can be applied to a wide variety of applications.

1.2.1 Electrophoresis

Under a wide range of circumstances, the application of an electric field will cause species in a microfluidic channel to drift with a velocity of

$$\upsilon = \mu E_x \tag{1.1}$$

$$\mu = \mu_{EOF} + \mu_{EP} \tag{1.2}$$

where μ_{EOF} is the electroosmotic mobility and μ_{ep} is the electrophoretic mobility of the species and E_x is the electric field [8]. Electroosmosis describes the flow of a solution containing ions and is the result of the formation of an electrical double layer on the channel wall. For instance, in glass, the silanol groups on the channel wall are ionized (for pH $> \sim$3) forming a negative charge on the channel wall. Cations from the solution are thus attracted to the channel wall forming an electric double layer. Under the application of an electric field, the cations are attracted to the negative electrode and drag the entire solution volume with them, creating a flow.

On the other hand, electrophoresis describes the transport of electrically charged species in the presence of an electric field. Thus for a charged species, the speed of passage through the capillary is due to a combination of electroosmosis and electrophoresis. Using this technique, a sample can be separated into its components

based on a variation in mobility between the components. However, we often want to eliminate the effects of electroosmosis and other capillary wall effects to improve the resolution and sensitivity. This is accomplished by using channel coatings to prevent interaction of the reagents with the channel wall.

Electrophoresis is commonly used in this way to separate DNA fragments. DNA fragments tend to be negatively charged (typically at pH $\approx$ 8) as a result of the DNA phosphate backbone and therefore migrate toward the positive electrode. A variation in electrophoretic mobility is achieved by filling the separation channel with a polymer sieving matrix. The polymer chains in the sieving matrix act to restrict the movement of the DNA fragment. Electrophoresis allows for a size-based separation since longer DNA fragments are slower to pass through the matrix and thus have a lower electrophoretic mobility.

The DNA fragments are labelled with a fluorescent dye allowing for optical detection at the end of the separation channel. The resultant electropherogram is a display of the detected fluorescence intensity as a function of time. The arrival time of a peak provides information on the size of the fragment and the peak intensity is indicative of the concentration of DNA. Similarly, electrophoresis can be used to separate other charged species such as amino acids, proteins and other small molecules.

1.3 Optical Detection Systems - Integrated Optics

Conventional fluorescence detection systems make use of expensive optical instruments such as gas lasers, photomultiplier tubes (PMTs), compound confocal microscope systems, dichroic mirrors and dielectric interference filters. While these high-end optics allow for high sensitivity, the size and cost of this equipment restrict their use to bench-top systems located within the laboratory.

In the same manner that fluid handling components have been miniaturised in the form of microfluidic LOC devices, the optical detection system must also be miniaturised to develop a fully integrated, portable biochemical analysis tool.

The increasing number of contributions to this field of research highlights the

growing importance of integrating optics into LOC systems. Several recent reviews describe the current issues and progress in this area [9–12]. There are four key components that are typically required in a fluorescence-based optical detection system: (i) light delivery / collection optics; (ii) optical filters; (iii) light sources; and (iv) photodetectors.

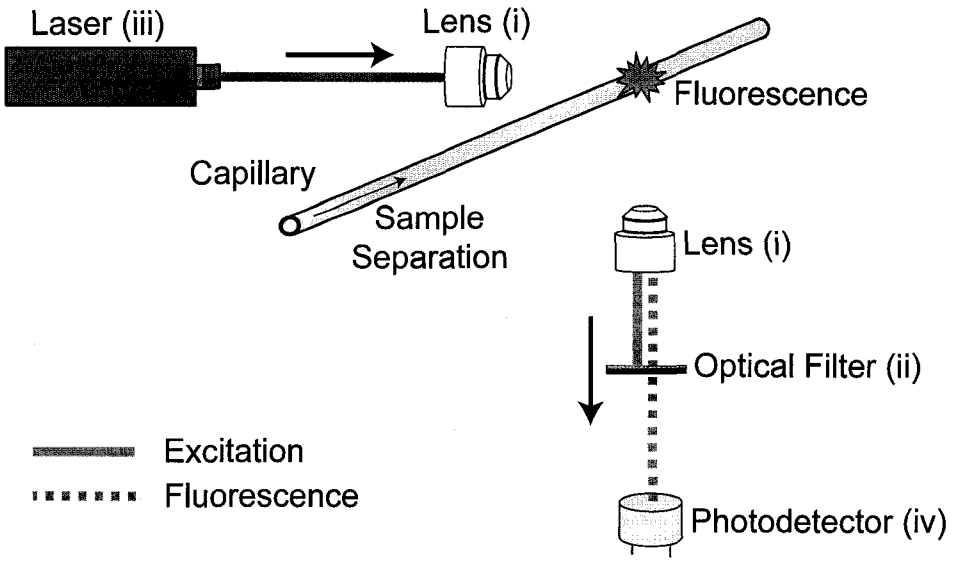

Figure 1.1: A schematic of a fluorescence detection system for capillary electrophoresis. Excitation light from a laser is focused onto the capillary using a microscope objective. A second microscope objective is used to collect the fluorescence emission. The collected light is passed through an optical filter to remove any scattered excitation light prior to reaching the photodetector.

1.3.1 Optical Waveguides

Since the inclusion of bulk lenses and microscope objectives is not desirable when designing an integrated system due to the large size of these components, light delivery and collection can instead be performed using optical waveguides. Optical waveguides can be readily integrated into microscale systems and can be fabricated using a variety of materials. Integrated optical waveguides are advantageous in that the detection efficiency can be increased through the precise alignment of the excitation and detection optics through photolithography during fabrication. This automatic alignment eliminates the requirement for micro-positioners. Integrated

planar waveguides can be used as multiplexing systems in order to deliver a single light source to many locations throughout the chip [10] or to compile light from multiple detection sites [13] to maximize the signal to noise ratio (SNR).

1.3.1.1 Theory

When light hits a boundary between two media of different refractive indices, the light will be reflected and may also be transmitted though the boundary after being bent, or refracted. This is shown schematically in Fig. 1.2. The angle of reflection, θ_r, is equal to the angle of incidence, θ_i. If refraction occurs, the angle of refraction, θ_t, can be calculated using Snell's law [14]

$$n_i \sin\theta_i = n_t \sin\theta_t \tag{1.3}$$

where n_i represents the refraction index of the incident medium and n_t is the refractive index of the medium into which the refracted ray is transmitted. The fraction of light which is reflected and transmitted can be determined using the Fresnel reflection and refraction coefficients, which can be found in ref. [14]. If $n_i > n_t$, the angle of refraction is greater than the incidence angle. However, the angle of refraction (θ_t) cannot be greater than 90^o. The angle of incidence required to set the angle of refraction to 90^o is defined as the critical angle. If the angle of incidence of the ray is larger than the critical angle the ray is said to be totally internally reflected. During total internal reflection (TIR), no light power is transmitted through the boundary and all of the optical power is reflected. This is the typical operation mode for a conventional waveguide.

Optical waveguides confine light through TIR at the cladding/core boundary. As described in Fig. 1.3, a conventional waveguide is formed by enclosing the waveguide core with a material of lower refractive index. It is important to know the range of angles over which the waveguide can accept or emit light. All angles less than the maximum incidence angle, θ_{inc} as shown schematically in Fig. 1.3, will result in angles greater than the waveguide critical angle, ensuring TIR within the waveguide. The maximum incidence angle is also the maximum angle at which a confined ray can exit the waveguide. Since the maximum incidence angle is dependent on the refractive index of the surrounding medium, n_s, the ability of a

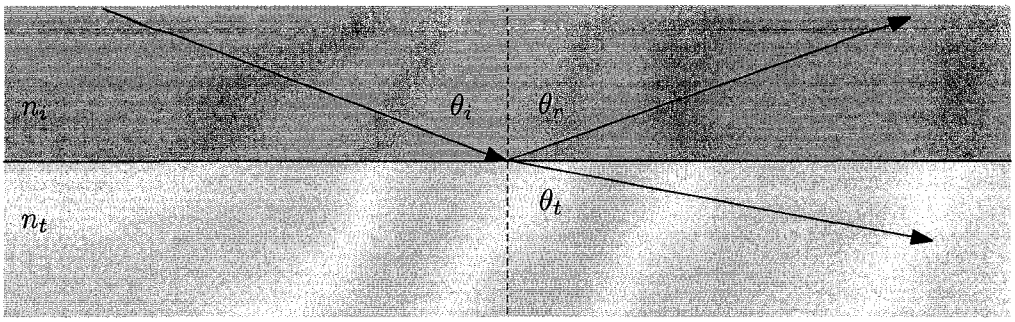

Figure 1.2: When a light ray encounters a shift in refractive index, a portion of the light is reflected and a portion is transmitted into the new medium according to the Fresnel reflection and refraction coefficients. The transmission angle is related to the incident angle and the refractive indices of each medium through Snell's law.

waveguide to accept incoming light rays is instead commonly described by the numerical aperture (NA) of the waveguide, which is independent of the index of the surrounding medium. The NA is given by

$$NA = \sqrt{{n_{core}}^2 - {n_{clad}}^2} \tag{1.4}$$

The numerical aperture can be used to determine the maximum acceptance angle of the waveguide by

$$\theta_{inc} = \sin^{-1} \frac{NA}{n_s} \tag{1.5}$$

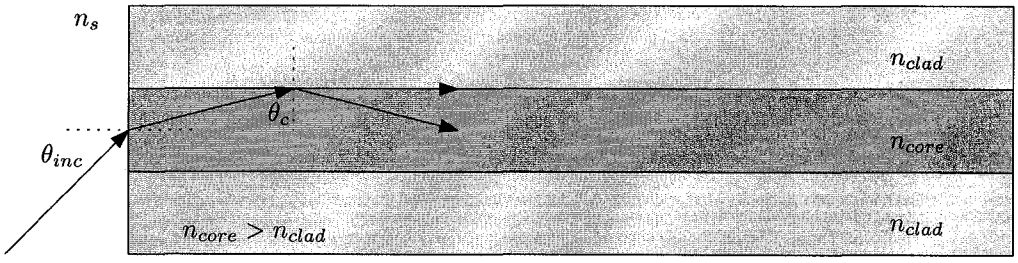

Figure 1.3: A schematic defining the acceptance angle of a waveguide. Light rays entering a waveguide at angles less than or equal to the acceptance angle will be confined to the waveguide through total internal reflection.

1.3.1.2 Fabrication

Initially, optical waveguides for LOC applications were formed through chemical vapor deposition (CVD) of dielectric materials and ion-implantation into glass. The monolithic integration of waveguides using CVD, fabricated of materials such as silicon oxynitrides [15] or germanium-doped glasses [16, 17], required lengthy deposition times along with several photolithography and etching steps. At time scales such as 192 hours in a 380°C molten bath [18], the ion replacement processes was extraordinarily lengthy. However, this time scale could be reduced to several hours [19, 20] using field-assisted ion replacement techniques. Ultimately, both CVD and ion-implantation techniques resulted in a substantial increase in device cost.

Recently, polymer waveguides have increased in popularity due to the reduced material cost and the simplification in the fabrication process. Polymer waveguides have been fabricated of SU-8 photoresist [21–24] and through laser fabrication using UV epoxy [25]. Using these polymer materials, waveguides could be fabricated simultaneously with the fluidic channels in a single photolithography step. PDMS waveguides are fabricated using simple soft lithography techniques [13, 26].

To further simplify the fabrication process, microfluidic waveguides have been built by filling microfluidic channels with high refractive index liquids [27–29]. Waveguides integrated into microfluidic devices in this manner do not require any additional processing steps. This is the waveguide fabrication approach taken in the work presented in this thesis.

1.3.1.3 Application

Integrated waveguides can be used in microscale LOC systems as an alternative to lenses for light delivery and collection in LIF. Just as the ability of a lens to collect light is a function of the numerical aperture, the NA also impacts the light collection efficiency (LCE) of a waveguide. However, additional factors, such as the waveguide aperture area and the distance between the waveguide and the microfluidic channel, can impact the LCE. A comparison of the performance of conventional lenses to integrated waveguides is provided in Chapter 2. If the excitation source

or detector are off-chip, interfacing between the waveguide and these components must also be considered. This typically involves the reliance on bulk optics, such as microscope objectives, to focus light on to or off of the integrated waveguides. In this work, we describe the design and fabrication of integrated fiber-to-waveguide couplers, which allow optical coupling through the insertion of optical fibers into the side of the chip. This is explored further in Chapter 2.

1.3.2 Optical Filters

Optical filters are required to isolate the fluorescence emission from the scattered / reflected excitation light. Since the excitation light power can be several orders of magnitude larger than the fluorescence emission (i.e. milliwatt excitation, picowatt emission) , the optical filter must be of a high quality to effectively suppress the excitation light while passing a large fraction of the impinging fluorescence. Efforts focusing on the integration of optical filters into LOC system generally fall into two categories based on optical interference and light absorption. A recent review provides a critical analysis of current progress in the development of optical filtering technologies for integrated fluorescence sensors [11].

1.3.2.1 Interference Filters

Interference filters typically consist of alternating layers of dielectric materials. Wavelengths that experience constructive interference pass through the filter while wavelengths that experience destructive interference are reflected [11]. While highly complex filters can be fabricated (with correspondingly high fabrication complexity), the types of optical filters designed for integration into LOC systems typically take the form of a common Bragg reflector consisting of a series of alternating high and low refractive index quarter-wavelength layers [11].

The primary advantages in using dielectric interference filters include the ability to tune the passband of the filter (by changing the thickness of the dielectric layers) and the compatibility of the material deposition process with microelectronics. Several examples of these filters have been presented in the literature [30–36]. However, multilayer interference filters are not without their disadvantages [11].

The fabrication of these types of optical filters tend to require 40 or more alternating layers to achieve adequate attenuation and sharpness of the passband [11]. Tight fabrication tolerances are required to achieve the designed filter properties, necessitating accuracy to within a few nanometers. Additionally, off-axis light impingent on the detector observes a larger spacing between layers and this results in a shift of the center wavelength and thus a degradation in the quality of the filter. For this reason, additional optics are required to collimate the light that enters the filter.

1.3.2.2 Absorbance Filters

Absorptive, or colour, filters operate by absorbing particular wavelengths and transmitting others. The transmission spectrum can be described using the Lambert-Beer law

$$I_O/I_I = 10^{-\epsilon l c} \tag{1.6}$$

where I_I and I_O are the intensities of light which enter and pass through the filter, respectively, ϵ is the wavelength dependent extinction coefficient of the absorbing material, l is the thickness of the filter, and c is the concentration of the absorbing material. The absorbing medium often consists of an organic material or polymer. Unlike the interference filters described above, the polymer filter can typically be deposited in a single layer. The deposition process also tends to be much simpler, through the use of techniques such as spin-coating or casting, and curing may be thermal, UV or chemical (cross-linking agent) [11]. Due to the simplified fabrication process, absorptive filters are a low cost alternative to interference filters. For this reason, absorptive filters have been used in integrated LOC-type systems by several groups [37–39]. We explore the use of integrated waveguides with built-in absorptive filters for fluorescence detection in Chapter 3.

While the performance of interference filters are sensitive to the incidence angle, absorptive filters do not suffer from a loss of performance at oblique angles. On the other hand, absorptive filters lack the design flexibility of interference filters since the transmission spectrum of absorptive filters cannot be modified and a change in fluorophore may require a change in filter material. It is also difficult to achieve a

sharp cut-off, defined as the width (in nm) of the transition between the passband (transmitted wavelengths) and stopband (absorbed wavelengths). Additionally, absorptive filters may also suffer from autofluorescence and this may contribute to background at the detector.

1.3.3 Integrated Sources

The integration of optical sources onto the LOC platform has been a significant challenge, partially due to the fact that silicon, the substrate of choice for microelectronics and many MEMS devices, does not function well as a light emitter. The majority of demonstrated work involving the integration of the light source consists of hybrid systems where the miniaturized light source is located on a separate substrate. Examples of hybrid systems involve the use of external polymer organic LEDs (OLEDs) [40, 41] and vertical cavity surface emitting lasers (VCSELs) fabricated on a secondary GaAs-based microchip [42–44]. While polymer OLEDs are attractive as an inexpensive technology that could be integrated directly onto a single-chip LOC system, a reduction in the spectral bandwidth and an increase in the luminosity are required in order for these devices to become useful as an excitation source in fluorescence sensing applications. Alternatively, microfluidic dye lasers have been used as a means of generating excitation light on-chip [45–48] and the laser emission is directly coupled into an integrated waveguide. However, the requirement for an external pump laser limits the usefulness of this technology as an integrated solution.

1.3.4 Integrated Photodetectors

In contrast to the difficulty in integrating the excitation source, the fabrication of photodiodes in silicon is a mature technology and thus photodiodes are readily integrated into silicon-based LOC systems. Since silicon is opaque for visible wavelengths, the fabrication of microfluidic chips consisting of silicon and either polymer or glass is required to allow optical access. Several systems have been demonstrated which incorporate the photodetector in this manner [16, 30–32, 48]. Alternatively, photodiodes have been integrated using a multi-chip method [33–35, 42–

44, 49–51], similar to the integrated optical sources described earlier. Alternate types of photodetectors such as micro avalanche photodiodes (μAPDs) [38, 52] and organic photodiodes [53, 54] have been integrated into multi-chip systems. While the single chip systems provide a higher level of integration, the cost of the chip, including the fabrication of microchannels, optical filters and photodetectors, will be significant. The multi-chip method provides the advantage that the microfluidic chip can be disposed of and replaced without replacing the optical source or photodetector, which is more costly to produce. We explore the use of a multi-chip hybrid method to integrate the photodetector into the miniaturised fluorescence detection system in Chapter 4.

1.4 Scope of Thesis

This thesis is divided into three core chapters, each of which explores the simplification and miniaturization of a particular aspect of the fluorescence detection system. Each successive chapter explores the integration of an additional key optical component, as described in 1.3, while building on the technology developed in the previous work.

In Chapter 2, the fabrication and performance of a microfluidic device with integrated liquid-core optical waveguides for laser induced fluorescence DNA fragment analysis is presented. The device was fabricated through PDMS soft lithography and waveguides are formed in dedicated channels through the addition of a liquid PDMS pre-polymer of higher refractive index. Once a master has been fabricated, microfluidic chips can be produced in less than 3 hours, without the requirement for a cleanroom, yet this method provides an optical system that has higher performance than a conventional confocal optical assembly. Optical coupling was achieved through the insertion of optical fibers into fiber-to-waveguide couplers at the edge of the chip and the liquid-fiber interface results in low reflection and scattering losses. We demonstrate that an inexpensive waveguide-based system can achieve a SNR comparable to, or better than, a commercially available confocal-based system for microchip capillary electrophoresis.

This chapter provides a foundation for the remainder of the work in this thesis. In this work, waveguides, rather than confocal optics, are used to deliver and collect light on the microchip. Where in confocal systems the focus and alignment must be adjusted prior to performing an experiment, the waveguides are automatically aligned during fabrication and no further alignment is required. The instrumentation convenience of the fiber-to-waveguide couplers developed in this work must be stressed. With a slight bit of experience, optical fibers can be repeatably inserted into the coupler within seconds and the fiber is automatically aligned to the core within approximately 5μm, allowing for rapid experimental setups. Additionally, the low cost of the PDMS chips allowed contaminated chips to be simply discarded rather than painstakingly cleaned with solvents and boiling acid treatments, a necessity with glass microchips. This work has recently been published in the journal *Lab on a Chip* [55].

In Chapter 3, we explore the use of organic dyes to dope PDMS and to create integrated absorptive filters. We discovered that liquid core waveguides built into dye-doped PDMS chips demonstrated optical filter properties, thus acting as wavelength-selective optical waveguides. Liquid-core waveguides are created within dye-doped PDMS microfluidic chips by filling channels with high refractive index liquids that allow dye molecules to diffuse into the waveguide core. The rate of diffusion is controlled by choosing either polar (low diffusion) or apolar (high diffusion) liquid waveguide cores. The dye is chosen to absorb excitation light and to transmit fluorescence emitted by the sample under test. This work has recently been submitted for publication in the journal *Lab on a Chip* [56].

In Chapter 4 we eliminate the need for the bulky PMT system used in the previous two chapters by using inexpensive silicon photodiodes. We report the development of a novel fluorescence-based capillary electrophoresis system that has the capability to be integrated onto a pocket-sized platform. The level of integration demonstrated in this work required the development of a compact optical detection system and high-voltage (HV) CMOS microelectronics. The design of the HV CMOS microelectronics was provided by students from the lab of Dr. Duncan Elliott, Department of Electrical & Computer Engineering, University of Alberta. On

the path toward our prototype system, we describe the development and characterization of a sequence of optical detection systems with increasing levels of integration. The HV CMOS microchip is capable of generating the high voltages required to drive the electrophoresis system and is key in eliminating the dependence on benchtop equipment for device operation. The final prototype system consists entirely of a polymer microfluidic chip, an inexpensive laser diode, a HV CMOS chip with a built-in high voltage power supply and some additional electronics. We demonstrate the clinical relevance of this device by detecting end-labelled DNA obtained from a BK virus PCR reaction. We lay out our roadmap to achieve a further increase in sensitivity and reduction in device size to allow for the fabrication of a "USB-key" style portable, handheld CE device.

Bibliography

[1] D. R. Reyes, D. Iossifidis, P. A. Auroux, and A. Manz, "Micro total analysis systems. 1. Introduction, theory, and technology," *Analytical Chemistry*, vol. 74, no. 12, pp. 2623–2636, 2002.

[2] P. A. Auroux, D. Iossifidis, D. R. Reyes, and A. Manz, "Micro total analysis systems. 2. Analytical standard operations and applications," *Analytical Chemistry*, vol. 74, no. 12, pp. 2637–2652, 2002.

[3] P. S. Dittrich, K. Tachikawa, and A. Manz, "Micro total analysis systems. Latest advancements and trends," *Analytical Chemistry*, vol. 78, no. 12, pp. 3887–3907, 2006.

[4] T. Vilkner, D. Janasek, and A. Manz, "Micro total analysis systems. Recent developments," *Analytical Chemistry*, vol. 76, no. 12, pp. 3373–3385, 2004.

[5] P. S. Dittrich and A. Manz, "Lab-on-a-chip: microfluidics in drug discovery," *Nature Reviews Drug Discovery*, vol. 5, no. 3, pp. 210–218, 2006.

[6] S. C. Terry, J. H. Jerman, and J. B. Angell, "Gas-chromatographic air analyzer fabricated on a silicon-wafer," *IEEE Transactions on Electron Devices*, vol. 26, no. 12, pp. 1880–1886, 1979.

[7] A. Manz, N. Graber, and H. M. Widmer, "Miniaturized total chemical-analysis systems - a novel concept for chemical sensing," *Sensors and Actuators B - Chemical*, vol. 1, no. 1-6, pp. 244–248, 1990.

[8] S. D. Senturia, *Microsystem Design*. New York, NY: Springer, 2001.

[9] E. Verpoorte, "Chip vision - optics for microchips," *Lab on a Chip*, vol. 3, no. 3, pp. 42N–52N, 2003.

[10] K. B. Mogensen, H. Klank, and J. P. Kutter, "Recent developments in detection for microfluidic systems," *Electrophoresis*, vol. 25, no. 21-22, pp. 3498–3512, 2004.

[11] M. Dandin, P. Abshire, and E. Smela, "Optical filtering technologies for integrated fluorescence sensors." *Lab on a Chip*, 2007. DOI:10.1039/b704008c.

[12] S. Gotz and U. Karst, "Recent developments in optical detection methods for microchip separations," *Analytical and Bioanalytical Chemistry*, vol. 387, no. 1, pp. 183–192, 2007.

[13] V. Lien, K. Zhao, Y. Berdichevsky, and Y. H. Lo, "High-sensitivity cytometric detection using fluidic-photonic integrated circuits with array waveguides," *IEEE Journal of Selected Topics in Quantum Electronics*, vol. 11, no. 4, pp. 827–834, 2005.

[14] E. Hecht, *Optics*, 4th ed. San Francisco, CA, USA: Addison Wesley, 2001.

[15] K. B. Mogensen, N. J. Petersen, J. Hubner, and J. P. Kutter, "Monolithic integration of optical waveguides for absorbance detection in microfabricated electrophoresis devices," *Electrophoresis*, vol. 22, no. 18, pp. 3930–3938, 2001.

[16] O. Leistiko and P. F. Jensen, "Integrated bio/chemical microsystems employing optical detection: the clip-on," *Journal of Micromechanics and Microengineering*, vol. 8, no. 2, pp. 148–150, 1998.

[17] P. Friis, K. Hoppe, O. Leistiko, K. B. Mogensen, J. Hubner, and J. P. Kutter, "Monolithic integration of microfluidic channels and optical waveguides in silica on silicon," *Applied Optics*, vol. 40, no. 34, pp. 6246–6251, 2001.

[18] R. Mazurczyk, J. Vieillard, A. Bouchard, B. Hannes, and S. Krawczyk, "A novel concept of the integrated fluorescence detection system and its application in a lab-on-a-chip microdevice," *Sensors and Actuators B - Chemical*, vol. 118, no. 1-2, pp. 11–19, 2006.

[19] J. N. McMullin, H. Qiao, S. Goel, C. L. Ren, and D. Q. Li, "Integrated optical measurement of microfluid velocity," *Journal of Micromechanics and Microengineering*, vol. 15, no. 10, pp. 1810–1816, 2005.

[20] H. Qiao, S. Goel, A. Grundmann, and J. N. McMullin, "Fabrication of micro-optical/microfluidic biochips," *Proc. SPIE Int. Soc. Opt. Eng.*, vol. 4833, no. 1, pp. 54–59, 2003.

[21] G. B. Lee, C. H. Lin, and G. L. Chang, "Micro flow cytometers with buried SU-8/SOG optical waveguides," *Sensors and Actuators A - Physical*, vol. 103, no. 1-2, pp. 165–170, 2003.

[22] A. R. Leeds, E. R. Van Keuren, M. E. Durst, T. W. Schneider, J. F. Currie, and M. Paranjape, "Integration of microfluidic and microoptical elements using a single-mask photolithographic step," *Sensors and Actuators A - Physical*, vol. 115, no. 2-3, pp. 571–580, 2004.

[23] Z. Wang, J. El-Ali, M. Engelund, T. Gotsaed, I. R. Perch-Nielsen, K. B. Mogensen, D. Snakenborg, J. P. Kutter, and A. Wolff, "Measurements of scattered light on a microchip flow cytometer with integrated polymer based optical elements," *Lab on a Chip*, vol. 4, no. 4, pp. 372–377, 2004.

[24] K. B. Mogensen, J. El-Ali, A. Wolff, and J. P. Kutter, "Integration of polymer waveguides for optical detection in microfabricated chemical analysis systems," *Applied Optics*, vol. 42, no. 19, pp. 4072–4079, 2003.

[25] J. N. McMullin, "Laser fabrication of integrated microfluidic/micro-optic systems," *Proc. SPIE Int. Soc. Opt. Eng.*, vol. 4087, no. 1, pp. 1050–1055, 2000.

[26] D. A. Chang-Yen, R. K. Eich, and B. K. Gale, "A monolithic PDMS waveguide system fabricated using soft-lithography techniques," *Journal of Lightwave Technology*, vol. 23, no. 6, pp. 2088–2093, 2005.

[27] O. J. A. Schueller, X. M. Zhao, G. M. Whitesides, S. P. Smith, and M. Prentiss, "Fabrication of liquid-core waveguides by soft lithography," *Advanced Materials*, vol. 11, no. 1, pp. 37–41, 1999.

[28] D. B. Wolfe, R. S. Conroy, P. Garstecki, B. T. Mayers, M. A. Fischbach, K. E. Paul, M. Prentiss, and G. M. Whitesides, "Dynamic control of liquid-core/liquid-cladding optical waveguides," *Proceedings of the National Academy of Sciences of the United States of America*, vol. 101, no. 34, pp. 12 434–12 438, 2004.

[29] D. B. Wolfe, D. V. Vezenov, B. T. Mayers, G. M. Whitesides, R. S. Conroy, and M. G. Prentiss, "Diffusion-controlled optical elements for optofluidics," *Applied Physics Letters*, vol. 87, no. 18, 2005.

[30] M. A. Burns, B. N. Johnson, S. N. Brahmasandra, K. Handique, J. R. Webster, M. Krishnan, T. S. Sammarco, P. M. Man, D. Jones, D. Heldsinger, C. H. Mastrangelo, and D. T. Burke, "An integrated nanoliter DNA analysis device," *Science*, vol. 282, no. 5388, pp. 484–487, 1998.

[31] J. R. Webster, M. A. Burns, D. T. Burke, and C. H. Mastrangelo, "Monolithic capillary electrophoresis device with integrated fluorescence detector," *Analytical Chemistry*, vol. 73, no. 7, pp. 1622–1626, 2001.

[32] V. Namasivayam, R. S. Lin, B. Johnson, S. Brahmasandra, Z. Razzacki, D. T. Burke, and M. A. Burns, "Advances in on-chip photodetection for applications in miniaturized genetic analysis systems," *Journal of Micromechanics and Microengineering*, vol. 14, no. 1, pp. 81–90, 2004.

[33] K. S. Shin, Y. H. Kim, J. A. Min, S. M. Kwak, S. K. Kim, E. G. Yang, J. H. Park, B. K. Ju, T. S. Kim, and J. Y. Kang, "Miniaturized fluorescence detection chip for capillary electrophoresis immunoassay of agricultural herbicide atrazine," *Analytica Chimica Acta*, vol. 573, pp. 164–171, 2006.

[34] Y. H. Kim, K. S. Shin, J. Y. Kang, E. G. Yang, K. K. Paek, D. S. Seo, and B. K. Ju, "Poly(dimethylsiloxane)-based packaging technique for microchip fluorescence detection system applications," *Journal of Microelectromechanical Systems*, vol. 15, no. 5, pp. 1152–1158, 2006.

[35] K. S. Shin, Y. H. Kim, K. K. Paek, J. H. Park, E. G. Yang, T. S. Kim, J. Y. Kang, and B. K. Ju, "Characterization of an integrated, fluorescence-detection hybrid device with photodiode and organic light-emitting diode," *IEEE Electron Device Letters*, vol. 27, no. 9, pp. 746–748, 2006.

[36] K. S. Shin, S. W. Lee, K. C. Han, S. K. Kim, E. K. Yang, J. H. Park, B. K. Ju, J. Y. Kang, and T. S. Kim, "Amplification of fluorescence with packed beads to enhance the sensitivity of miniaturized detection in microfluidic chip," *Biosensors & Bioelectronics*, vol. 22, no. 9-10, pp. 2261–2267, 2007.

[37] O. Hofmann, X. H. Wang, A. Cornwell, S. Beecher, A. Raja, D. D. C. Bradley, A. J. deMello, and J. C. deMello, "Monolithically integrated dye-doped PDMS long-pass filters for disposable on-chip fluorescence detection," *Lab on a Chip*, vol. 6, no. 8, pp. 981–987, 2006.

[38] M. L. Chabinyc, D. T. Chiu, J. C. McDonald, A. D. Stroock, J. F. Christian, A. M. Karger, and G. M. Whitesides, "An integrated fluorescence detection system in poly(dimethylsiloxane) for microfluidic applications," *Analytical Chemistry*, vol. 73, no. 18, pp. 4491–4498, 2001.

[39] J. A. Chediak, Z. S. Luo, J. G. Seo, N. Cheung, L. P. Lee, and T. D. Sands, "Heterogeneous integration of CdS filters with GaN LEDs for fluorescence detection microsystems," *Sensors and Actuators A - Physical*, vol. 111, no. 1, pp. 1–7, 2004.

[40] J. B. Edel, N. P. Beard, O. Hofmann, J. C. DeMello, D. D. C. Bradley, and A. J. deMello, "Thin-film polymer light emitting diodes as integrated excitation sources for microscale capillary electrophoresis," *Lab on a Chip*, vol. 4, no. 2, pp. 136–140, 2004.

[41] O. Hofmann, X. H. Wang, J. C. deMello, D. D. C. Bradley, and A. J. deMello, "Towards microalbuminuria determination on a disposable diagnostic microchip with integrated fluorescence detection based on thin-film organic light emitting diodes," *Lab on a Chip*, vol. 5, no. 8, pp. 863–868, 2005.

[42] E. Thrush, O. Levi, W. Ha, K. Wang, S. J. Smith, and J. S. Harris, "Integrated bio-fluorescence sensor," *Journal of Chromatography A*, vol. 1013, no. 1-2, pp. 103–110, 2003.

[43] E. Thrush, O. Levi, W. Ha, G. Carey, L. J. Cook, J. Deich, S. J. Smith, W. E. Moerner, and J. S. Harris, "Integrated semiconductor vertical-cavity surface-emitting lasers and PIN photodetectors for biomedical fluorescence sensing," *IEEE Journal of Quantum Electronics*, vol. 40, no. 5, pp. 491–498, 2004.

[44] E. Thrush, O. Levi, L. J. Cook, J. Deich, A. Kurtz, S. J. Smith, W. E. Moerner, and J. S. Harris, "Monolithically integrated semiconductor fluorescence sensor for microfluidic applications," *Sensors and Actuators B - Chemical*, vol. 105, no. 2, pp. 393–399, 2005.

[45] B. Helbo, A. Kristensen, and A. Menon, "A micro-cavity fluidic dye laser," *Journal of Micromechanics and Microengineering*, vol. 13, no. 2, pp. 307–311, 2003.

[46] B. Helbo, S. Kragh, B. G. Kjeldsen, J. L. Reimers, and A. Kristensen, "Investigation of the dye concentration influence on the lasing wavelength and threshold for a micro-fluidic dye laser," *Sensors and Actuators A - Physical*, vol. 111, no. 1, pp. 21–25, 2004.

[47] Z. Y. Li and D. Psaltis, "Optofluidic distributed feedback dye lasers," *IEEE Journal of Selected Topics in Quantum Electronics*, vol. 13, no. 2, pp. 185–193, 2007.

[48] S. Balslev, A. M. Jorgensen, B. Bilenberg, K. B. Mogensen, D. Snakenborg, O. Geschke, J. P. Kutter, and A. Kristensen, "Lab-on-a-chip with integrated optical transducers," *Lab on a Chip*, vol. 6, no. 2, pp. 213–217, 2006.

[49] T. Kamei, B. M. Paegel, J. R. Scherer, A. M. Skelley, R. A. Street, and R. A. Mathies, "Integrated hydrogenated amorphous Si photodiode detector for microfluidic bioanalytical devices," *Analytical Chemistry*, vol. 75, no. 20, pp. 5300–5305, 2003.

[50] T. Kamei, N. M. Toriello, E. T. Lagally, R. G. Blazej, J. R. Scherer, R. A. Street, and R. A. Mathies, "Microfluidic genetic analysis with an integrated a-Si : H detector," *Biomedical Microdevices*, vol. 7, no. 2, pp. 147–152, 2005.

[51] T. Kamei and T. Wada, "Contact-lens type of micromachined hydrogenated amorphous Si fluorescence detector coupled with microfluidic electrophoresis devices," *Applied Physics Letters*, vol. 89, no. 11, 2006.

[52] J. Kruger, K. Singh, A. O'Neill, C. Jackson, A. Morrison, and P. O'Brien, "Development of a microfluidic device for fluorescence activated cell sorting," *Journal of Micromechanics and Microengineering*, vol. 12, no. 4, pp. 486–494, 2002.

[53] X. Wang, O. Hofmann, R. Das, E. M. Barrett, A. J. deMello, J. C. deMello, and D. D. C. Bradley, "Integrated thin-film polymer/fullerene photodetectors for on-chip microfluidic chemiluminescence detection." *Lab on a Chip*, 2007. DOI:10.1039/b611067c.

[54] O. Hofmann, P. Miller, P. Sullivan, T. S. Jones, J. C. deMello, D. D. C. Bradley, and A. J. deMello, "Thin-film organic photodiodes as integrated detectors for microscale chemiluminescence assays," *Sensors and Actuators B - Chemical*, vol. 106, no. 2, pp. 878–884, 2005.

[55] C. Bliss, J. McMullin, and C. Backhouse, "Rapid fabrication of a microfluidic device with integrated optical waveguides for DNA fragment analysis," *Lab on a Chip*, 2007. DOI: 10.1039/b708485d.

[56] C. Bliss, J. McMullin, and C. Backhouse, "Integrated wavelength-selective optical waveguides for microfluidic-based laser induced fluorescence detection," *Lab on a Chip*, 2007. Submitted.

Chapter 2

Rapid Fabrication of a Microfluidic Device with Integrated Optical Waveguides for DNA Fragment Analysis

2.1 Introduction

The development of microfluidic-based technologies for biochemical analysis has led to an increased research interest in lab-on-a-chip (LOC) systems [1–3], which is now finding many commercial analytical and medical applications [4, 5]. Advantages such as reduced sample and reagent volumes, system cost, size and power requirements, as compared to conventional systems, are key in addressing the need for point-of-care (POC) disease diagnosis. However, reduced analysis volumes lead to low signal levels since fewer molecules are present in the detection region. Though a number of detection strategies exist [6], laser induced fluorescence (LIF) has remained the most popular in LOC systems due to the high sensitivity achievable through the use of this technique.

Confocal detection configurations are commonly used to achieve high signal-to-noise ratios (SNR) through excellent suppression of scattered light and allow for high resolution detection, making even single molecule detection possible [7, 8]. However, confocal detection systems include expensive bulk optics that do not lend themselves to miniaturization - particularly an issue in the development of hand-held POC diagnostic systems. On the other hand, LOCs with integrated op-

tical components promise a reduction in the size, cost and complexity of the system [9]. Integrated optical waveguides can be used to direct light to within microns of the sample. Also, waveguide splitters and combiners allow for a parallel architecture with multiple excitation or detection points per input or output [10]. Microscope translation stages and micro-positioners are not required since precise alignment of the optics to the detection region is achieved automatically through photolithography. Waveguides for LOC applications have been previously fabricated through oxide deposition [11–13], ion-exchange [14, 15] and anisotropic etching of silicon [16]. However, waveguide systems made of polymers such as SU-8 [17–20], UV-laser-written optical adhesives [21] and poly(dimethylsiloxane) (PDMS) [10, 22–24] have grown in popularity due to the low cost of these materials and the rapid fabrication processes based upon them.

In this chapter, we describe microfluidic chips with integrated waveguides fabricated by PDMS soft lithography [25]. Waveguides are formed by filling microfluidic channels with a high refractive index liquid PDMS pre-polymer. The waveguides are used to deliver excitation light to the microchannels and to collect fluorescence from the samples under test. Optical coupling between external sources/detectors and the waveguides is achieved through optical fibers inserted into the liquid-core waveguides at the edge of the chips. The PDMS pre-polymer coats the inserted fiber, reducing reflections and scattering at the optical interface, thus increasing the coupling efficiency. Unlike previous work [10], only a single PDMS polymer precursor is added to the waveguide channel to prevent subsequent curing that would encapsulate the interfacing optical fibers. This allows for cleaning and reuse of the chip. In addition, the design was optimized to suppress the collection of excitation (laser) light and maximize the collection of the emitted fluorescence enabling us to achieve greater sensitivity, in terms of SNR, than a commercially available confocal-based system.

Numerous human diseases are detectable through genetic testing of bodily fluids. Pathogen detection in food and water is becoming more common as the availability of affordable DNA analysis technologies increases. The analysis of amplified DNA fragments is commonly used as a "fingerprinting" tool in diagnostic as-

says [26]. We have previously demonstrated a microfluidic-based bench-top system capable of the sensitive analysis of BK virus (viral load) from an unprocessed urine sample using a commercial confocal detection system [27]. In the current work, we present the results of a DNA fragment analysis of a BK virus (BKV) polymerase chain reaction (PCR) product using microchip capillary electrophoresis (CE) in the miniaturized waveguide system described here. We compare these results to those obtained using a commercially available microchip-based electrophoresis system, the Microfluidic Toolkit or μTK (Micralyne, AB, Canada), using identical microchips, samples and reagents.

Detection schemes which rely on integrated optics have been successfully demonstrated for micro flow cytometry [10, 28] or protein analysis [29, 30] and other groups have previously used integrated optics for DNA fragment analysis. In particular, Wang *et al.* have developed a miniaturized CE system with greatly simplified optics. This system is capable of the analysis of intercalator-labelled DNA using Teflon-coated glass capillaries as waveguides with inexpensive LED excitation [31]. In an impressive demonstration of the integration achievable through LOC technology, Burns *et al.* reported the amplification, digestion, separation and detection of DNA samples on a microfluidic chip containing integrated optical filters and photosensors [32]. Though the intercalating dyes used in both of the above cases tend to be much brighter than end-labelled dyes since multiple fluorophores label a single DNA fragment, this comes at the expense of decreased separation efficiency [33]. In our work, we are able to maintain high SNRs while using end-labelled DNA. It is also desirable that the microfluidic chip in a handheld POC diagnostic system be disposable to prevent cross contamination between samples and therefore cost is an important issue. The individual microfluidic chip cost can be drastically reduced by moving the photodetector and optical interference filter off-chip, while retaining the critical optical components. Once a master has been fabricated, the material cost of each chip in our system is much less than one dollar and a set of chips can be fabricated in less than 3 hours without the requirement for a cleanroom. The cost per analysis is simply the cost of an individual chip, or less if the chip were re-used, since the cost of the buffer and sieving matrix is negligible relative to the cost of the

chip.

In Section 2.2, we describe in detail the microfluidic chip design, the fabrication procedure, the waveguide propagation and fiber-coupling properties, and compare the light-gathering efficiency of the waveguide system to a confocal system. In Section 2.3, a performance comparison of the waveguide system with a commercial confocal system is carried out through a separation analysis of BKV DNA fragments obtained through PCR. It is shown that the SNR of the waveguide system is higher than that of the confocal system while maintaining a comparable separation efficiency. Section 2.4 concludes the chapter with a summary and discussion of the results.

This chapter is based on a recently published journal paper by Bliss *et al.* [34].

2.2 Device Design, Fabrication and Optical Characterization

2.2.1 Design and Fabrication

A schematic of the PDMS device is shown in Fig. 2.1. The microfluidic channels connecting the sample (S), sample waste (SW), buffer (B) and buffer waste (BW) wells are 100 x 60 μm^2 (WxH), with a 19 mm long injection channel (S to SW) and a 22 mm long separation channel (B to BW). The liquid-core waveguides are 70 x 60 μm^2 (WxH). Each of the waveguides were designed to interface to an optical fiber. The optical fibers have a 62.5 μm diameter core and have a total outer diameter of 125 μm when the fiber jackets are removed. Fiber-to-waveguide couplers are fabricated by flaring out the waveguide near the edges of the chip to facilitate fiber insertion (Fig. 2.1). The PDMS conforms to the inserted optical fiber and the fiber core lines up well with the waveguide core at the narrow end of the taper, as can be seen in Fig. 2.2. The fibers can be manually inserted into the coupler using a microscope with a 5x objective. Over a series of five fiber re-insertions, the average lateral misalignment was found to be less than 5μm. The misalignment was determined by inspecting an image of the coupler taken by a microscope that was calibrated to perform length measurements. The PDMS pre-polymer waveguide

core coats the inserted fiber thus increasing the coupling efficiency by removing the air gap between the fiber and waveguide (Fig. 2.2).

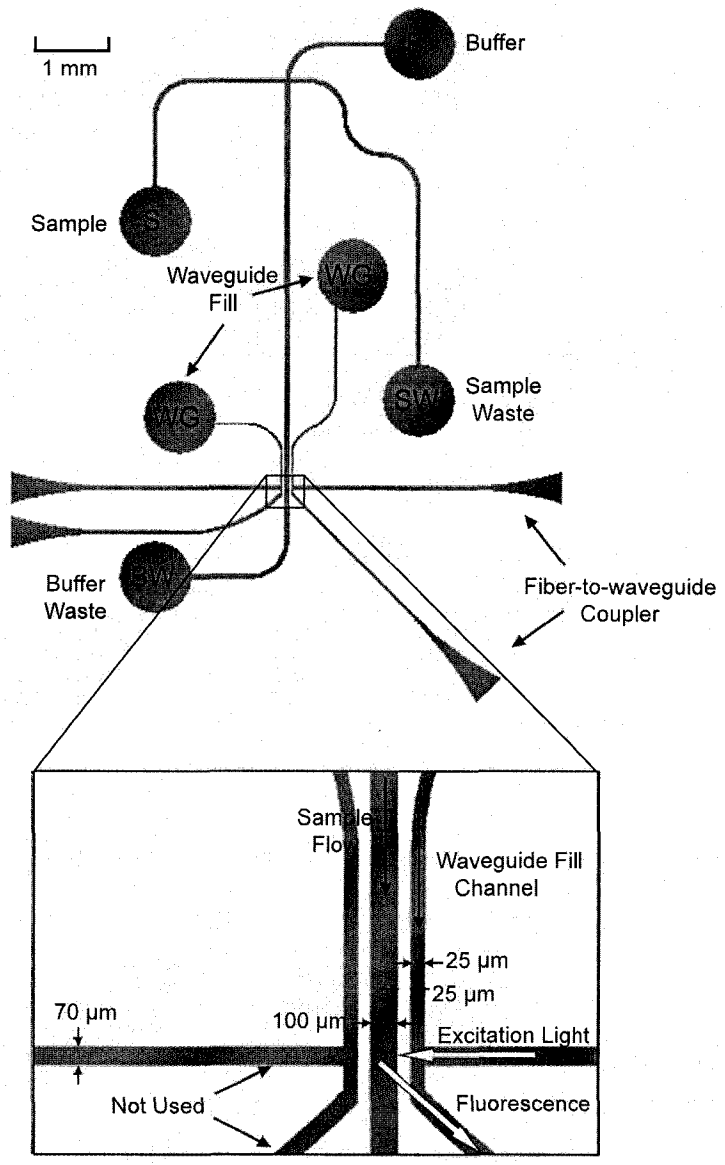

Figure 2.1: A schematic of the microfluidic device with an expanded view of the detection region. The waveguides to the right of the separation channel are used for LIF, while the waveguides to the left are not used in this work.

The design was produced in L-Edit v3.0 (MEMS Pro 8, MEMS CAP, CA, USA) and a chrome mask was created using a pattern generator (DWL 200, Heidelberg

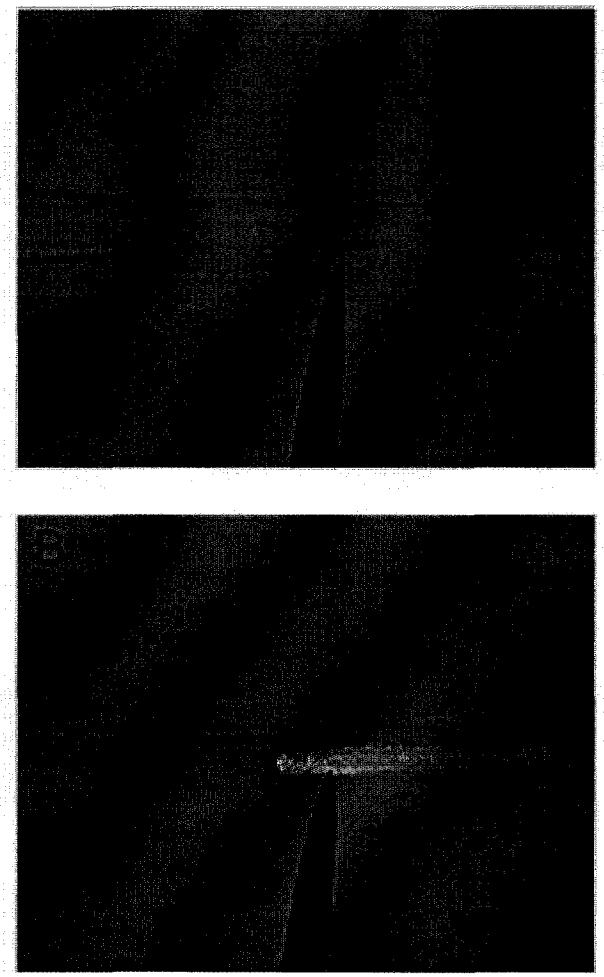

Figure 2.2: Photographs from an optical microscope showing (A) an empty fiber-to-waveguide coupler partially filled with liquid and (B) scattered light observed when a live fiber is inserted into the coupler.

Instruments, CA, USA). The mask was used to fabricate a master on a 10.16 x 10.16 x 0.11 cm^3 (LxWxH) borofloat substrate (Paragon Optical Company, PA, USA). A 60 μm layer of SU-8 2050 (MicroChem Corp., MA, USA) was patterned using the vendor specified protocol [35] to form the master. The master was hard baked on a contact hotplate for 1 hour at 150°C to anneal any residual cracks and to improve adhesion between the SU-8 and glass. The SU-8 master was silanized for 2 hours in a desiccator under vacuum using tridecafluoro-1,1,2,2-tetrahydrooctyl-1-trichlorosilane (United Chemical Technologies, PA, USA) to prevent adhesion between the master and the PDMS.

PDMS pre-polymer and curing agent (Sylgard 184, Dow Corning, NC, USA) were mixed at a 10:1 (w/w) ratio. The PDMS mixture was degassed for 30 minutes under vacuum prior to pouring onto the master and curing at 80°C for 2 hours. A similar, featureless PDMS slab was fabricated to facilitate sealing of the microfluidic channels. The 1-mm thick PDMS slabs were removed from the mould, exposed to an oxygen plasma at 100 W for 30 s and placed in contact with eachother to produce an irreversible bond. The refractive index of the cured Sylgard PDMS was verified to be 1.410 ± 0.005 at 633 nm using a Metricon Model 2010 Prism Coupler (Metricon Corp., NJ, USA). The waveguide cores were formed by adding a PDMS pre-polymer (OE-43-Part B, Gelest, PA, USA) to the waveguide channels fabricated within the bulk PDMS. The refractive index of the uncured pre-polymer was measured to be 1.429 ± 0.002 at 589 nm using a Bausch and Lomb 33-45-58 Abbe-type refractometer.

2.2.2 Waveguide Characterization

Two important characteristics of optical waveguides that affect the performance of the overall system are the propagation loss per unit length and the fiber-to-waveguide coupling coefficient. Using the setup displayed in Fig. 2.3A, loss measurements were performed at 532 nm and at 633 nm to represent excitation and fluorescence wavelengths, respectively. The light was launched into a 3-cm long straight waveguide containing PDMS pre-polymer through an optical fiber inserted into a fiber-to-waveguide coupler. Light scattered at 90° is collected by a 1-mm plastic optical fiber, which is positioned under the microfluidic chip, at several points along the waveguide and is measured using an optical power meter (1930-C, Newport, CA, USA). Sample plots of the normalized intensity (in dB) of the scattered light are shown in Fig. 2.3B along with least square linear curve fits. Assuming the power of light scattered from the waveguide is proportional to the power of the confined light at each point, the propagation loss, α_{WG}, of the waveguide in dB cm^{-1} is obtained from the average slope of the plot. The measured losses were 2.9 dB cm^{-1} and 2.2 dB cm^{-1} at 532 nm and 633 nm, respectively. However, the waveguides used in the DNA fragment experiment described below were fabricated

using a different SU-8 master and the propagation loss for this device was determined to be 1.8 dB cm^{-1} and 1.0 dB cm^{-1} at 532 nm and 633 nm, respectively. It is thought that the waveguide propagation loss is highly dependent on the quality of the SU-8 master and that the losses are primarily due to scattering by surface roughness on the waveguide walls. In future work, losses could likely be further reduced by optimizing the master fabrication process, possibly by using an edgebead removal compatible photoresist spinner or an I-line bandpass filter to improve the photolithography resolution.

The total fiber-to-waveguide coupling loss was determined by coupling a known amount of optical power from a fiber into a 1-cm long waveguide and measuring the output power from a similar fiber inserted into the taper at the opposite end. By subtracting the expected propagation loss of the 1-cm waveguide (1.0 dB at 633 nm), the total coupling loss was found. The total coupling loss includes both the fiber-to-waveguide and waveguide-to-fiber coupling losses. After a series of 8 measurements with 62.5 μm core excitation and detection fibers, where both fibers were removed, cleaned and reinserted after each measurement, the total coupling loss (L_{coup}) was found to increase from 7.3 dB to 8.4 dB with an average value of 7.6 dB. The increase in coupling loss is attributed to minor damage to the PDMS couplers due to multiple fiber re-insertions. A reduction in fiber-to-waveguide coupling loss was observed when the detection fiber was switched to a larger 100 μm core optical fiber (L_{coup} = 4.8±0.5 dB). However, the 100 μm core fiber was coated with a polyimide buffer, requiring removal with a flame prior to insertion into the microfluidic chip. For this reason, the 62.5 μm core fiber was found to be more convenient to use in our system and was used for the remainder of the experiments. By choosing to use the 62.5 μm core fiber, the coupling loss is increased by 7.6-4.8 = 2.8 dB. As described near the end of this section, we estimate that this would result in a decrease in the SNR by a factor of $10^{2.8/20}$ = 1.38. We felt this was a minimal change given the comparative ease of use of the polyimide-free fiber. The total optical loss through the system is given by $L_{total} = L_{coup} + \alpha_{WG}$ x (total waveguide length in cm). For the waveguides used in the DNA fragment experiment described below, the total optical loss is 8.6±0.5 dB at 633 nm.

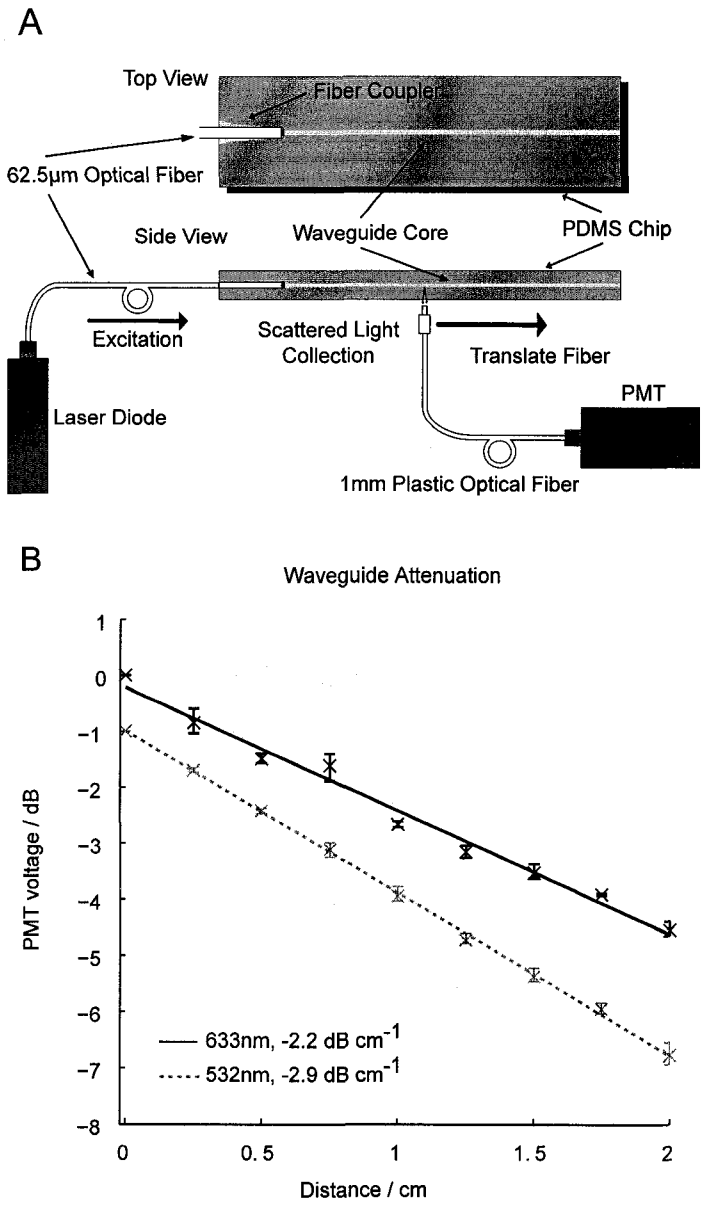

Figure 2.3: (A) Experimental setup for performing waveguide loss measurements. (B) Plots of the normalized intensity along the PDMS waveguide demonstrating the propagation loss at 532 nm and 633 nm. The average waveguide attenuation is determined from a linear fit to the raw data. For clarity, the data points at 532 nm are shifted down by -1.0 dB. The primary source of uncertainty in the propagation loss measurements is drift in the laser diode intensity.

The strength of the acquired fluorescence signal and noise due to collection of excitation light are both factors which determine the overall sensitivity of the system. The light collection efficiency (LCE) is defined as the fraction of the isotropic fluorescence emission collected and is given by $\Omega/4\pi$ where Ω is the solid angle subtended by the collection optics. An estimate of the LCE can be obtained by assuming the entire fluorescence emission originates from a point source in the center of the excitation region. For a microscope (Fig. 2.4A), the fraction of the isotropic emission collected by the objective lens, including all refractions at the interfaces between the sample medium and the lens, is given by [36]

$$LCE = \frac{\Omega}{4\pi} = \frac{1}{2}(1 - \cos\theta_{max}) \tag{2.1}$$

where θ_{max} is the half-angle of the maximum cone of light collected by the lens. When the microscope is collecting light from a sample medium of index n_s, θ_{max} is related to the numerical aperture of the lens by [37]

$$NA = n_s \sin\theta_{max} \tag{2.2}$$

In this work, the commercial confocal system used has a microscope objective with a NA of 0.55 and the sample medium has a refractive index n_s = 1.33, resulting in a collection efficiency of approximately 4.5%.

For a waveguide system (Fig. 2.4B) of width w and height h at a distance d from the point source, the approximate solid angle subtended by the end of the waveguide is Ω = wh/d^2 and therefore

$$LCE = \frac{wh}{4\pi d^2} \tag{2.3}$$

For our waveguide system, w x h = 70 x 60 μm^2, d = 160 μm and n_s = 1.33 implying a collection efficiency of approximately 1.3%. However, when d is small and Ω is large, the maximum angle of collected light is limited by the waveguide numerical aperture [37]

$$NA = \sqrt{n_{core}^2 - n_{clad}^2} \tag{2.4}$$

which in our system is NA = $\sqrt{1.43^2 - 1.41^2}$ = 0.24. As above, the numerical aperture and maximum angle of light collected from a medium of index n_s are

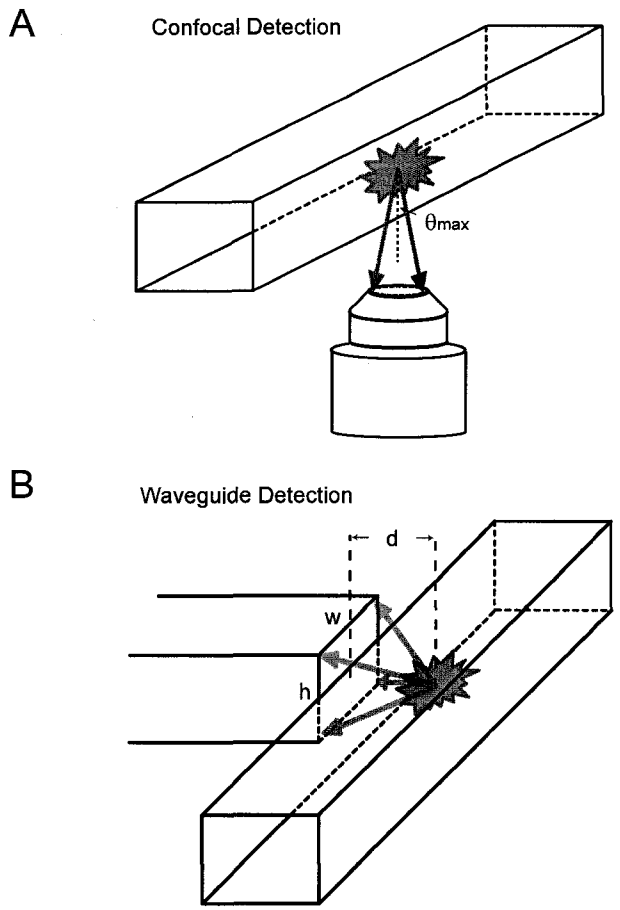

Figure 2.4: A comparison of (A) confocal and (B) waveguide fluorescence collection.

related by eqn. 2.2. For small cone angles (as is the case here), $\sin\theta_{max} \approx \theta_{max}$ and the approximate solid angle is $\Omega = \pi\theta_{max}^2$. The resulting NA-limited collection efficiency is found to be

$$LCE_{max} = \frac{NA^2}{4n_s^2} \tag{2.5}$$

or approximately 1% in our system and is similar to the simple geometrical estimate made above. These calculations show that a small aperture waveguide placed close to the sample volume can achieve a LCE of the same magnitude as that of a confocal microscope system.

A performance indicator for the device is the SNR, which can be optimized by maximizing the LCE while limiting sources of detector noise. The benefits of an

increased SNR include a lower limit of detection (LOD), typically defined as the smallest sample concentration detectable with a SNR equal to 3. The background noise in photomultiplier tube (PMT) based LIF systems is ideally shot-noise-limited and increases as the square root of the signal baseline. Careful design of the detection geometries and the use of optical filters assist in preventing scattered excitation light from reaching the detector, reducing both the signal baseline and detector shot-noise. Additionally, electrical and software low-pass filters can be used to remove high frequency shot or analog-to-digital converter (ADC) noise to increase the SNR. Additional losses in the detection optics such as vignetting and poor light collimation in confocal systems or waveguide propagation loss and fiber coupling losses in waveguide-based systems will reduce the amount of light reaching the sensor. These losses will have equal effects on the amount of fluorescence and excitation light which reach the detector and will result in a decrease in the SNR by a factor of $10^{\frac{L}{10}}/\sqrt{10^{\frac{L}{10}}} = 10^{\frac{L}{20}}$, where L is the optical loss in dB.

2.3 Application: DNA Fragment Analysis

The μTK is a commercially available microchip-based electrophoresis system and is used as a benchmark in comparison with our custom-built system. The μTK provides optical detection from the underside of the microfluidic chip as seen in Fig. 2.5A. The light emitted from the objective was measured to be approximately 1.70±0.03 mW by focusing the source onto a handheld laser power meter (T54-018, Edmund Optics, NJ, USA). As part of the μTK, the PMT data is sampled using a 16-bit ADC at 200 Hz. Further system details can be found in ref. [38]. In our system (Fig. 2.5B), an excitation waveguide delivers light to the separation channel and the fluorescence is collected by a waveguide at an angle of 45° to the excitation waveguide (Fig. 2.1). Light is coupled into the excitation fiber by focusing the output from a 5 mW, 532 nm green laser diode (Holograms & Lasers Int., TX, USA) into the fiber core using a 10x microscope objective. The light emitted from the free end of the optical fiber was measured to be 3.0±0.1 mW using an optical power meter (1930-C, Newport, CA, USA) prior to insertion into the

excitation waveguide. Fluorescence light is captured by the collection waveguide and is coupled into a second optical fiber, which delivers light to the in-line optical filter (OD_{532nm} ~6.7, T_{590nm} ~81%, D590/55m, Chroma, VT, USA) prior to detection at the PMT (H5784-20, Hamamatsu, Japan). Both the excitation and detection waveguides are 5 mm in length. The PMT is sampled at 48 kHz and averaged in real-time to give an equivalent sample rate of 50 Hz.

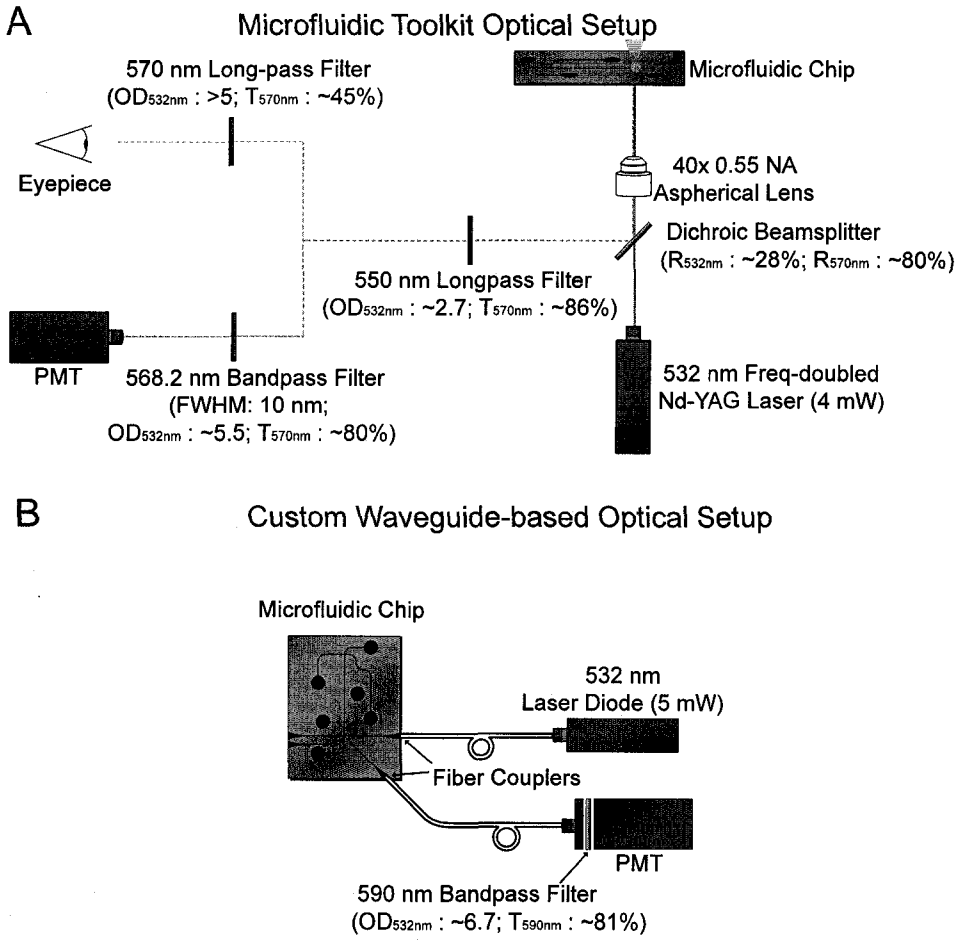

Figure 2.5: A comparison of the optical setups of (A) the μTK [38] and (B) our integrated system.

New PDMS chips were conditioned prior to use for the first time to minimize surface effects. The channels were filled with a solution of 5% linear polyacrylamide (LPA - MW 600k - 1,000k) (Polysciences Inc., PA, USA) and 17% Dynamic

	Control Voltage (V)	Cathode Radiant Sensitivity @ 550 nm (A W^{-1})	Gain	Effective Amplifier Feedback Resistance (Ω)	Sensitivity @ 550 nm (V nW^{-1})
μTK PMT[a]	0.5	3.5E-02	2.0E+04	5.2E+07	36
Waveguide PMT[b]	0.8	7.8E-02	5.0E+05	1.0E+06	39

Table 2.1: The sensitivities of the PMTs used in each system are compared at 550 nm, the emission peak for the VIC fluorescent dye. The PMT sensitivity is a product of the cathode radiant sensitivity, the gain and the effective amplifier feedback resistance. The PMT gain is tuned by setting the PMT control voltage. [a] H5773-01, Hamamatsu, Japan [b] H5784-20, Hamamatsu, Japan

Coating (The Gel Co., CA, USA), allowed to sit for 15 minutes and then were rinsed with de-ionized water. For each experiment, the PDMS chip was loaded with 6% LPA as a sieving matrix for the electrophoretic separations. The wells B, SW and BW were loaded with 3 μL of 1xTTE buffer (Tris-Taurine- Ethylenediaminetetraacetic acid) and the sample well (S) was loaded with 2.4 μL of autoclaved water, 0.3 μL 1xTTE and 0.3 μL BKV PCR product, which was synthesized as described elsewhere [27]. The BKV PCR product is end-labelled with VIC dye (Applied Biosystems, CA, USA) and has a fluorescence emission peak at approximately 550 nm with a tail that extends into the red. In each system, the DNA sample was injected at a field of 158 V cm^{-1} for 100 seconds and separated at 136 V cm^{-1} for 110 seconds. Subsequent injections in the same load were reduced to 10 seconds. Optical detection was performed at a distance of 11.5 mm from the intersection in both the μTK and the waveguide-based system.

The optical sensitivities of the waveguide system and μTK were set to 39 V nW^{-1} and 36 V nW^{-1}, respectively, by configuring the PMT gain as shown in Table 2.1. The gain of the PMT in each case is chosen to maximize the detected peak height without saturating the PMT or the ADC. The SNR of signals received from both PMTs vary little with gain for gains greater than 20,000, suggesting that the PMTs in both systems are shot-noise limited [39].

The results from 3 chip loads, averaged over 3 consecutive injection/separation

runs per load, are compiled in Table 2.2, where each new load required replacing the sieving matrix, buffer and sample in the microfluidic chip. The SNR is indicative of the overall sensitivity of the system and is determined by dividing the average peak height above the background by the standard deviation of the background signal immediately prior to the product peak. The average SNR of the waveguide and μTK systems was found to be 570±30 and 330±30, respectively, demonstrating that the waveguide system consistently outperformed the confocal system in terms of sensitivity. Run-to-run variations can be attributed to slight variations in the confocal focus within the channel, fiber-to-waveguide coupling and placement of the electrodes within the wells. The position of the electrode with respect to the channel entrance can impact electrophoresis reproducibility through a non-uniform space charge distribution of ions or a change in pH [40] near the channel entrance. Since these effects are more pronounced near the electrode, close positioning of the electrode to the channel entrance has been found to decrease repeatability and increase instability in the electrophoresis currents. As explained in the following paragraph, the higher performance of the waveguide system is due to its lower level of detected excitation light even though the optical filters in the μTK provide an additional factor of 30 in terms of excitation light suppression over the waveguide system.

Results comparing typical DNA fragment separations in freshly loaded chips in each system are shown in Fig. 2.6. The shift in peak position is due to the slightly larger (+6 V cm^{-1}) separation field strength that was used in the waveguide system. A calibration of the custom power supply used in the waveguide system should be performed to correct this problem in future work. In order to directly compare the two results, the signals have been normalized to the height of the primer peak. The SNR is calculated using the baseline noise just before the PCR product peaks that occur in the 70-80 s range. It can be seen that the μTK baseline is approximately twice that of the waveguide system and has a correspondingly higher noise assuming shot-noise-limited detection.

		Noise: $V_{noise,std\ dev}$ (V)	Baseline: $V_{baseline}$ (V)	Signal: $V_{peak,avg}$ (V)	SNR: Signal-to-noise ratio	SBR: Signal-to-baseline ratio	Theoretical Number of Plates
Confocal	Load 1[a]	3.9E-03	1.0E-01	1.2	310	12	3.2E+04
	Load 2[a]	3.6E-03	1.0E-01	1.1	320	11	2.0E+04
	Load 3[a]	4.0E-03	1.1E-01	1.4	360	13	2.6E+04
	Average	**3.9E-03**	**1.1E-01**	**1.3**	**330**	**12**	**2.6E+04**
	Std Dev (% of Avg)	**5.3%**	**5.6%**	**12.5%**	**8.6%**	**6.1%**	**22.5%**
Waveguide	Load 1[a]	1.1E-02	2.1E-01	5.7	550	26	2.0E+04
	Load 2[a]	1.3E-02	2.8E-01	7.3	610	26	2.5E+04
	Load 3[a]	6.5E-03	1.4E-01	3.5	560	25	1.9E+04
	Average	**1.0E-02**	**2.1E-01**	**5.5**	**570**	**26**	**2.1E+04**
	Std Dev (% of Avg)	**31.7%**	**33.4%**	**34.4%**	**5.6%**	**2.6%**	**15.1%**

Table 2.2: Comparison of the SNR, SBR and theoretical number of plates obtained from CE runs using confocal and waveguide LIF detection systems. The noise and the baseline are calculated in the region immediately prior to the arrival of the product peak. The signal is an average of the background-corrected primer and product peak heights, where background-correcting involves subtracting the baseline from the measured peak height. [a] the results for each chip load provided above are averaged over three consecutive runs

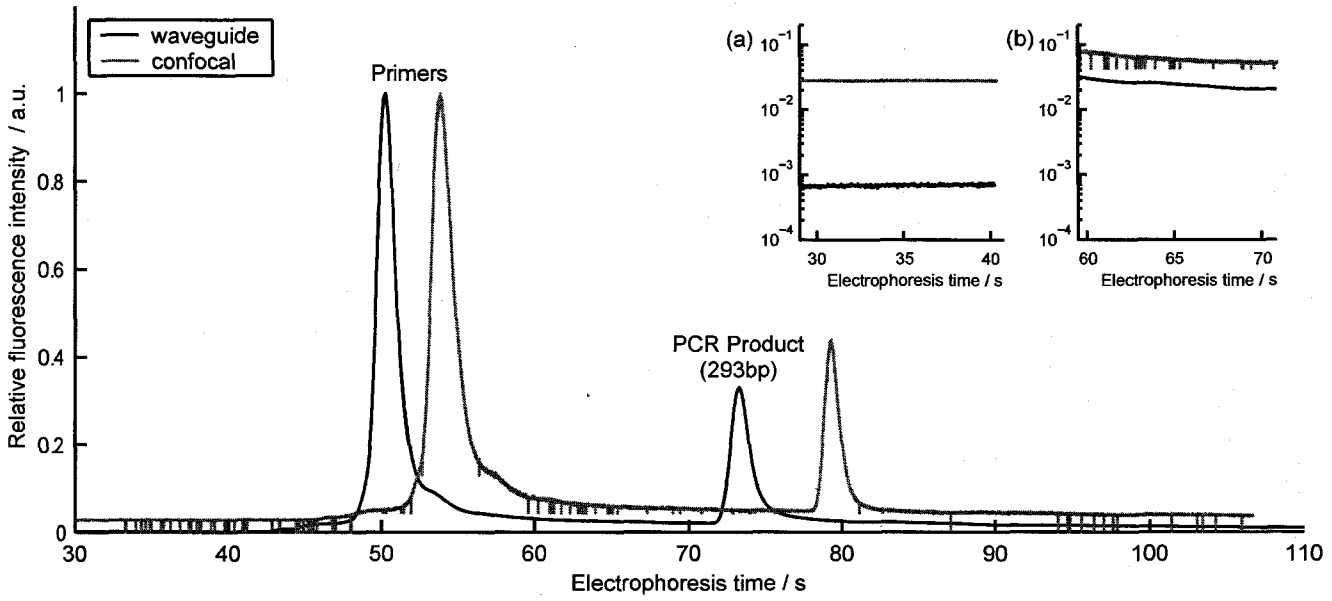

Figure 2.6: An electropherogram demonstrating the detection of the BKV PCR product using the μTK and our integrated system in a freshly loaded chip. In order to directly compare the two systems, the plots have been normalized to the height of the primer peak. The shift in peak position is attributed to a 6V cm^{-1} variation in the separation field strength between the two systems. Inset (a): An analysis of the baseline prior to the arrival of DNA highlights the contribution of excitation light to the baseline. The baseline is approximately 40 times lower for the waveguide-based system than for the μTK, suggesting improved excitation light suppression. Inset (b): An increase in the baseline on arrival of the primers is presumed to be due to DNA flow as a result of sample leakage at the injection channel. Occasional spikes in the confocal intensity data are thought to be a result of data lost due to ADC errors in the μTK system.

The baseline signal has two components - fluorescence from DNA that leaks into the separation channel and scattered excitation light. The contribution due to scattered excitation light in each system can be determined by considering the baseline during the time before any DNA reaches the detection region (prior to 40 s). The signals in this region for both systems are shown on a logarithmic scale in inset (a) of Fig. 2.6. Here, the waveguide system baseline is 32 dB lower than the primer peak, whereas the μTK baseline is only 16 dB lower than the primer peak indicating that the waveguide system receives approximately 40 times less excitation light at the detector, relative to the primer peak, than the confocal system. The waveguide system has no surfaces which directly reflect excitation light into the detection waveguide whereas an estimated 3% of the excitation light in the confocal system is reflected back into the objective from the underside of microfluidic chip, assuming near-normal incident angle Fresnel reflection coefficients. After the passage of the primers, there is an increase in the signal baseline (Fig. 2.6, inset b) that is attributed to fluorescence emitted by DNA which enters the separation channel as a result of sample leakage (from diffusion) at the intersection between the injection and separation channels [41]. This fluorescence approximately doubles the baseline in the μTK system while accounting for almost all (97%) of the baseline in the waveguide system. In future work, further improvement in the sensitivity of the waveguide system over the μTK could be achieved by applying pull-back voltages to the sample and sample waste wells during separation to reduce DNA leakage [41].

In addition, the low-pass filter effect of real-time data averaging during sample collection provides a factor of $M^{1/2}$ increase in the SNR, where M is the number of data points averaged [42]. In this work, we gain a factor of approximately 30 in SNR through data averaging. Since the SNR is inversely proportional to the square root of the measurement system bandwidth, similar performance gains could be expected by instead adding a bandwidth-limiting low-pass filter to the PMT output.

Due to the proprietary nature of the μTK hardware, we are unable to accurately determine the effective bandwidth of the detection electronics. While it is possible that the μTK performance could be improved through further bandwidth reduc-

tion, the fact remains that, as currently configured, the inexpensive microfabricated waveguide system outperforms the commercial confocal system.

The number of theoretical plates, N, of a separation column is a measure of the separation efficiency, and is given by [43]

$$N = 8 \ln 2 \left(\frac{t_m}{W_t} \right)^2 \tag{2.6}$$

where t_m is the retention time of the product and W_t is the full width at half max (FWHM) of the product peak. The average number of theoretical plates for the confocal and waveguide-based systems are $2.6 \pm 0.63 \text{x} 10^4$ and $2.1 \pm 0.3 \text{x} 10^4$, respectively. The slightly poorer resolution observed with the waveguide system can be attributed to the larger probe volume present within this system and the slight variation in migration time between the two systems. The tradeoff between probe volume size and resolution will be investigated in future designs.

2.4 Conclusion

The cost-effective integration of optical components onto microfluidic LOC devices is a precursor to the successful development of hand-held POC diagnostic systems. We have developed a miniaturized system capable of DNA fragment analysis through the use of integrated optical waveguides. We have demonstrated that waveguide detection of a viral PCR product can provide equal or greater sensitivity to that of a commercially available confocal system for LIF applications, while maintaining similar peak resolution. Though the confocal system is estimated to be able to collect a greater fraction of the fluorescence emission from the sample, the configuration of the waveguides in the miniaturized system helped to prevent excitation light from entering the collection waveguide, providing less noise at the detector. Our custom-built miniaturized system has the potential to be integrated into a handheld system. A complete miniaturized LOC system including a fiber-pigtailed excitation laser diode, PMT, high voltage power supply, microcontroller and LCD display, can be built for less than 5% of the cost of commercially available confocal bench-top systems with comparable performance. Cost-effective mass production of the microfluidic opto-biochips through injection moulding techniques is easily

envisioned. Though disposable, single microfluidic chips have been reused for more than 15 electrophoretic separations involving numerous optical fiber removals and reinsertions. Future work will involve the integration of additional assays onto the LOC device and improvement and optimization of the optical detection system.

Bibliography

[1] D. R. Reyes, D. Iossifidis, P. A. Auroux, and A. Manz, "Micro total analysis systems. 1. Introduction, theory, and technology," *Analytical Chemistry*, vol. 74, no. 12, pp. 2623–2636, 2002.

[2] P. A. Auroux, D. Iossifidis, D. R. Reyes, and A. Manz, "Micro total analysis systems. 2. Analytical standard operations and applications," *Analytical Chemistry*, vol. 74, no. 12, pp. 2637–2652, 2002.

[3] T. Vilkner, D. Janasek, and A. Manz, "Micro total analysis systems. Recent developments," *Analytical Chemistry*, vol. 76, no. 12, pp. 3373–3385, 2004.

[4] C. Haber, "Microfluidics in commercial applications; an industry perspective," *Lab on a Chip*, vol. 6, no. 9, pp. 1118–1121, 2006.

[5] C. D. Chin, V. Linder, and S. K. Sia, "Lab-on-a-chip devices for global health: Past studies and future opportunities." *Lab on a Chip*, vol. 7, no. 1, pp. 41–57, 2007.

[6] K. B. Mogensen, H. Klank, and J. P. Kutter, "Recent developments in detection for microfluidic systems," *Electrophoresis*, vol. 25, no. 21-22, pp. 3498–3512, 2004.

[7] H. Craighead, "Future lab-on-a-chip technologies for interrogating individual molecules," *Nature*, vol. 442, no. 7101, pp. 387–393, 2006.

[8] A. J. de Mello, "Seeing single molecules," *Lab on a Chip*, vol. 3, no. 2, pp. 29N–34N, 2003.

[9] E. Verpoorte, "Chip vision - optics for microchips," *Lab on a Chip*, vol. 3, no. 3, pp. 42N–52N, 2003.

[10] V. Lien, K. Zhao, Y. Berdichevsky, and Y. H. Lo, "High-sensitivity cytometric detection using fluidic-photonic integrated circuits with array waveguides," *IEEE Journal of Selected Topics in Quantum Electronics*, vol. 11, no. 4, pp. 827–834, 2005.

[11] K. B. Mogensen, N. J. Petersen, J. Hubner, and J. P. Kutter, "Monolithic integration of optical waveguides for absorbance detection in microfabricated electrophoresis devices," *Electrophoresis*, vol. 22, no. 18, pp. 3930–3938, 2001.

[12] O. Leistiko and P. F. Jensen, "Integrated bio/chemical microsystems employing optical detection: the clip-on," *Journal of Micromechanics and Microengineering*, vol. 8, no. 2, pp. 148–150, 1998.

[13] P. Friis, K. Hoppe, O. Leistiko, K. B. Mogensen, J. Hubner, and J. P. Kutter, "Monolithic integration of microfluidic channels and optical waveguides in silica on silicon," *Applied Optics*, vol. 40, no. 34, pp. 6246–6251, 2001.

[14] H. Qiao, S. Goel, A. Grundmann, and J. N. McMullin, "Fabrication of micro-optical/microfluidic biochips," *Proc. SPIE Int. Soc. Opt. Eng.*, vol. 4833, no. 1, pp. 54–59, 2003.

[15] R. Mazurczyk, J. Vieillard, A. Bouchard, B. Hannes, and S. Krawczyk, "A novel concept of the integrated fluorescence detection system and its application in a lab-on-a-chip microdevice," *Sensors and Actuators B - Chemical*, vol. 118, no. 1-2, pp. 11–19, 2006.

[16] D. Spicer, J. N. McMullin, and H. Rourke, "A multi-layer biochip with integrated hollow waveguides," *Journal of Micromechanics and Microengineering*, vol. 16, no. 8, pp. 1674–1680, 2006.

[17] K. B. Mogensen, J. El-Ali, A. Wolff, and J. P. Kutter, "Integration of polymer waveguides for optical detection in microfabricated chemical analysis systems," *Applied Optics*, vol. 42, no. 19, pp. 4072–4079, 2003.

[18] S. H. Huang and F. G. Tseng, "Development of a monolithic total internal reflection-based biochip utilizing a microprism array for fluorescence sensing," *Journal of Micromechanics and Microengineering*, vol. 15, no. 12, pp. 2235–2242, 2005.

[19] M. A. Powers, S. T. Koev, A. Schleunitz, H. M. Yi, V. Hodzic, W. E. Bentley, G. F. Payne, G. W. Rubloff, and R. Ghodssi, "A fabrication platform for electrically mediated optically active biofunctionalized sites in BioMEMS," *Lab on a Chip*, vol. 5, no. 6, pp. 583–586, 2005.

[20] S. Balslev, A. M. Jorgensen, B. Bilenberg, K. B. Mogensen, D. Snakenborg, O. Geschke, J. P. Kutter, and A. Kristensen, "Lab-on-a-chip with integrated optical transducers," *Lab on a Chip*, vol. 6, no. 2, pp. 213–217, 2006.

[21] J. N. McMullin, "Laser fabrication of integrated microfluidic/micro-optic systems," *Proc. SPIE Int. Soc. Opt. Eng.*, vol. 4087, no. 1, pp. 1050–1055, 2000.

[22] D. A. Chang-Yen, R. K. Eich, and B. K. Gale, "A monolithic PDMS waveguide system fabricated using soft-lithography techniques," *Journal of Lightwave Technology*, vol. 23, no. 6, pp. 2088–2093, 2005.

[23] V. Lien, Y. Berdichevsky, and Y. H. Lo, "A prealigned process of integrating optical waveguides with microfluidic devices," *IEEE Photonics Technology Letters*, vol. 16, no. 6, pp. 1525–1527, 2004.

[24] O. J. A. Schueller, X. M. Zhao, G. M. Whitesides, S. P. Smith, and M. Prentiss, "Fabrication of liquid-core waveguides by soft lithography," *Advanced Materials*, vol. 11, no. 1, pp. 37–41, 1999.

[25] D. C. Duffy, J. C. McDonald, O. J. A. Schueller, and G. M. Whitesides, "Rapid prototyping of microfluidic systems in poly(dimethylsiloxane)," *Analytical Chemistry*, vol. 70, no. 23, pp. 4974–4984, 1998.

[26] C. H. Mastrangelo, M. A. Burns, and D. T. Burke, "Microfabricated devices for genetic diagnostics," *Proceedings of the IEEE*, vol. 86, no. 8, pp. 1769–1787, 1998.

[27] G. V. Kaigala, R. J. Huskins, J. Preiksaitis, X. L. Pang, L. M. Pilarski, and C. J. Backhouse, "Automated screening using microfluidic chip-based PCR and product detection to assess risk of BK virus-associated nephropathy in renal transplant recipients," *Electrophoresis*, vol. 27, no. 19, pp. 3753–3763, 2006.

[28] Z. Wang, J. El-Ali, M. Engelund, T. Gotsaed, I. R. Perch-Nielsen, K. B. Mogensen, D. Snakenborg, J. P. Kutter, and A. Wolff, "Measurements of scattered light on a microchip flow cytometer with integrated polymer based optical elements," *Lab on a Chip*, vol. 4, no. 4, pp. 372–377, 2004.

[29] S. K. Hsiung, C. H. Lin, and G. B. Lee, "A microfabricated capillary electrophoresis chip with multiple buried optical fibers and microfocusing lens for multiwavelength detection," *Electrophoresis*, vol. 26, no. 6, pp. 1122–1129, 2005.

[30] J. Vieillard, R. Mazurczyk, C. Morin, B. Hannes, Y. Chevolot, P. L. Desbene, and S. Krawczyk, "Application of microfluidic chip with integrated optics for electrophoretic separations of proteins," *Journal of Chromatography B*, vol. 845, no. 2, pp. 218–225, 2007.

[31] S. L. Wang, X. F. Fan, Z. R. Xu, and Z. L. Fang, "A simple microfluidic system for efficient capillary electrophoretic separation and sensitive fluorimetric detection of DNA fragments using light-emitting diode and liquid-core waveguide techniques," *Electrophoresis*, vol. 26, no. 19, pp. 3602–3608, 2005.

[32] M. A. Burns, B. N. Johnson, S. N. Brahmasandra, K. Handique, J. R. Webster, M. Krishnan, T. S. Sammarco, P. M. Man, D. Jones, D. Heldsinger, C. H. Mastrangelo, and D. T. Burke, "An integrated nanoliter DNA analysis device," *Science*, vol. 282, no. 5388, pp. 484–487, 1998.

[33] V. J. Sieben and C. J. Backhouse, "Rapid on-chip postcolumn labeling and high-resolution separations of DNA," *Electrophoresis*, vol. 26, no. 24, pp. 4729–4742, 2005.

[34] C. Bliss, J. McMullin, and C. Backhouse, "Rapid fabrication of a microfluidic device with integrated optical waveguides for DNA fragment analysis," *Lab on a Chip*, 2007. DOI: 10.1039/b708485d.

[35] MicroChem, *SU-8 2000 Permanent Epoxy Negative Photoresist - Processing Guidelines For: SU-8 2025, SU-8 2035, SU-8 2050 and SU-8 2075* Newton, MA, USA: MicroChem, 2007.

[36] S. L. Wu and N. J. Dovichi, "High-sensitivity fluorescence detector for fluorescein isothiocyanate derivatives of amino-acids separated by capillary zone electrophoresis," *Journal of Chromatography*, vol. 480, pp. 141–155, 1989.

[37] E. Hecht, *Optics*, 4th ed. San Francisco, CA, USA: Addison Wesley, 2001.

[38] Micralyne, *Microfluidic Tool Kit Operating Manual*, v3.30.00 Edmonton, Alberta, Canada: Micralyne Inc., 2002.

[39] Hamamatsu, *Photomultiplier Tubes: Basics and Applications*, 3rd ed. Hamamatsu City, Japan: Hamamatsu Photonics K.K., 2006.

[40] M. Macka, P. Andersson, and P. R. Haddad, "Changes in electrolyte pH due to electrolysis during capillary zone electrophoresis," *Analytical Chemistry*, vol. 70, no. 4, pp. 743–749, 1998.

[41] C. S. Effenhauser, A. Paulus, A. Manz, and H. M. Widmer, "High-speed separation of antisense oligonucleotides on a micromachined capillary electrophoresis device," *Analytical Chemistry*, vol. 66, no. 18, pp. 2949–2953, 1994.

[42] R. Higgins, *Electronics with Digital and Analog Integrated Circuits*. Englewood Cliffs, N.J.: Prentice Hall, 1983, signal Averaging: pp 559-560.

[43] D. J. Harrison, A. Manz, Z. H. Fan, H. Ludi, and H. M. Widmer, "Capillary electrophoresis and sample injection systems integrated on a planar glass chip," *Analytical Chemistry*, vol. 64, no. 17, pp. 1926–1932, 1992.

Chapter 3

Integrated Wavelength-selective Optical Waveguides for Microfluidic-based Laser Induced Fluorescence Detection

3.1 Introduction

The integration of optical filters into fluorescence-based lab-on-a-chip (LOC) systems is key in reducing the size and cost of the detection optics. This enables the development of point-of-care diagnostic systems while retaining adequate sensitivity for a clear diagnosis. Dandin *et al.* recently provided a comprehensive review on optical filtering technologies for integrated fluorescence sensors [1]. Reflective interference filters are common in applications involving photodetector integration and materials such as SiO_2 and either TiO_2 [2–8] or Si_3N_4 [1] are deposited directly onto the photodetector surface. However, the fabrication of biochips with multilayer optical filters and photodiodes is time consuming and expensive with requirements for 40 or more alternating layers to achieve adequate attenuation [6]. Additionally, dielectric filters rely on optical interference where the filter strength varies with the angle of incidence. Therefore, additional light collimation optics are required for efficient light filtering.

Alternatively, absorptive (or colour) filters have been used by several groups [9–11]. Absorbance-based filters are inexpensive to fabricate and the strength of the filter is not sensitive to the incident angle since the material absorbs light rather

than reflecting it through interference effects. Hofmann *et al.* have recently demonstrated an interesting and cost-effective approach to integrate a long-pass absorptive filter on-chip by doping bulk PDMS with lysochrome dyes [9]. In that work, Hofmann *et al.* produce and characterize featureless sheets of dye-doped PDMS. They discuss the potential for this material to be used in a monolithic fluorescence detection scheme consisting of a microfluidic chip sandwiched between an LED and a photodetector. However, unless the optical attenuation provided by the dye-doped PDMS is very strong, this configuration will saturate the photodetector with excitation light. Unfortunately, the maximum optical density of the integrated filter is restricted since the quantity of dye that can be incorporated into the PDMS matrix is limited by both the solubility of the dye in toluene and the volume of toluene that can be added to the PDMS without inhibiting curing. This means that an increase in optical density requires an increase in filter thickness.

With this in mind, the monolithic detection scheme requires a compromise between excitation light suppression and fluorescence collection. An increase in optical density will require an increase in filter thickness, but an increased filter thickness implies a greater distance between the sample and photodetector resulting in a reduction in the light collection efficiency (LCE) of the detector (the fraction of sample fluorescence that reaches the detector). For example, Chabinyc *et al.* reported a light collection efficiency of only 0.2% by a 30 μm diameter avalanche photodiode at a distance of only 200 μm from the channel system [10]. If this distance were increased to 1 mm, the LCE would be further reduced to $\sim$0.005%. An increase in LCE could be achieved by increasing the detector size, but at the cost of separation efficiency due to the convolution effect (band broadening) as the sample passes over the detector.

We have recently demonstrated a waveguide-based excitation and detection scheme for laser induced fluorescence (LIF) with performance comparable to a commercial confocal system [12]. Our goal is to integrate the entire diagnostic system while minimizing the device cost and a significant challenge is to integrate the optical filter, a critical component in LIF systems. An interesting and elegant solution would be to integrate the optical filter directly into the fluorescence collection waveguide.

Unlike the system developed by Hofmann *et al.*, the optical density of the filter could be increased without reducing the LCE of the detection optics by increasing the length of the waveguide since the waveguide numerical aperture remains constant.

The Whitesides group has demonstrated the use of liquid-core waveguides using glycerol and other high refractive index liquids as core materials in PDMS microfluidic channels [13] and in liquid-liquid (L^2) waveguides [14]. In an extension to the L^2 work, liquid core materials containing dissolved dyes are used to isolate particular wavelength ranges from a single white light source using a diffusion-controlled waveguide splitter [15]. However, this integrated filter technology has not yet been applied to fluorescence detection.

Yin *et al.* demonstrate integrated filter functionality using liquid-core ARROW waveguides, which selectively confine particular wavelengths within a low index core by tailoring the design of the Fabry-Perot cladding [16]. However, ARROW waveguides are inherently "leaky" and require additional reflecting layers to decrease the propagation loss. While this technique provides a high degree of flexibility in terms of tuning the optical passband and stopband, deposition of the alternating dielectric layers that form the cladding is time consuming and expensive and therefore the ARROW waveguide is not a likely candidate for integration onto a disposable lab-on-a-chip (LOC) device.

We demonstrate for the first time the use of waveguides containing dissolved dyes as a detection filter for fluorescence sensing applications. In an extension to our previous work and the work of Hofmann *et al.*, we report the integration of dye-doped PDMS into our waveguide-based microfluidic DNA analysis device to create novel wavelength-selective waveguides which rely on diffusion to "pull" dye out of the bulk material into the waveguide core. The dye is chosen such that the detection waveguide selectively attenuates stray excitation light, while efficiently transmitting the fluorescence signal. Since the bulk chip material consists of dye-doped PDMS, it rapidly absorbs any reflected or scattered excitation light preventing this light from reaching the detector. This provides an advantage over simply creating a waveguide core containing a dissolved dye within an undoped PDMS chip.

As well, a reduction in the signal baseline is achieved by positioning the detection waveguide at an angle of 45° to the excitation waveguide. This reduces the amount of unabsorbed stray excitation light that reaches the detector. The use of dye-doped PDMS as an absorbing waveguide effectively eliminates the requirement for an interference filter at the detector since signal collection and noise suppression are both performed using the same element.

Scattered excitation light is present in all LIF systems resulting in an increased signal baseline and shot noise at the detector. The system reported in this work dramatically reduces the effects of stray excitation light through three effects: (i) the dye-doped bulk material in the chip is strongly absorbing at the excitation wavelength and scattered excitation light is quickly absorbed before it can be collected by the detection waveguide; (ii) the detection waveguide is placed at an angle of 45° to the excitation waveguide acting as a spatial filter to prevent direct coupling of excitation light into the detection waveguide; (iii) excitation light collected by the detection waveguide is absorbed by dye molecules which have diffused from the bulk PDMS into the liquid core of the waveguide, while the fluorescence from the sample is delivered to the detector with much less attenuation.

The microfluidic devices are fabricated though PDMS soft lithography. However, a toluene-dye solution is mixed with the uncured PDMS prior to casting to create dye-doped PDMS. Following chip fabrication (after curing and bonding), two types of waveguides are formed by adding high refractive index liquids into dedicated channels within the chip. High performance, wavelength-selective, attenuating waveguides are formed by using a liquid PDMS pre-polymer as the core material. In this case, the liquid core is miscible with other apolar liquids so residual toluene from the bulk chip, including the dissolved dye, is free to diffuse from the bulk PDMS into the core. The high performance attenuating waveguides are used for detection since a high dye concentration in the waveguide core will result in high attenuation of the unwanted excitation light. The use of a more polar liquid will limit the diffusion of dye into the core and will thus reduce the waveguide attenuation strength. Excitation waveguides are filled with a polar liquid (glycerol) to reduce dye diffusion into the core, allowing excitation light to reach the sample with

minimal attenuation. The excitation and detection waveguides are fabricated in the same plane, but a 45^o angular offset provides spatial filtering by minimising direct coupling of excitation light into the detection waveguide. The proposed system eliminates the requirement for nearly all external passive optics, while maintaining an excellent SNR.

In the next section, we describe the microfluidic chip design, fabrication procedure and waveguide propagation properties. In Section 3.2.3, we demonstrate the effectiveness of the wavelength-selective waveguide as an integrated optical filter. We achieve this through the analysis of BK virus (BKV) DNA fragments, obtained through polymerase chain reaction (PCR) with end-labelled primers, using our custom microchip electrophoresis system. We compare the sensitivity, in terms of SNR, to similar experiments performed using an undoped PDMS microchip with traditional, non-attenuating waveguides and a commercial external interference filter placed in-line with the photodetector. We show that an external interference filter is required to allow reliable detection of BKV when using an undoped, colourless PDMS microchip. However, when the external interference filter is removed, we show that dye-doped microchips containing attenuating waveguides can provide clear detection of the PCR product and compare well in terms of sensitivity to results obtained using an undoped chip with the external filter. Thus, the wavelength-selective waveguides are an effective replacement of the external optical filter and represent a significant step toward miniaturizing the entire optical system.

This chapter is based on a recently submitted journal paper by Bliss *et al.* [17]

3.2 Results and Discussion

3.2.1 Device Fabrication

The microfluidic devices (Fig 3.1A) were fabricated through PDMS soft lithography, as described elsewhere [12], modified to allow the incorporation of lysochrome dye into the bulk material. The uniform dispersal of lysochrome dye molecules into PDMS and subsequent optical transmission properties has been reported previously by Hofmann *et al.* [9]. Briefly, the PDMS pre-polymer and curing agent (Syl-

gard 184, Dow Corning, NC, USA) were mixed at a 10:1 (w/w) ratio. Sudan II dye (Sigma-Aldrich, MO, USA) was then dissolved in toluene and the solution was added to the PDMS mixture followed by thorough mixing. In order to ensure complete curing of the PDMS, the toluene content was restricted to below 10% (v/v) [9]. Concentrations of 1200 μg/mL, the optimum dye loading as determined by Hofmann *et al.*, were formed by adding 19.8 mg of Sudan II dye to 1 mL of toluene and 16.5 g of the PDMS. The PDMS mixture was degassed for 30 minutes under vacuum prior to pouring onto the master and curing at 80°C for 4 hours. To form microfluidic devices, featureless PDMS slabs fabricated in a similar fashion were bonded to the PDMS replica mould after treatment with an oxygen plasma. Colourless PDMS microchips, containing no toluene or Sudan II dye, were fabricated as well for comparison purposes.

Refractive index measurements were performed to ensure that the addition of toluene (n=1.50) or Sudan II dye did not modify the refractive index of the bulk PDMS. This could possibly prohibit light confinement in the waveguides if the refractive index was increased beyond that of the core material. Samples of unmodified PDMS, PDMS containing toluene and PDMS containing both toluene and Sudan II were spun onto a silicon substrate at 6100 rpm for 30 seconds. The PDMS films were approximately 6 μm thick. The PDMS was prepared and cured as previously described. The refractive index of each sample was measured to be 1.410±0.005 at 633 nm using the prism coupling method (Model 2010 Prism Coupler, Metricon Corp., NJ, USA), thus the PDMS dye-doping protocol has a negligible impact on the refractive index. The waveguide cores were formed by adding either PDMS pre-polymer (OE-43-Part B, Gelest, PA, USA) or glycerol to microfluidic channels fabricated within the bulk PDMS. The refractive index of glycerol is 1.47 and the refractive index of uncured pre-polymer was measured to be 1.429±0.002 at 589 nm using a Bausch and Lomb 33-45-58 Abbe-type refractometer.

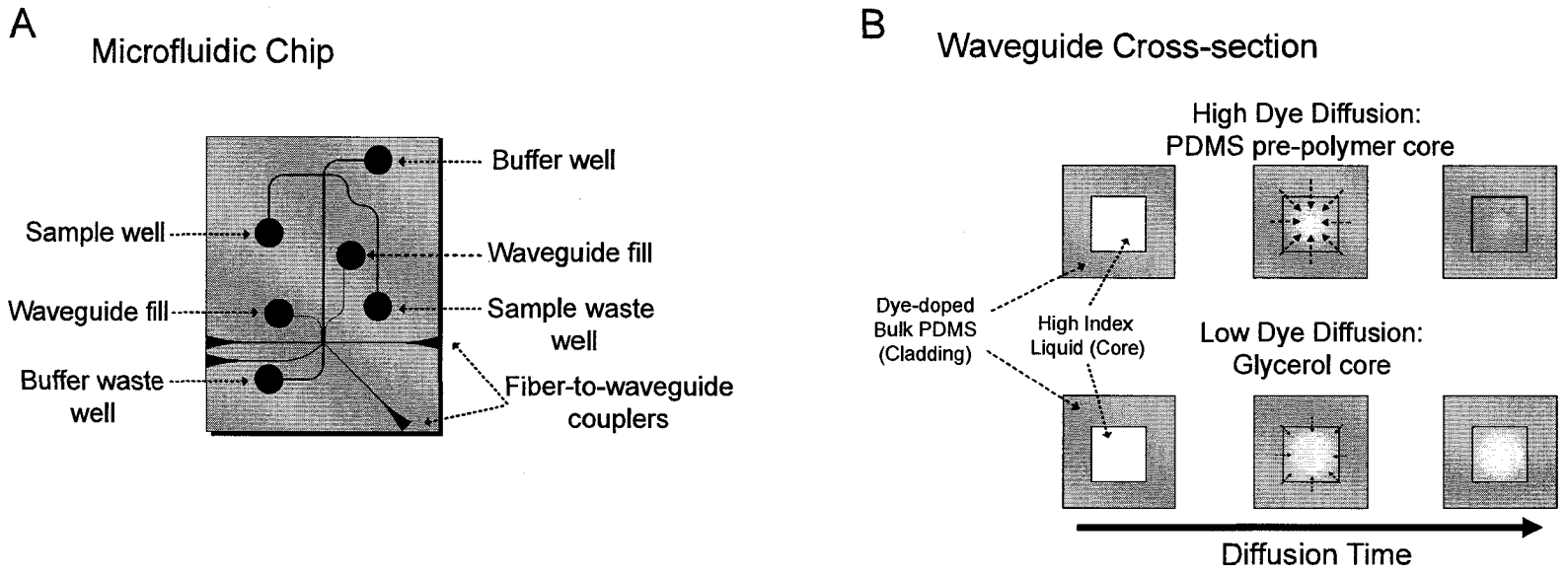

Figure 3.1: (A) A schematic of the dye-doped PDMS microfluidic device. (B) A cross-sectional view of the two types of dye-doped waveguides. Waveguides filled with PDMS pre-polymer experience higher dye diffusion into the core since toluene and the dye are soluble in the pre-polymer, resulting in a stronger optical filter effect. Since toluene and the dye are relatively insoluble in glycerol, glycerol filled waveguides experience less dye diffusion and weaker optical filter effects.

We predicted that we would observe light attenuation through one of three mechanisms: (i) dye would diffuse from the bulk PDMS into the core material resulting in increased attenuation as a function of increased concentration or diffusion time; (ii) the high refractive index liquid core material would diffuse into the bulk PDMS creating a graded-index effect. Light would begin to travel in regions of the bulk material that had absorbed the high index liquid and the dye in the bulk material would absorb light, increasing the waveguide attenuation; (iii) evanescent interaction between the guided light and the dye-doped cladding would result in light attenuation. While we expected (iii) to dominate, we noticed an increase in attenuation with time suggesting that diffusion effects were dominating. This time dependence is described in detail in the next section. We discounted (ii) since an image of the waveguide cross section (not shown) indicated very little light propagation in regions beyond the fabricated waveguide boundaries. We concluded that a significant portion of the waveguide attenuation is a result of light absorption by dye which has diffused from the bulk dye-doped PDMS into the liquid waveguide core. This conclusion was supported by the observation of an orange hue in the pre-polymer core material upon removal from the waveguide. As shown in Fig 3.1B, the strength of the filter can be adjusted by controlling the rate of dye diffusion into the core. Since the Sudan II dye is more soluble in non-polar liquids, the strength of the filter is enhanced by using a non-polar liquid (PDMS pre-polymer) or minimized by using a polar liquid (glycerol) as a core material. It is also possible that the dye-doping of the core is dominated by the diffusion of residual toluene (and dissolved dyes) from the bulk PDMS into the liquid core rather than by the diffusion of the dye itself.

3.2.2 Wavelength-selective Waveguide Characterization

The transmission spectrum of the dye-doped PDMS was determined using a PerkinElmer Lambda 900 UV/VIS/NIR spectrophotometer (PerkinElmer, MA, USA). Data was collected at 1 nm resolution over a range of 350 - 850 nm with a slit width of 1 nm. The PMT integration time was set to 2 seconds to obtain a large enough SNR such that the minimum measurable transmittance was 0.001%. Transmission measure-

ments were performed on featureless dye-doped PDMS samples with thicknesses of approximately 1 mm at dye loadings of 720 μg/mL and 1200 μg/mL in reference to air (Fig. 3.2). The filter quality is assessed using the figure of merit Q = $T(\lambda_{transmit})/T(\lambda_{block})$, as defined by Hofmann *et al.* [9], where $T(\lambda_{transmit})$ and $T(\lambda_{block})$ represent the % transmission through the filter at a wavelength above and below the filter cut-off, respectively. In this work, the figure of merit Q is determined at $\lambda_{transmit}$ = 633 nm and λ_{block} = 532 nm. We achieve a Q of 6 and 66 for samples with dye loadings of 720 μg/mL and 1200 μg/mL, respectively. A more thorough approximation to the filter quality would consider the wavelength dependence of the filter spectrum along with the excitation and fluorescence spectra as described in ref. [9], but the simplified model provides a reasonable estimate of the filter quality.

As previously mentioned, guided-mode waveguides are formed through the addition of high index liquids into microfluidic channels. In the case of the high performance attenuating waveguides, the PDMS pre-polymer core is initially colourless with low absorption at visible wavelengths. However, dye molecules quickly diffuse into the pre-polymer core from the dye-doped bulk PDMS creating an attenuating waveguide with transmission properties similar to those described above. Dye diffusion cannot be completely avoided by using glycerol and thus the low-loss waveguides still absorb light according to the above spectral curve, but to a lesser extent due to the lower uptake by the polar glycerol.

The optical filter strength is determined by measuring the waveguide propagation loss at 532 nm and 633 nm to represent wavelengths in the stopband and the passband of the optical filter, respectively. Approximately 2 mW of light from either a red or green laser diode is coupled into the waveguide and scattered light is collected at 90° using a 1-mm plastic optical fiber at several positions along the waveguide [12]. If we assume that the density of light scattering centers, due to fabrication defects or waveguide core impurities, is roughly constant throughout the length of the waveguide, light scattered from the waveguide is proportional to the power of the confined light. In order to monitor the effects of diffusion on the waveguide attenuation, we also studied the waveguide loss as a function of time. A

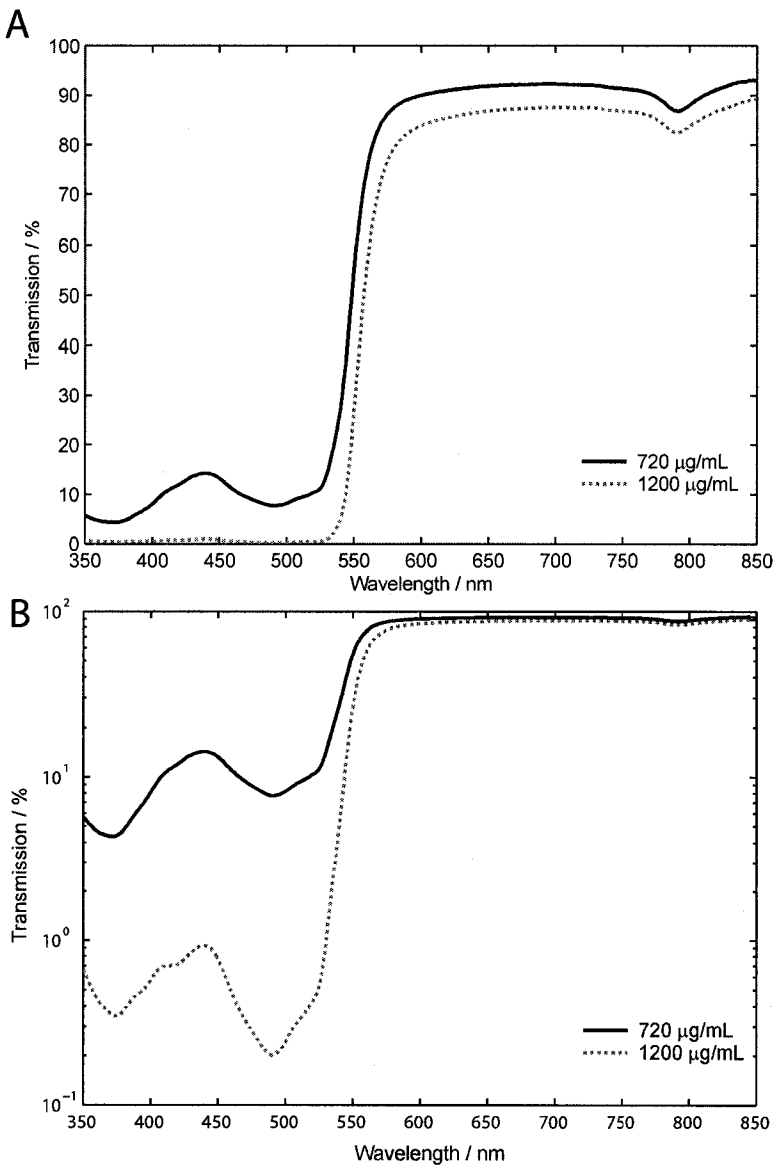

Figure 3.2: The transmission spectrum of 1-mm dye-doped PDMS on a (A) linear and (B) logarithmic plot. The quality factor of the optical filter increases by an order of magnitude (Q = 6 to 66) when the dye concentration in the PDMS is increased from 720 μg/mL to 1200 μg/mL.

summary of the per unit length waveguide attenuation results are tabulated in Table 3.1.

As expected, we observe similar waveguide propagation losses at both 532 nm and 633 nm when using the colourless, undoped PDMS waveguides with OE-43-B PDMS pre-polymer cores. This was consistent with the idea that losses were primarily a result of scattering by surface roughness on the waveguide walls. However, very little scattered light was observed when using glycerol and we could not observe any measurable loss using our current measurement technique. The decreased performance of the PDMS pre-polymer in comparison to glycerol is thought to be due to additional light scattering from the PDMS pre-polymer, possibly due to scattering from the PDMS monomers. This may also explain why, when using the PDMS pre-polymer core, we typically observe a slightly higher propagation loss ($\sim$1 dB cm^{-1}) at 532 nm since the degree of scattering for a particular wavelength is known to be dependent on the physical size of the scatterer [18].

The waveguides formed in microfluidic chips fabricated using dye-doped PDMS exhibit significant attenuation due to Sudan II dye diffusion into the waveguide core. However, in contrast to the observations of Hofmann *et al.*, we noticed considerable autofluorescence from the Sudan-doped PDMS. This is particularly apparent when we compare the spectrum of the emission from a green laser diode (Fig. 3.3A) to the output of a 3-mm long dye-doped waveguide (Fig. 3.3B) excited using the same laser. After passing the excitation light through the short waveguide, we see spectral content in the region between 550-750 nm due to autofluorescence of the Sudan II dye.

The waveguide propagation loss is determined from the slope of the decay in intensity along the dye-doped waveguides, as shown in Fig. 3.4. When 532 nm light is coupled into a dye-doped waveguide, virtually no scattered light is observed. This is because any scattered light is absorbed by the dye in the bulk material prior to passing through the chip. However, we found that we could relate the intensity of the 532 nm light in the waveguide to the amount of autofluorescence generated by the dye. The waveguide attenuation can thus be determined by monitoring the decay in autofluorescence along the waveguide.

Bulk Material (Cladding)	Core Material	Diffusion Time	Waveguide Attenuation (dB cm^{-1}) 532 nm	633 nm
Undoped PDMS	OE-43-B	-	2.9	2.2
	Glycerol	-	*	*
Sudan-doped PDMS ($1200\mu g/mL$)	OE-43-B	1 hour	118	3.3
		3 hours	120	3.5
		24 hours	120	4.4
		48 hours	120	4.9
	Glycerol	1 hour	7.6	*
		3 hours	6.5	0.2
		24 hours	8.2	1.1
		48 hours	9.8	1.0

Table 3.1: Measured waveguide attenuation. * loss too small to measure using our current setup.

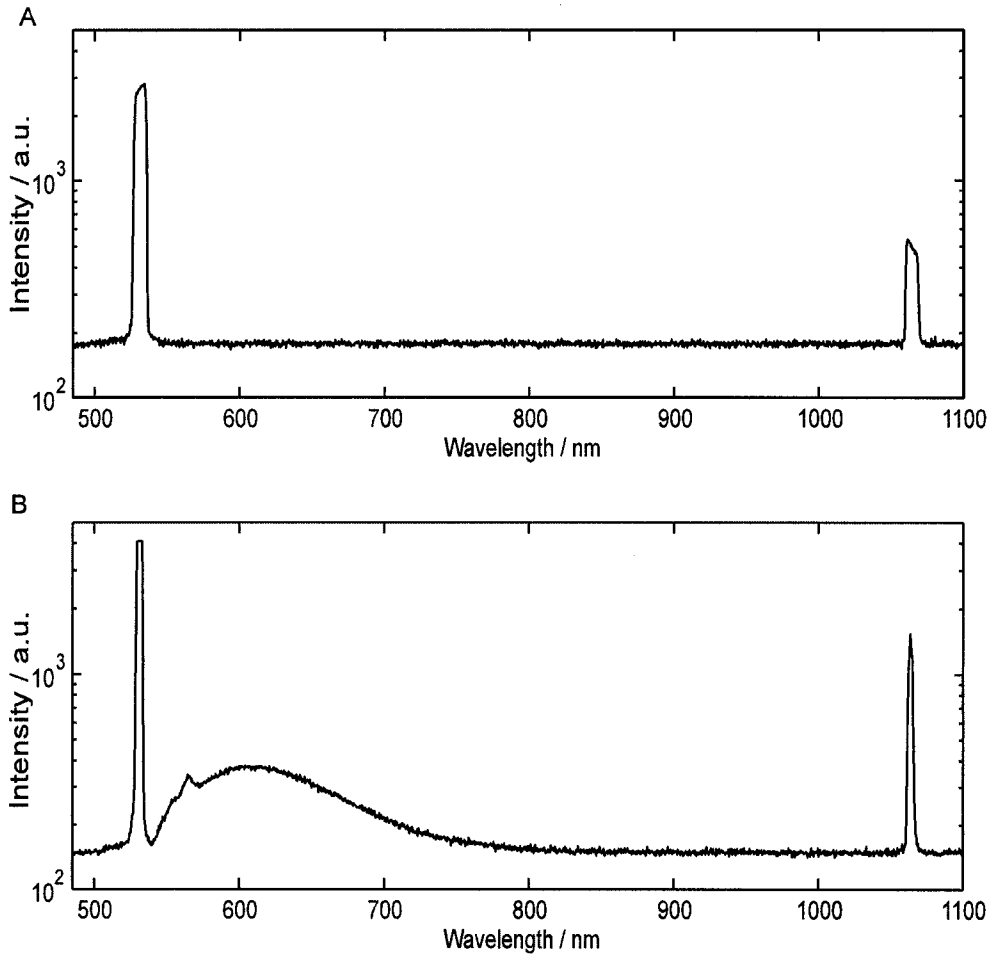

Figure 3.3: A comparison between the spectrum of (A) a green diode laser and (B) the output of a 3-mm dye-doped waveguide excited using the same laser on a logarithmic scale as measured by a fiber-coupled spectrometer (USB2000, Ocean Optics, FL, USA). The primary laser diode emission at 532 nm is frequency doubled from a 1064 nm Nd:YAG laser and a significant component at 1064 nm is still present after passing through an IR filter. Significant autofluorescence generated from the Sudan II dye is observed between 550-750nm.

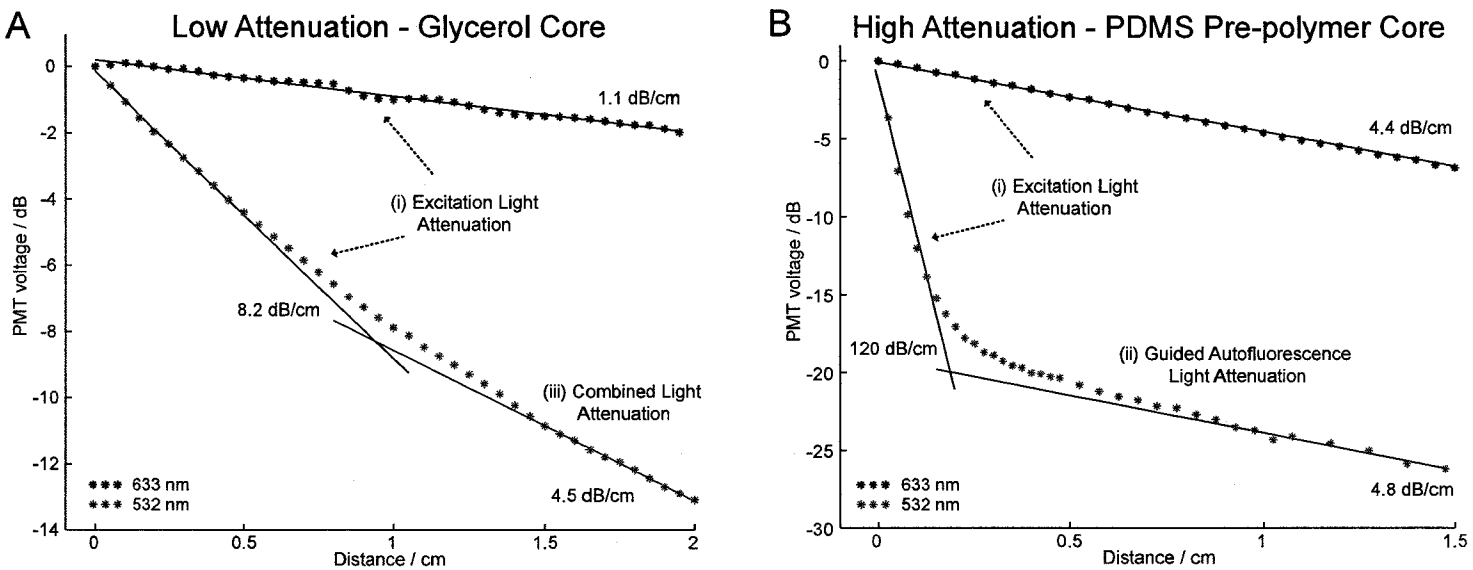

Figure 3.4: Plot of the normalized intensity of light collected along the length of the waveguide. The propagation loss for dye-doped PDMS (1200 μg/mL) waveguides with (A) glycerol and (B) PDMS pre-polymer core materials are given after a diffusion time of 24 hours. The losses at 633 nm remain low as compared to the attenuation at 532 nm and are constant over the test length. At 532 nm, the waveguide losses are significantly higher when the PDMS pre-polymer rather than glycerol is used as the core material. Three regions become apparent depending on the dominant source of light exiting the waveguide and this provides information on the spectral content of the waveguide (see text).

At 633 nm, we observe the expected linear relation between the optical power in the waveguide and distance, with the slope representing the propagation loss. However, at 532 nm we observe two attenuation regions. In Fig. 3.4B at 532 nm, we observe a period of high attenuation followed by a region of low attenuation. The first region represents the rate at which excitation light is absorbed by the waveguide and as expected, the attenuation is high. However, the dye emits some of the absorbed energy as autofluorescence and a fraction of this light remains confined to the waveguide. Eventually the spectral content of the waveguide shifts from 532 nm to ~600 nm, the peak autofluorescence wavelength of the dye. This occurs at ~0.5 cm in Fig. 3.4B. At this point, the waveguide propagation loss closely matches the losses measured at 633 nm. We name these regions (i) Excitation Light Attenuation and (ii) Guided Autofluorescence Light Attenuation, respectively.

The propagation loss measurement of the lower attenuation waveguide (glycerol core) is provided in Fig. 3.4A. At 532 nm, the waveguide propagation loss does not level out to match the loss at 633 nm as it did in Fig. 3.4B. However, we believe that second linear fit is somewhere in the "knee" of the curve and that if our test waveguide was longer, we would eventually observe the losses to decrease to approximately 1.1 dB cm^{-1}. We term the region in the knee (iii) Combined Light Attenuation since the spectral content in the waveguide is a combination of light at 532 nm and ~600 nm.

From Fig. 3.4B, we observe that a ~5 mm dye-doped waveguide filled with PDMS pre-polymer will provide similar performance to a commercial interference filter. A D590/55m Chroma filter provides an attenuation of ~67 dB at 532 nm and ~80% light transmission at 590 nm whereas a ~5 mm dye-doped waveguide filled with pre-polymer (1200 μg/mL) provides an attenuation of 60 dB at 532 nm and ~60% light transmission at 633 nm. This is equivalent to Q-values of $4x10^6$ and $6x10^5$ for the dielectric filter and the waveguide filter, respectively. However, during operation, the small portion of the autofluorescence generated from the Sudan II dye that is confined within the detection waveguide is not efficiently removed by the integrated filter and becomes a source of background light at the photodetector. From Fig. 3.4B, we see that Sudan II autofluorescence limits the maximum perfor-

mance of the waveguide filter to a Q-value of $1x10^2$ or a difference in attenuation of 20 dB between the two curves.

3.2.3 Application: DNA Fragment Analysis

In order to demonstrate the effectiveness of the wavelength-selective waveguide, we compare the separation and detection of BKV PCR product using 4 different detection configurations (Fig. 3.5). The first two configurations use PDMS chips that have not been doped with the Sudan II dye to set a benchmark for comparison to the dye-doped chips. Configuration A (Fig. 3.5A) includes a clear, undoped PDMS chip with a commercial optical interference filter positioned in-line with the PMT. This configuration is identical to the waveguide system described in our previous work [12]. Configuration B (Fig. 3.5B) is identical to the benchmark except that the optical filter is removed from the system in order to quantify the noise-reduction provided by the commercial filter.

In configurations C and D, Sudan II dye-doped PDMS (1200 μg/mL) is used to replace the requirement for an external optical filter. In configuration C (Fig. 3.5C), the excitation fiber is inserted perpendicularly to the separation channel in a "buried optical fiber" configuration to prevent absorption of the excitation light before it can reach the sample . In this configuration, light leaves the excitation fiber and directly excites the sample without first passing through a waveguide. Sample fluorescence is then captured by the detection waveguide and any collected excitation light is attenuated by the dye in the waveguide core. The buried optical fiber approach is not convenient since a fragile optical fiber must be fed into or encapsulated in the microfluidic chip. In configuration D (Fig. 3.5D), the excitation waveguide is filled with glycerol to reduce the diffusion of dye into the waveguide core (Fig. 3.1B). Since the waveguides used in the first three configurations are loaded using the same fluidic network, it is difficult to fill each waveguide with a separate material. In this configuration, the waveguides on the left side of the separation channel are loaded with glycerol and the waveguides on the right side with PDMS pre-polymer. Excitation light is delivered to the sample with a relatively small amount of attenuation since the glycerol reduces dye diffusion into the waveguide core and scatters less

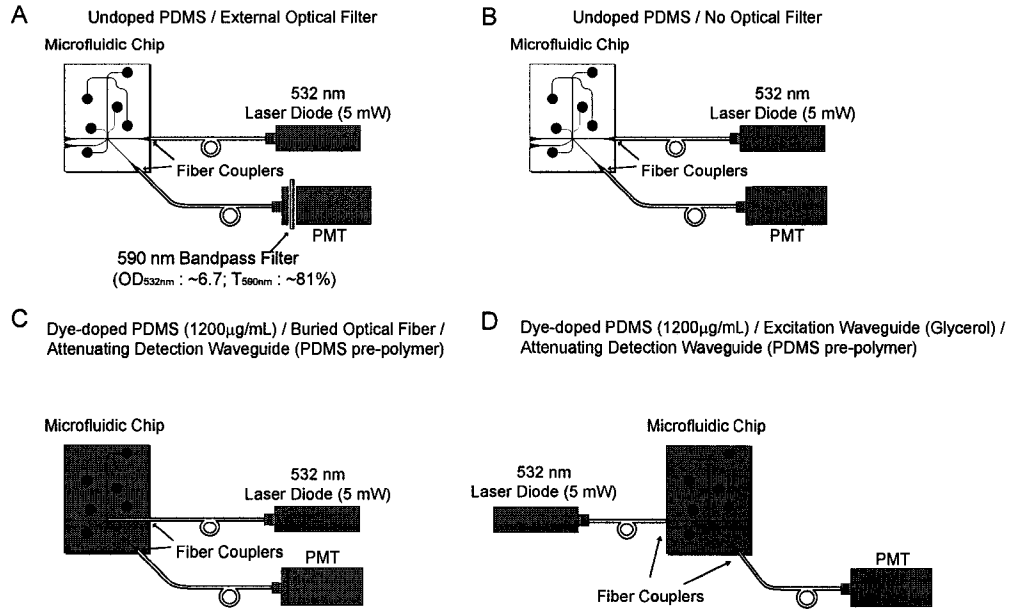

Figure 3.5: Four optical detection scenarios are explored. (A) A colourless, undoped PDMS chip with a commercial external interference filter is used as a benchmark in this study. (B) The noise-reduction ability of the external filter is quantified by performing the same test as (A), but without the external filter. (C) By using a buried optical fiber for excitation, the optical filter properties of the attenuating waveguides are investigated without the influence of light absorption during the delivery of excitation light. (D) An all-waveguide solution. Low attenuation glycerol filled waveguides are used to deliver excitation light to the sample and detection is achieved using high attenuation PDMS pre-polymer attenuating waveguides.

light than the PDMS pre-polymer. The sample fluorescence is collected by the opposing waveguide at an angle of 45° and any collected excitation light is absorbed by the attenuating waveguide.

The details on the microchip electrophoresis protocol can be found in our previous work [12]. In brief, new PDMS chips were conditioned with a solution of linear polyacrylamide (LPA - MW 600k - 1,000k) (Polysciences Inc., PA, USA) and Dynamic Coating (The Gel Co., CA, USA) prior to use for the first time to minimize surface effects. The PDMS chips were loaded with a sieving matrix (6% LPA), the sample well was loaded with 0.3 μL BKV PCR product and 2.7 μL 0.1xTTE buffer (tris- taurine- ethylenediaminetetraacetic acid), while the remaining wells were loaded with 3 μL 1xTTE buffer. The BKV PCR product is end-labelled with VIC dye (Applied Biosystems, CA, USA) and has a fluorescence emission peak at approximately 550 nm with a tail that extends into the red ($\sim$650 nm). Details of the BKV PCR product synthesis are described elsewhere [19]. DNA sample injection and separation was performed using a field of 158 V cm^{-1} for 100 seconds and 136 V cm^{-1} for 110 seconds, respectively. The injection time was reduced to 10 seconds for subsequent runs during the same experiment. The intersection between the waveguide and the microchannel is 11.5 mm from the injection point.

Except for configuration C, which uses a buried optical fiber for excitation, an excitation waveguide delivers light to the separation channel and the fluorescence is collected by a waveguide at an angle of 45° to the excitation waveguide (Fig. 3.5). The excitation and detection waveguides are each 5 mm in length. A 5 mW, 532 nm green laser diode (Holograms & Lasers Int., TX, USA) passes through an IR filter to remove any remaining 1064 nm light and is focused into the excitation optical fiber with 60% efficiency using a 10x microscope objective. Fluorescence is captured by the collection waveguide and is coupled into a second optical fiber that delivers light to a PMT (H5784-20, Hamamatsu, Japan). In configuration A (Fig. 3.5A), an in-line optical filter (D590/55m, Chroma, VT, USA) is placed prior to the PMT. In all configurations, the PMT is sampled using an ADC at 48 kHz (NI USB-6008, National Instruments, TX, USA) and averaged in real-time to give an equivalent sample rate of 50 Hz.

The results from 3 chip runs using each of the outlined detection configurations is compiled in Table 3.2 and a comparison of typical DNA fragment separations is shown in Fig. 3.6. Configuration A (Fig. 3.5A) was our benchmark and this achieved the highest average SNR of 545. When the commercial external interference filter was removed, configuration B (Fig. 3.5B), we observed a factor of 60 reduction in the average SNR (SNR: 545 vs. 9) since a larger fraction of the excitation light reached the detector resulting in an increased signal baseline and detector shot noise [12]. The significance of the drop in SNR upon removal of the optical filter is observed by comparing the clear primer and product peaks of configuration A (Fig. 3.6A) with the barely discernable peaks of configuration B (Fig. 3.6B).

In configuration C (Fig. 3.5C), the undoped PDMS chip from configuration B is replaced with a dye-doped PDMS chip. A buried optical fiber approach is taken for excitation to prevent attenuation of the excitation light prior to sample excitation while detection is performed using an attenuating waveguide. An average SNR of 300 is observed with configuration C (without the use of an external optical filter), which is a 30-fold improvement over the similar configuration using the undoped PDMS (Fig. 3.5B) due to a large drop in the amount of excitation light reaching the detector and thus reduced shot noise. In configuration D (Fig. 3.5D), a low attenuation glycerol waveguide is used for excitation and a high attenuation waveguide PDMS pre-polymer waveguide is used for detection. Through this configuration, we gain an order of magnitude in terms of SNR as compared to configuration B (SNR: 138 vs. 9). In detection configurations without the use of an external optical filter, the improvement in SNR when using the dye-doped PDMS rather than undoped PDMS is clearly observed by comparing Fig. 3.6C, D to Fig. 3.6B. It is also observed that the addition of the Sudan II pigment into the PDMS microfluidic chip has no observable impact on other aspects of the separation, such as the peak resolution.

		(A) Clear PDMS with External Filter	(B) Clear PDMS without External Filter	(C) Dye-doped PDMS without External Filter[a]	(D) Dye-doped PDMS without External Filter[b]
SNR: Signal-to-noise ratio	Run 1	521	12	338	127
	Run 2	508	6	339	88
	Run 3	607	10	231	198
	Average	**545**	**9**	**303**	**138**
	Std Dev (% of Avg)	**9.8%**	**29.7%**	**20.5%**	**40.6%**

Table 3.2: Comparison of the SNR obtained from microchip CE runs using each waveguide LIF detection system. The noise and the baseline are calculated in the region immediately prior to the arrival of the product peak. The signal is an average of the background-corrected primer and product peak heights, where background-correcting involves subtracting the baseline from the measured peak height. [a] excitation via buried optical fiber. [b] glycerol excitation waveguide from opposite side as detection waveguide.

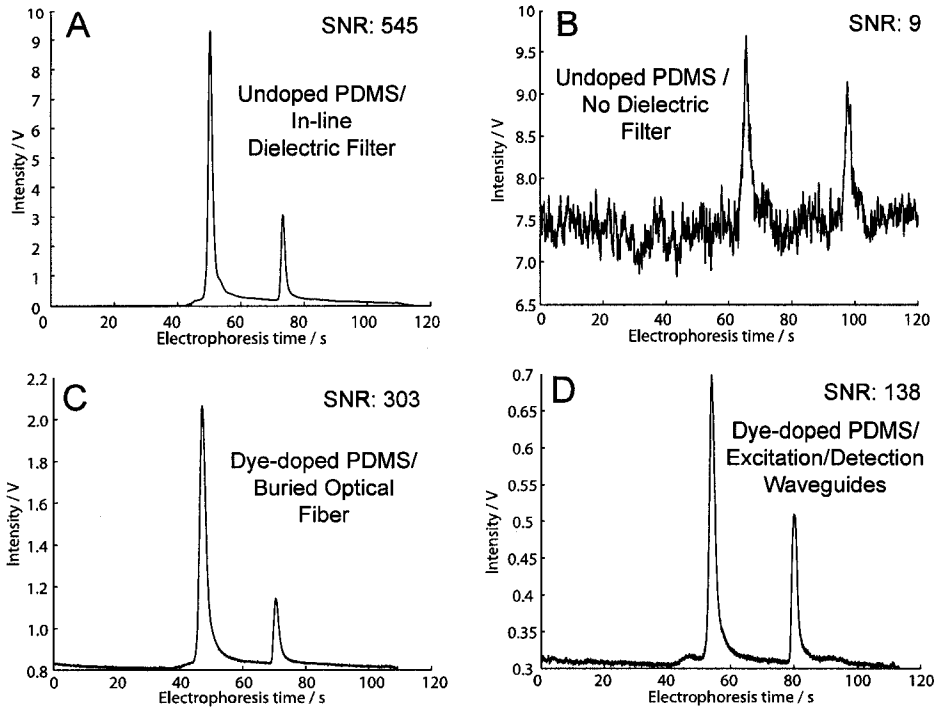

Figure 3.6: The separation of the BK virus PCR product using each detection configuration. (A) Configuration A: The benchmark, undoped PDMS with an external optical filter, shows clear peaks with low noise. (B) Configuration B: The removal of the external optical filter results in a factor of 60 decrease in SNR and the peaks are difficult to detect. (C) Configuration C: When using dye-doped PDMS without an external optical filter, attenuating detection waveguides provide an optical filter effect providing a dramatic increase in SNR as compared to (B). (D) An all-waveguide approach within a dye-doped PDMS chip. Glycerol waveguides provide lower light attenuation at 532 nm during excitation and PDMS pre-polymer waveguide provide high attenuation at 532 nm during detection. The SNR is an order of magnitude larger than in (B). Since the glycerol excitation does exhibit non-negligible attenuation at 532 nm, the excitation power is lower than in configuration (C) resulting in a lower SNR.

3.3 Conclusions

We have demonstrated that the incorporation of Sudan II dye into PDMS microfluidic chips can be used to create waveguides with built-in optical filters that are useful in removing excitation light while preserving the fluorescence signal during LIF. While a monolithic approach to sandwich a dye-doped chip between the source and

detector would be a simple solution for a point-of-care diagnostic system, the optical density of the dye-doped PDMS may not be great enough to remove all of the excitation light prior to detection. Our new approach avoids this issue since the effective optical density of the attenuating waveguides can be increased by extending the length of the waveguide without a reduction in the amount of light captured by the waveguide. For a system that does not contain an external optical filter, we can improve the SNR by as much as 30 times using dye-doped PDMS. We have also shown that our wavelength-selective waveguide system provides results that are very comparable to our benchmark system, which relies on external optical filters. Thus a simplification in the detection system and a reduction in system cost can be achieved through the elimination of external optical interference filters and the use our novel dye-doped waveguide system. While the dye-doped waveguides demonstrate similar attenuation to a commercial interference filter, autofluorescence of the dye currently limits the overall performance of the filter. The performance of the filter could be improved in future work by selecting a dye that generates less autofluorescence or adding quenching species to absorb the autofluorescence.

Bibliography

[1] M. Dandin, P. Abshire, and E. Smela, "Optical filtering technologies for integrated fluorescence sensors." *Lab on a Chip*, 2007. DOI:10.1039/b704008c.

[2] M. A. Burns, B. N. Johnson, S. N. Brahmasandra, K. Handique, J. R. Webster, M. Krishnan, T. S. Sammarco, P. M. Man, D. Jones, D. Heldsinger, C. H. Mastrangelo, and D. T. Burke, "An integrated nanoliter DNA analysis device," *Science*, vol. 282, no. 5388, pp. 484–487, 1998.

[3] J. R. Webster, M. A. Burns, D. T. Burke, and C. H. Mastrangelo, "Monolithic capillary electrophoresis device with integrated fluorescence detector," *Analytical Chemistry*, vol. 73, no. 7, pp. 1622–1626, 2001.

[4] K. S. Shin, Y. H. Kim, J. A. Min, S. M. Kwak, S. K. Kim, E. G. Yang, J. H. Park, B. K. Ju, T. S. Kim, and J. Y. Kang, "Miniaturized fluorescence detection chip for capillary electrophoresis immunoassay of agricultural herbicide atrazine," *Analytica Chimica Acta*, vol. 573, pp. 164–171, 2006.

[5] Y. H. Kim, K. S. Shin, J. Y. Kang, E. G. Yang, K. K. Paek, D. S. Seo, and B. K. Ju, "Poly(dimethylsiloxane)-based packaging technique for microchip

fluorescence detection system applications," *Journal of Microelectromechanical Systems*, vol. 15, no. 5, pp. 1152–1158, 2006.

[6] V. Namasivayam, R. S. Lin, B. Johnson, S. Brahmasandra, Z. Razzacki, D. T. Burke, and M. A. Burns, "Advances in on-chip photodetection for applications in miniaturized genetic analysis systems," *Journal of Micromechanics and Microengineering*, vol. 14, no. 1, pp. 81–90, 2004.

[7] K. S. Shin, Y. H. Kim, K. K. Paek, J. H. Park, E. G. Yang, T. S. Kim, J. Y. Kang, and B. K. Ju, "Characterization of an integrated, fluorescence-detection hybrid device with photodiode and organic light-emitting diode," *IEEE Electron Device Letters*, vol. 27, no. 9, pp. 746–748, 2006.

[8] K. S. Shin, S. W. Lee, K. C. Han, S. K. Kim, E. K. Yang, J. H. Park, B. K. Ju, J. Y. Kang, and T. S. Kim, "Amplification of fluorescence with packed beads to enhance the sensitivity of miniaturized detection in microfluidic chip," *Biosensors & Bioelectronics*, vol. 22, no. 9-10, pp. 2261–2267, 2007.

[9] O. Hofmann, X. H. Wang, A. Cornwell, S. Beecher, A. Raja, D. D. C. Bradley, A. J. deMello, and J. C. deMello, "Monolithically integrated dye-doped PDMS long-pass filters for disposable on-chip fluorescence detection," *Lab on a Chip*, vol. 6, no. 8, pp. 981–987, 2006.

[10] M. L. Chabinyc, D. T. Chiu, J. C. McDonald, A. D. Stroock, J. F. Christian, A. M. Karger, and G. M. Whitesides, "An integrated fluorescence detection system in poly(dimethylsiloxane) for microfluidic applications," *Analytical Chemistry*, vol. 73, no. 18, pp. 4491–4498, 2001.

[11] J. A. Chediak, Z. S. Luo, J. G. Seo, N. Cheung, L. P. Lee, and T. D. Sands, "Heterogeneous integration of CdS filters with GaN LEDs for fluorescence detection microsystems," *Sensors and Actuators A - Physical*, vol. 111, no. 1, pp. 1–7, 2004.

[12] C. Bliss, J. McMullin, and C. Backhouse, "Rapid fabrication of a microfluidic device with integrated optical waveguides for DNA fragment analysis," *Lab on a Chip*, 2007. DOI: 10.1039/b708485d.

[13] O. J. A. Schueller, X. M. Zhao, G. M. Whitesides, S. P. Smith, and M. Prentiss, "Fabrication of liquid-core waveguides by soft lithography," *Advanced Materials*, vol. 11, no. 1, pp. 37–41, 1999.

[14] D. B. Wolfe, R. S. Conroy, P. Garstecki, B. T. Mayers, M. A. Fischbach, K. E. Paul, M. Prentiss, and G. M. Whitesides, "Dynamic control of liquid-core/liquid-cladding optical waveguides," *Proceedings of the National Academy of Sciences of the United States of America*, vol. 101, no. 34, pp. 12 434–12 438, 2004.

[15] D. B. Wolfe, D. V. Vezenov, B. T. Mayers, G. M. Whitesides, R. S. Conroy, and M. G. Prentiss, "Diffusion-controlled optical elements for optofluidics," *Applied Physics Letters*, vol. 87, no. 18, 2005.

[16] D. Yin, D. W. Deamer, H. Schmidt, J. P. Barber, and A. R. Hawkins, "Integrated optical waveguides with liquid cores," *Applied Physics Letters*, vol. 85, no. 16, pp. 3477–3479, 2004.

[17] C. Bliss, J. McMullin, and C. Backhouse, "Integrated wavelength-selective optical waveguides for microfluidic-based laser induced fluorescence detection," *Lab on a Chip*, 2007. Submitted.

[18] E. Hecht, *Optics*, 4th ed. San Francisco, CA, USA: Addison Wesley, 2001.

[19] G. V. Kaigala, R. J. Huskins, J. Preiksaitis, X. L. Pang, L. M. Pilarski, and C. J. Backhouse, "Automated screening using microfluidic chip-based PCR and product detection to assess risk of BK virus-associated nephropathy in renal transplant recipients," *Electrophoresis*, vol. 27, no. 19, pp. 3753–3763, 2006.

Chapter 4

Towards a Pocket-sized Microchip Capillary Electrophoresis Diagnostic Tool

4.1 Introduction

Capillary electrophoresis (CE) has been available on microfluidic platforms for 15 years [1] and the technology is relatively mature, yet a hand-held portable CE system is not yet commercially available. Conventional CE systems containing high performance confocal optics and sensitive photomultiplier tubes (PMTs) often outperform miniaturized systems in terms of sensitivity. However, such equipment also prevents the use of conventional systems for point-of-care (POC) applications due to the size, cost and complexity of these systems. Furthermore, the microfluidics-based systems reported in the literature tend also to rely on expensive bulk optics and external high-voltage (HV) power supplies. Thus such "miniaturized" tools remain restricted to bench-top use, where they cannot effectively compete with higher sensitivity conventional systems.

In recent work, we have demonstrated a waveguide-based excitation and detection scheme for laser induced fluorescence (LIF) with performance comparable to a commercial confocal system [2]. Additionally, we have eliminated the requirement for a commercial interference filter through the integration of dye-doped waveguides, which selectively attenuate excitation wavelengths while transmitting the fluorescence signal with a high efficiency [3]. In the present work, we have de-

veloped a series of simple, compact and inexpensive fluorescence detection systems by replacing the PMT with a low-cost photodiode. The simplified detection systems do not rely on expensive and bulky gas lasers, microscope objectives, dichroic mirrors or PMTs, which are typically found in commercial confocal LIF detection systems. We explored the use of absorptive pigmented photoresist thin films which act as integrated optical filters. Additionally, we have developed a CMOS-based chip which is capable of supplying the high voltage electric fields required for CE and providing optical detection using an integrated photodiode. The application of the HV CMOS device is highlighted in this work, while details on the design and development of the HV CMOS chip can be found elsewhere [4, 5]. To our knowledge, this is the first demonstration of electrophoresis using a microchip-based high voltage power supply. The high-voltage CMOS process was developed by DALSA Semiconductor.

Through the combined use of a microfluidic chip and a HV CMOS chip, we demonstrate a novel prototype, proof-of-concept device that demonstrates the feasibility of building an inexpensive, "USB-key" size microchip CE system consisting of little else other than these two chips. This pocket-sized system is not dependant on any bench-top equipment for operation and can be entirely powered and operated through a laptop USB port.

Several groups have sought to integrate waveguides, optical filters and photodetectors onto a lab-on-a-chip (LOC) platform and integrated optics has been the focus of several recent reviews [6–9]. Chabinyc *et al.* have developed a miniaturized fluorescence detection system in PDMS for the detection of proteins and other small molecules [10]. An encapsulated optical fiber is used to deliver excitation light from a blue LED. A μAPD embedded in PDMS, along with a thin polycarbonate color filter, was used for detection. This work provides an excellent demonstration of the use of low-cost optics, such as polymer filters and sensitive μAPDs, and is fabricated of inexpensive PDMS. The reversible seal between the μAPD and the microfluidic chip is advantageous because the microfluidic chip could be replaced without discarding the detector setup. However, the buried optical fiber approach necessitates the fiber be aligned with the fluidic channels during fabrication, in-

creasing the fabrication time and cost. Thus, this approach does not result in a product that could be mass produced.

Other groups have developed miniaturized systems for DNA fragment analysis. The Burns group have presented several reports involving the fabrication of microfluidic channels on a silicon wafer containing photodiodes and thin film interference filters [11–13]. In one case, the amplification, digestion, separation and detection of an intercalator-labelled PCR product was demonstrated using a blue LED for excitation and a lock-in-amplifier for noise reduction [11]. Kamei *et al.* demonstrated a multi-chip system for DNA fragment analysis consisting of a glass microfluidic chip with a half-ball lens and fluorescence detector that included an interference filter integrated with an a-Si PIN photodiode [14].

Each of these DNA fragment analysis systems demonstrated the impressive integration achievable using LOC technology. However, the fabrication of multilayer dielectric interference filters is complicated and expensive. Our system is based on PDMS soft-lithography and the spin-coating of photoresist-based optical filters, which leads to quick and inexpensive device fabrication. DNA fragments labelled with intercalating dyes are often much brighter than end-labelled dyes since multiple fluorophores label a single DNA fragment. However, this comes at the cost of decreased separation efficiency [15] and increased sample processing. In our work, we are able to maintain high signal-to-noise ratios (SNRs) while using DNA amplified using end-labelled primers. Though each of the cases in the previous two paragraphs presented important advancements in the development of integrated optical systems, each of the systems relies on external high-voltage power supplies to perform CE. Our HV CMOS-based system is capable of generating high-voltage electric fields on-chip using a low-power 5Vdc source.

We present a three stage development toward a prototype for a fully integrated portable, hand-held microchip CE system. The first system uses an integrated waveguide to deliver excitation light to the sample and a graded index (GRIN) lens is used to collect the fluorescence. The collected light passes through a commercial interference filter and is focused onto a photodiode. The microfluidic chip in the second system is similar to the first except a layer of pigmented photoresist on

the bottom surface of the substrate acts as an absorptive filter, eliminating the requirement for the commercial interference filter. The two preliminary systems rely upon an external high voltage power supply to drive the capillary electrophoresis separation.

The third system does not use any imaging optics for fluorescence collection and instead relies on the proximity afforded by LOC. A custom CMOS photodiode is bonded to a ceramic DIP package and is coated with pigmented photoresist. A microfluidic chip is placed in close contact with the CMOS chip and the photodiode is centered under the detection region of the microchannel. Excitation is provided by a laser diode which is focused onto the detection region. This third microchip system is entirely self-contained and does not require a separate electrophoresis system for operation. We have replaced the external HV system and switching with a HV CMOS-based chip. This system is novel in that both the optical detector (a simple P-N junction photodiode) and power supply (an inductive DC-DC boost converter) are implemented using a HV CMOS process, allowing for complete future integration, portability and potential disposability (due to low cost). Our system essentially consists of a laser diode, a microfluidic chip and inexpensive microelectronics. However, we are working to integrate all of the electronics onto a single HV CMOS chip along with a second microchip to add USB communications functionality. This future system could easily fit on a device the size of a current USB memory stick.

In the next section we provide details on the microchip design and fabrication process. We also provide an analysis of each of the three optical systems and compare the efficiency of the excitation and detection systems. In Section 4.3 we demonstrate the functionality of each of these three systems through the detection of unpurified, end-labelled BK virus (BKV) PCR products. BKV is a clinically relevant virus that is a cause of renal transplant rejection when present in high concentrations. The detection of BKV is representative of any viral, bacterial or biomarker identification. The performance of each system is compared through an analysis of the signal-to-noise ratio (SNR). We conclude the paper in Section 4.4 with a summary of the results and suggestions for future work.

4.2 Materials and Methods

4.2.1 Design and Fabrication

The microfluidic devices are fabricated through PDMS soft lithography using the same chip design as previously reported [2, 3]. The channels connecting the sample, sample waste, buffer and buffer waste wells are 100x60 μm^2 while the waveguide channels are 70x60 μm^2. A schematic of the design is given in Fig. 4.1A. The superstrate containing the microchannels is fabricated of PDMS and is common between each of the configurations. PDMS pre-polymer and curing agent (Sylgard 184, Dow Corning, NC, USA) were mixed at a 10:1 (w/w) ratio, degassed for 30 minutes under vacuum, poured onto an SU-8 master and cured at 80°C for 2 hours.

The featureless substrates vary between microchip configurations as seen in Fig. 4.1. Microchip A is fabricated as described in ref. [2]. Briefly, a featureless PDMS slab was fabricated similarly to the superstrate to facilitate sealing of the microfluidic channels. The ~1-mm thick PDMS superstrate and substrate were removed from the mould, exposed to an oxygen plasma at 100W for 30 seconds and placed in contact to produce an irreversible bond.

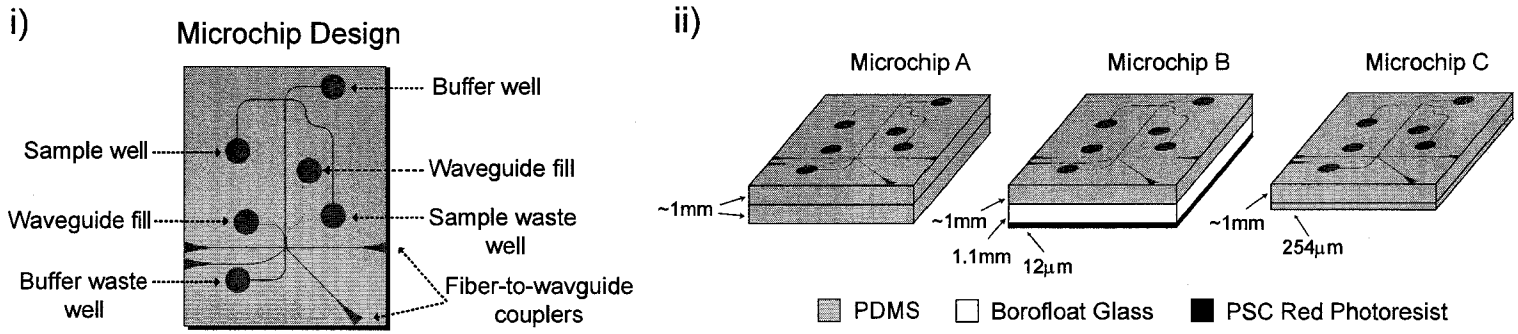

Figure 4.1: (i) A schematic of the microfluidic device used in this work. As the sample is electrophoretically injected from the sample well to the sample waste well, a plug is formed at the intersection between the injection and separation channels. The sample plug is separated within a sieving matrix by applying an electric field between the buffer and buffer waster wells. Detection is performed at the region where the waveguides intersect the separation channel. (ii) Schematics of each of the three different microchips used in this work.

The substrate of microchip B is glass coated with a pigmented photoresist, which acts as an integrated absorptive filter. PSC Red (Brewer Science, MO, USA) is a negative working, photosensitive, pigmented, acrylic resin and is used in fabricating color filters for flat panel display and sensor applications. The 1.1 mm borofloat glass substrate is Piranha cleaned (3:1 v/v, H_2SO_4:H_2O_2) and is coated with an adhesion promoter (APX, Brewer Science, MO, USA) (500rpm, 35 seconds) then baked (contact hotplate with vacuum hold at 150°C for 2 minutes) to increase the bond strength between the glass and PSC Red resist. The PSC Red resist was deposited as per the manufacturer's recommendations. The resist is spun (1000 rpm, 30 seconds), soft-baked (contact hotplate with vacuum hold at 100°C for 2 minutes), blanket exposed (I-line, 300 mJ/cm^2) and cured (convection oven, 190°C for 1 hour). This is repeated five times to create a filter with a total thickness of 12 μm. In future work, this process could be optimized to produce a similar film thickness in fewer coats. The photoresist-coated wafer is diced into 2.1x1.6 cm^2 pieces to match the size of the PDMS chips. The PDMS chip is bonded to the glass-side of the substrate after exposure to an oxygen plasma (100W, 30 seconds).

Microchip C is fabricated by bonding the PDMS superstrate containing the microchannels to a thin (~254 μm) featureless PDMS sheet (HT-6135, Bisco Silicones, IL, USA) after exposure to an oxygen plasma (100W, 30 seconds). As described in detail in the next section, microchip C is used in conjunction with a CMOS-based die that contains a photodiode along with other microelectronics (Sec. 4.2.3). The CMOS chip, fabricated using a HV CMOS process developed by DALSA Semiconductor Inc., has been post-processed to add an integrated optical filter (Fig. 4.2). The HV CMOS die is first wire-bonded to a ceramic DIP package. The packaged HV CMOS chip was coated with 50 μL of APX adhesion promoter using a pipette to drop the liquid onto the die. The packaged die was baked at 200°C for 1 hour. A 50 μL drop of PSC Red was deposited on the die and the die was baked at 100°C for 1 hour. This was repeated to add a second layer of PSC Red. The resultant film was determined to be ~22 μm thick using a contact profilometer. The uniformity and repeatability achieved through this photoresist deposition technique has not been explored. Future work will focus on photoresist deposition

by spin-coating at the wafer level, rather than using an "eye-dropper" technique, to enhance both the uniformity and repeatability.

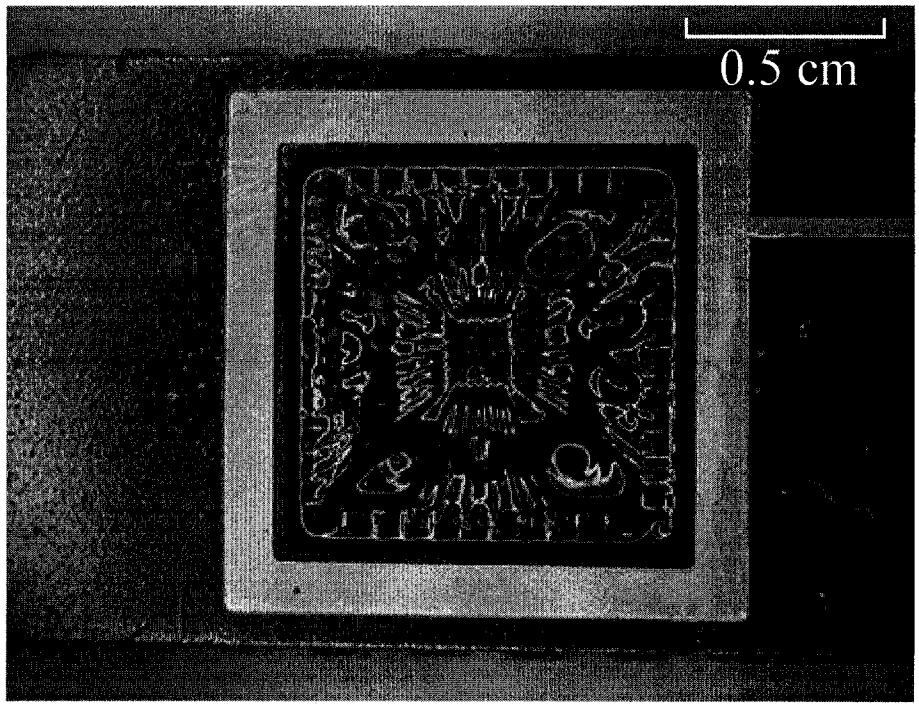

Figure 4.2: A photograph of the wire-bonded HV CMOS die coated in PSC Red pigmented photoresist.

4.2.2 Detection System Characterization

We investigate the advantages gained through miniaturization through a three stage development process (Fig. 4.3). All of the systems have been designed to minimize the size and cost of the detection system; however each successive system contains a higher level of integration. Microchip systems A and B are preliminary steps toward microchip system C, our fully integrated prototype system.

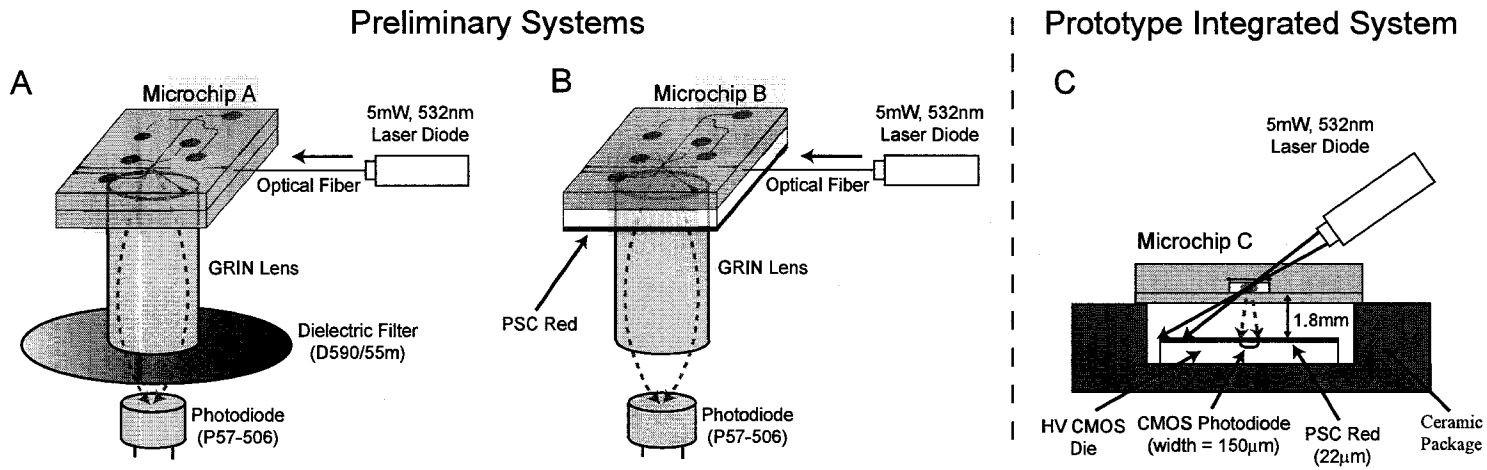

Figure 4.3: Schematics of the three fluorescence detection configurations studied in this work. (A) Microchip System A: Excitation light is coupled to the sample through a waveguide and fluorescence is collected using a GRIN lens that focuses the light through an interference filter onto a photodiode. (B) Microchip System B: Similarly to system A, a waveguide delivers light to the sample and fluorescence is collected using a GRIN lens. The dielectric interference filter is replaced with a pigmented resist that has been fabricated directly on microchip B. (C) Microchip System C: The microchip is placed directly on top of a CMOS die that has been wire-bonded to a ceramic DIP package. The excitation source is focused onto the channel from above and the fluorescence is collected by an integrated photodiode which has been coated with pigmented photoresist.

4.2.2.1 Microchip System A: Preliminary System

In microchip system A (Fig. 4.3A), an optical waveguide is used to deliver excitation light to the sample under test. The optical waveguides are formed by filling microfluidic channels with a high refractive index liquid (Series A: n_D=1.5060, Cargille Laboratories, NJ, USA) and the waveguide interfaces to the fiber-coupled laser diode through a fiber-to-waveguide coupler consisting of a microfabricated taper at the edge of the chip [2]. The waveguide propagation loss was previously measured to be 1.8 dB cm^{-1} and 1.0 dB cm^{-1} at 532 nm and 633 nm, respectively, for similar waveguides [2]. Light is coupled into the excitation fiber by focusing the output from a 5 mW, 532 nm green laser diode (Holograms & Lasers Int., TX, USA) through an IR filter to remove any remaining 1064 nm light and into the fiber core using a 10x microscope objective. Prior to performing CE, the light emitted from the free end of the optical fiber was measured to be 3.0 $\pm$ 0.1 mW using an optical power meter (1930-C, Newport, CA, USA).

The excitation loss is determined by calculating the total loss in delivering light from the laser diode to the sample

$$L_{ex} = L_{L-F} + L_{F-WG} + \alpha_{WG} \cdot l_{WG} \tag{4.1}$$

where L_{ex} is the excitation loss, L_{L-F} is the laser diode to fiber coupling loss, L_{F-WG} is the fiber to waveguide coupling loss, α_{WG} is the waveguide propagation loss in dB/cm and l_{WG} is the length of the waveguide in centimeters. For microchip system A, these values are as follows: L_{L-F} = ~1.75 dB, L_{F-WG} = ~3 dB, α_{WG} = 1.8 dB/cm, l_{WG} = 0.5 cm. This results in a total excitation loss of ~6 dB or an excitation efficiency of ~25%. We estimate that we excite the sample with ~1 mW or ~2.4x10^4 W/cm^2 emitted through a waveguide with an aperture of 70x60 μm^2.

The isotropic fluorescence emission is captured by a 1.8 mm diameter and 5.37 mm long GRIN lens (LGI630-6, Newport, CA, USA) and focused onto a 0.2mm^2 (~450x450 μm^2) photodiode (P57-506, Edmund Optics, NJ, USA). A commercial interference filter (D590/55m, Chroma, VT, USA) is placed between the GRIN lens and the photodiode to remove scattered excitation light that has been collected by the lens. The light collection efficiency can be estimated by approximating the

sample as a point source with an isotropic fluorescence emission. The solid angle, Ω, of the isotropic fluorescence emission that reaches the photodiode is limited by the numerical aperture of the collection lens. As in ref. [2], we estimate the light collection efficiency of the GRIN lens to be

$$LCE = \frac{\Omega}{4\pi} = \frac{1}{2}(1 - \cos\theta_{max}) \tag{4.2}$$

where θ_{max} is the aperture half-angle and is related to the numerical aperture through NA= $n_s \sin\theta_{max}$ where n_s=1.33 is the index of refraction of the sample medium. For the GRIN lens used in this system, the effective numerical aperture is given by [16]

$$NA_{eff} = \sqrt{\frac{r^2}{r^2 + d^2 + \frac{1}{(n_0\sqrt{A})^2}}} \tag{4.3}$$

where r is the lens radius (0.9 mm), d is the distance between the sample and the lens ($\sim$1 mm), n_0 is the index of refraction of the lens on the central axis (1.608) and sqrt(A) is the gradient-index constant (0.339 mm^{-1}). This leads to NA_{eff} = 0.4 and LCE = 2.3%. The overlap between the volume that is excited by the waveguide and the volume which is imaged onto the photodetector is defined as the probe volume. In this configuration, a 450μm segment of the microfluidic channel is imaged onto photodiode with a magnification of $\sim$1 (Fig. 4.4), but only a 70μm region is excited by the waveguide, resulting in a probe volume of $\sim$400pL. A trade-off between the width of the electrophoretic peaks and the fluorescence signal strength occurs when the size of the photodiode active area is adjusted relative to the microchannel. As the probe volume increases, the quantity of fluorescence collected is increased however the separation efficiency in terms of the number of theoretical plates is decreased. The decrease in separation efficiency is due an increased convolution effect since the time an individual fluorophore spends above the photodiode is extended.

The spatial filtering provided by the system due to the perpendicular excitation/detection configuration reduces the amount of excitation light that reaches the detector. This can be quantified by comparing the amount of scattered light that reaches the detector to the total amount of excitation light which reaches the sample. The fraction of scattered excitation light collected by the GRIN lens is measured by

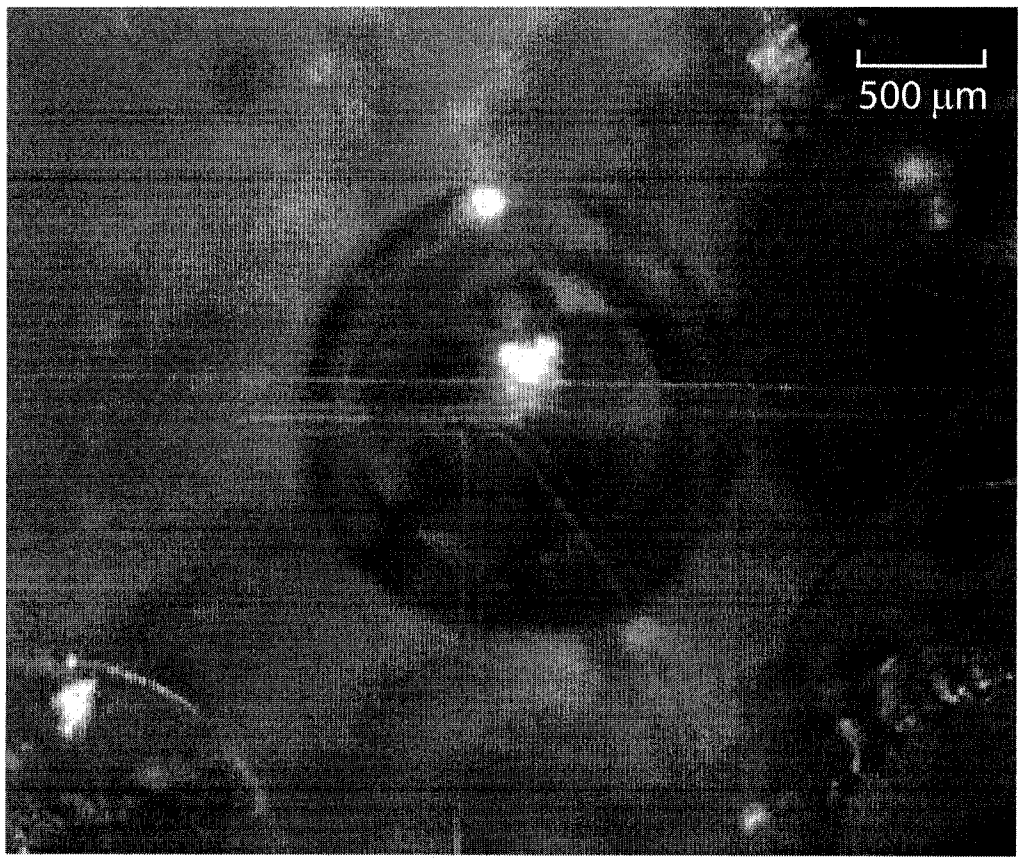

Figure 4.4: A photograph of the microfluidic channel at the detection region. The photodiode is imaged by the GRIN lens onto the microfluidic channel and is visible since the dielectric filter has been removed.

replacing the photodiode and interference filter with an optical power meter. With ~2.5 mW of excitation light (532 nm) emitted from the tip of the fiber, the fiber is inserted into the fiber to waveguide coupler. The scattered light collected by the GRIN lens is measured to be 0.67 ± 0.05 μW using an optical power meter (1930-C, Newport, CA, USA), which corresponds to ~0.03% of the light emitted from the tip of the fiber or ~0.07% of the light that has reached the sample volume, assuming a loss of $L_{F-WG} + \alpha_{WG}* l_{WG}$ = ~3.9 dB. A dark measurement of 60 pW on the optical power meter was observed with all light sources turned off.

The optical filtering capability (or optical density) of the commercial interference filter (D590/55m, Chroma, VT, USA) was found to be ~OD7 (attenuation by 67dB or by a factor of $\sim 10^7$) at 532 nm at normal incidence with a transmittance of 81% at 590nm. Rays entering at oblique angles observe a larger gap between layers. Since these filters rely on optical interference between a stack of dielectric thin films, the effective increase in the gap between layers results in a shift in the cutoff wavelength for these oblique rays. For this reason, we observe reduced filter effectiveness at 532 nm due to rays which exit the lens at large angles (nearly 30° for the GRIN lens used in this work). This is an important consideration when developing integrated detection systems that involve dielectric stack interference filers. When the commercial interference filter was added back to the detection system and ~2.5 mW (532 nm) was emitted from the tip of the fiber, the scattered light reaching the detector was measured to be 0.72 ± 0.02 nW with a dark reading of 60pW when all light sources are turned off. This is only a factor of 1000 less than without any filter at all. This indicates that the quality of the filter was reduced from OD7 to OD3 at 532 nm due to light passing through the filter at oblique angles. A plot of the optical filter attenuation as a function of incidence angle is given in Fig. 4.5.

The responsivity of the commercial photodetector increases approximately linearly as a function of wavelength from ~0.15 A/W (500 nm) to ~0.43 A/W (700 nm), as reported in the specification sheet. The photocurrent is amplified using a transimpedance amplifier with a gain of 1 V/nA, is sampled at 48 kHz (NI USB-6008, National Instruments, TX, USA) and averaged in real-time to give an equivalent sample rate of 50 Hz. The same amplifier / ADC system is used in all three

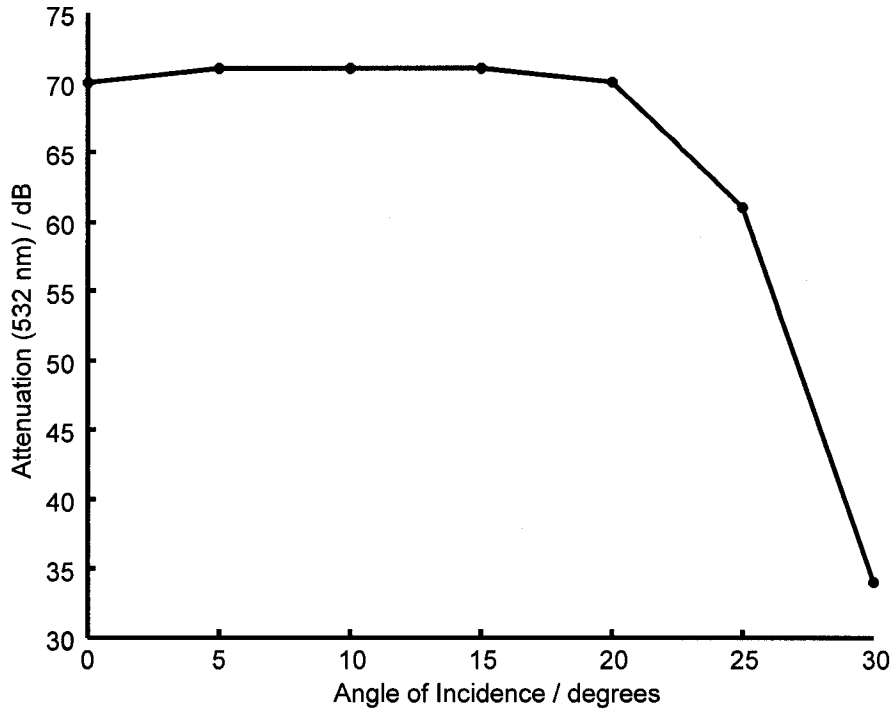

Figure 4.5: The optical density (OD) of a Chroma D590/55m interference filter was measured by placing a collimated 532 nm laser in-line with the filter and an optical power meter. As the filter is rotated, the optical density as a function of the filter angle is recorded. The OD falls off rapidly for angles larger than 20^{o} to normal incidence.

systems.

The functionality of microchip A is demonstrated in Sec. 4.3 through the analysis of fluorescently labelled DNA fragments.

4.2.2.2 Microchip System B: Preliminary System

Microchip system B (Fig. 4.3B) is similar to system A, except the microfluidic chip has been modified such that the PDMS substrate is replaced with a 1.1 mm glass substrate coated with a pigmented photoresist. The pigmented photoresist acts as an absorptive filter with a cutoff of ~600nm and replaces the commercial interference filter used in system A. Since the excitation optics are nearly identical, we assume an excitation efficiency of ~27%. The isotropic fluorescence emission passes through the integrated absorbance filter and is captured by the GRIN lens and focused onto the same photodiode as described in system A. As in system A, the GRIN lens will have a LCE of approximately 2.3% and the spatial filtering provided by the orthogonal detection setup will limit the excitation light which reaches the detector to ~0.07% of the light emitted from the excitation waveguide.

In this system, the commercial optical filter is replaced with a pigmented photoresist filter (PSC Red) deposited directly onto the microchip. In Fig. 4.6, the transmission spectra of the commercial interference filter and the pigmented photoresist is overlaid on the emission spectrum of the fluorescent dye used in the DNA fragment analysis experiments described below. While the commercial filter is a better match to the emission of the dye used in this work (VIC, Applied Biosystems, CA, USA), fluorescent dyes such as ROX, with a fluorescence emission maximum of ~600nm, could be used in future work to increase the performance of systems incorporating the pigmented photoresist. The photodetector, amplifier and ADC used in microchip system B are identical to those used in system A.

Absorptive optical filters are advantageous since light attenuation is not dependant on the angle of incidence. As we have demonstrated above, this is of particular importance when developing integrated optics since light may enter the filter at oblique angles. For a 12 μm film of the pigmented photoresist (6 layers as fabricated using the manufacturer's recommended process), the attenuation at 532 nm

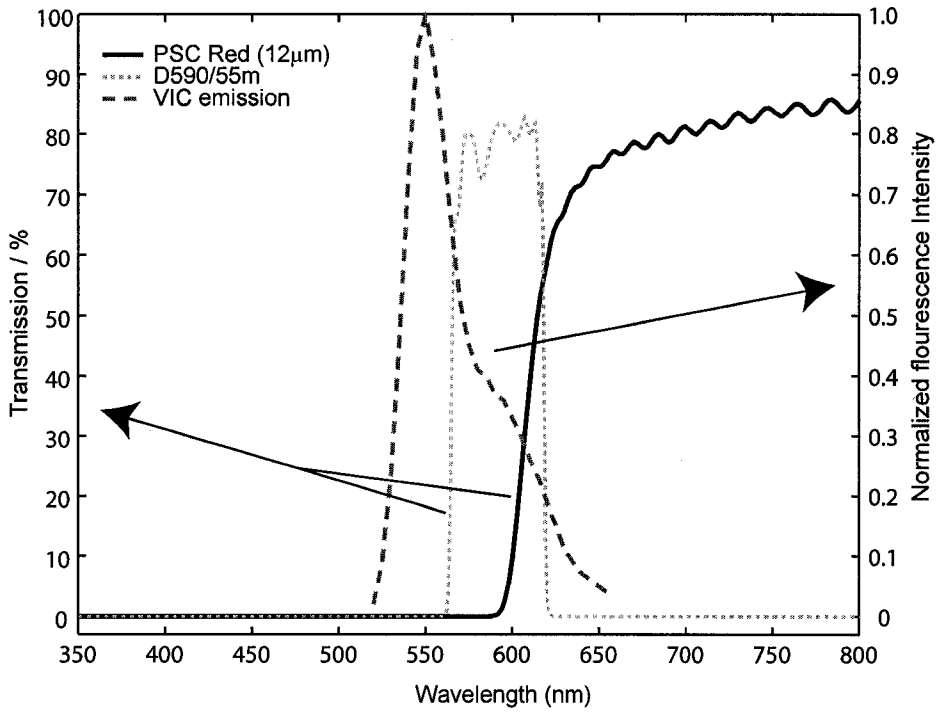

Figure 4.6: Transmission spectra of a 12 μm film of PSC Red photoresist and a D590/55m interference filter (Chroma) in comparison to the emission spectrum of the VIC fluorophore (Applied Biosystems, CA, USA) [17].

was measured to be ~140,000 (~OD5, 51dB) and the transmission at 633 nm was measured to be 70%. The disadvantage of absorbance-based filters is their tendency to release absorbed light as autofluorescence. In our device, the GRIN lens is in direct contact with the absorbance filter and therefore ~2.3% of any autofluorescence generated by the photoresist is captured and contributes to background at the photodetector.

The effective optical filtering capability of the PSC film is measured by replacing the photodiode with an optical power meter and comparing this measurement with the expected amount of scattered excitation light that would be collected if the PSC filter were not present. We expect the performance of the PSC filter to be reduced when integrated into the system due to the collection of autofluorescence. With ~2.5 mW of excitation light (532 nm) emitted from the tip of the fiber, the fiber is inserted into the fiber to waveguide coupler. The light collected by the GRIN lens / photodiode detection system after passing through the PSC film is measured to be 1.8 $\pm$ 0.1 nW using an optical power meter (1930-C, Newport, CA, USA). We can assume that the scattered light that would be collected by the system if the integrated filter were removed is close to the ~0.67 $\pm$ 0.05 μW as measured for microchip system A since the change in substrate from PDMS to glass would have a minimal impact on the optical path of the scattered light. We observe a factor of 370 reduction in the amount of light reaching the detector (OD3, 26dB at 532 nm). A spectral analysis of the light collected by the GRIN lens (Fig. 4.7) reveals that the captured light has a negligible component at the excitation wavelength of 532 nm and is therefore nearly completely composed of autofluorescence from the PSC Red photoresist.

Again, the functionality of this system is demonstrated in Sec. 4.3 through the analysis of fluorescently labelled DNA fragments.

4.2.2.3 Microchip System C: Prototype Integrated System

Microchip system C (Fig. 4.3C) provides a significant increase in integration over systems A or B and is a prototype for a pocket-sized microchip CE device. In this setup, the emission from a green laser diode is focused directly onto the microflu-

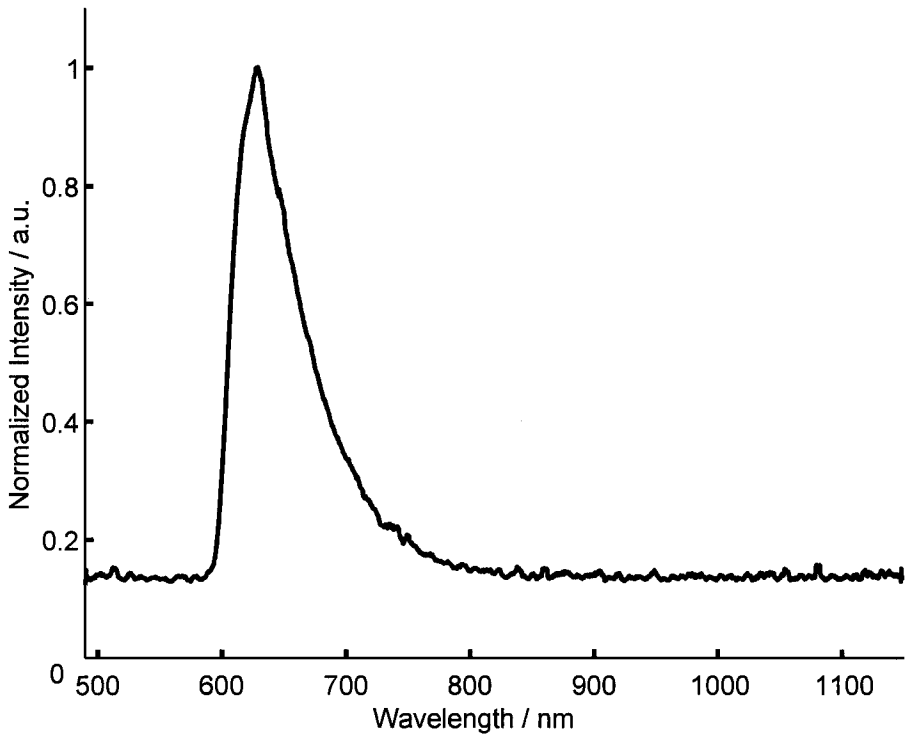

Figure 4.7: A spectrum of the light impinging on the photodetector in microchip system B as measured using a spectrometer (USB2000, Ocean Optics, FL, USA). The light is dominated by autofluorescence generated from the pigmented photoresist and negligible scattered light at the excitation wavelength of 532 nm is observed.

idic channel rather than through a waveguide. A HV CMOS chip containing a photodiode is wire-bonded into ceramic DIP package and is coated with pigmented photoresist. The package containing the HV CMOS chip is placed in contact with the microfluidic chip and the photodiode is positioned beneath the region of the channel under illumination from the excitation source.

In this configuration, the output of a frequency-doubled 532 nm laser diode passes through an IR filter to remove any emission at 1064 nm and is focused to a point $\sim$100-150 μm in diameter onto the microfluidic channel at an angle of $\sim 30^o$ normal to the surface of the chip. The 30^o excitation angle prevents blinding of the photodiode since the center of the focused beam lands $\sim$1mm to the side of the photodiode. The output power of the laser diode was measured to be $\sim$4.5mW. While there is no fiber or waveguide coupling loss, imperfect focusing of the divergent beam and small misalignments between the beam spot and the channel is estimated to reduce the coupling efficiency. The performance of the system could likely be improved through the use of a laser with lower divergence and a low-aberration lens.

The sample fluorescence is captured on the 150x150 μm^2 photodiode without the use of any collection optics. In this prototype system, the closest proximity we could achieve between the die and the microchannel is 1.8 mm due to the ceramic package housing our prototype HV CMOS chip. To achieve this, the microfluidic chip is fabricated using a thin 254 μm PDMS substrate. For a square detector, the light collection efficiency is calculated by dividing the solid angle of the isotropic fluorescence sphere that reaches the detector, Ω, by the solid angle of the entire sphere [7]

$$LCE = \frac{\alpha}{2\pi} \sin\left(\frac{\alpha}{2}\right) = \frac{a}{2\pi\sqrt{\frac{a^2}{4} + d^2}} \cos^{-1}\left(\frac{d}{\sqrt{\frac{a^2}{4} + d^2}}\right) \tag{4.4}$$

where α is the polar angle subtended by the photodetector, d is the distance between the sample and photodetector and a is the width of the photodetector. The width of the photodetector is 150 μm resulting in an estimated LCE of 0.06%.

Two layers of pigmented photoresist are deposited on the packaged die and we measured the thickness of the deposited PSC Red film to be $\sim$22 μm. The effec-

tive optical filtering capability of the PSC Red film was measured by comparing the photocurrent generated from the CMOS photodiode before and after the deposition of the pigmented resist. In each case, the photodiode was illuminated by a mercury lamp filtered to individually isolate wavelengths at 550 nm and 600 nm. The attenuation of the 22 μm PSC Red film was determined to be OD5 (47dB) at 550 nm while the transmission was 22% at 600nm. As in system B, the autofluorescence rather than the penetrating excitation limit is likely the primary source of background at the photodetector.

The photodiode is operated unbiased in photovoltaic mode, so no dark current is generated. However, an electronic offset of 0.098 $\pm$ 0.002 V from our amplifier system was observed. During operation, we observed a background of 0.65 $\pm$ 0.02V. The contribution due to autofluorescence and scattered excitation light was determined by subtracting the electronic offset from the observed background and calculating the power of the background light based on the amplifier gain and photodiode responsivity. The responsivity of the HV CMOS photodiode was measured to be 0.16 A/W at 550 nm and the gain of our transimpedance amplifier is 1 V/nA. From this simple back-calculation, the background due to autofluorescence and scattered excitation light is determined to be $\sim$3.5 nW.

As in system A, the photocurrent is amplified using a transimpedance amplifier with a gain of 1V/nA, is sampled at 48 kHz and averaged in real-time to give an equivalent sample rate of 50 Hz. Additionally, the resultant data is passed through a 5 point moving average window to assist in removing electronic noise at 60 Hz.

4.2.3 Capillary Electrophoresis System

Details on the microchip electrophoresis protocol can be found in our previous work [2]. The microfluidic channels were filled with a solution of 5% linear polyacrylamide (LPA - MW 600k - 1,000k) (Polysciences Inc., PA, USA) and 17% Dynamic Coating (The Gel Co., CA, USA) and allowed to sit for 15 min. This is done to condition the microchips prior to use for the first time to minimize surface effects. The microchips are loaded with 6% LPA as a sieving matrix. In microchips A and B, the sample well was loaded with 0.3μL BKV PCR product and 2.7μL 0.1xTTE

buffer (Tris-Taurine- Ethylenediaminetetraacetic acid). In microchip C, the BKV PCR product was increased to 2μL along with 1μL 0.1xTTE buffer. In all configurations, the sample waste, buffer and buffer waste wells were loaded with 3 μL 1xTTE buffer. The BKV PCR product is end-labelled with VIC dye (Applied Biosystems, CA, USA) and has a fluorescence emission peak at approximately 550 nm (Fig. 4.6). The BKV PCR product synthesis is described in detail in our previous work [18].

The custom CE system used to operate microchips A and B applied a voltage of 300 V during injection (158 V cm^{-1}, 100 seconds) and separation (136 V cm^{-1}, 150 seconds). The electric fields are produced using a miniature high voltage power supply (TS-0.3P, Matsusada Precision Inc., Kyoto, Japan). The injection time was reduced to 10 seconds for subsequent runs during the same experiment. The detection point was located at the intersection between the waveguide and the microchannel at a distance of 11.5 mm from the intersection between the injection and separation channels. While all of the equipment required to perform CE and LIF on microchip systems A and B could be packaged into a portable system, a 12Vdc supply is still required and the system is still oversized. The HV CMOS chip is capable of generating the electric fields necessary for CE on a microchip platform and can be operated using a low-power 5Vdc supply. In this work, microchip system C consists of a laser diode (containing a lens), a microfluidic chip, two HV CMOS chips and inexpensive microelectronics (Fig. 4.8). The HV CMOS chip used to operate microchip C was restricted to an operating voltage of 150V for DNA sample injection (79 V cm^{-1}, 200 seconds) and separation (68 V cm^{-1}, 300 seconds), however improvements to the design will allow the operating voltage of the HV CMOS chip to be increased to 300V in future work. The injection time was reduced to 20 seconds for subsequent runs during the same experiment. The detection point was located $\sim$13 mm from the intersection between the injection and separation channels.

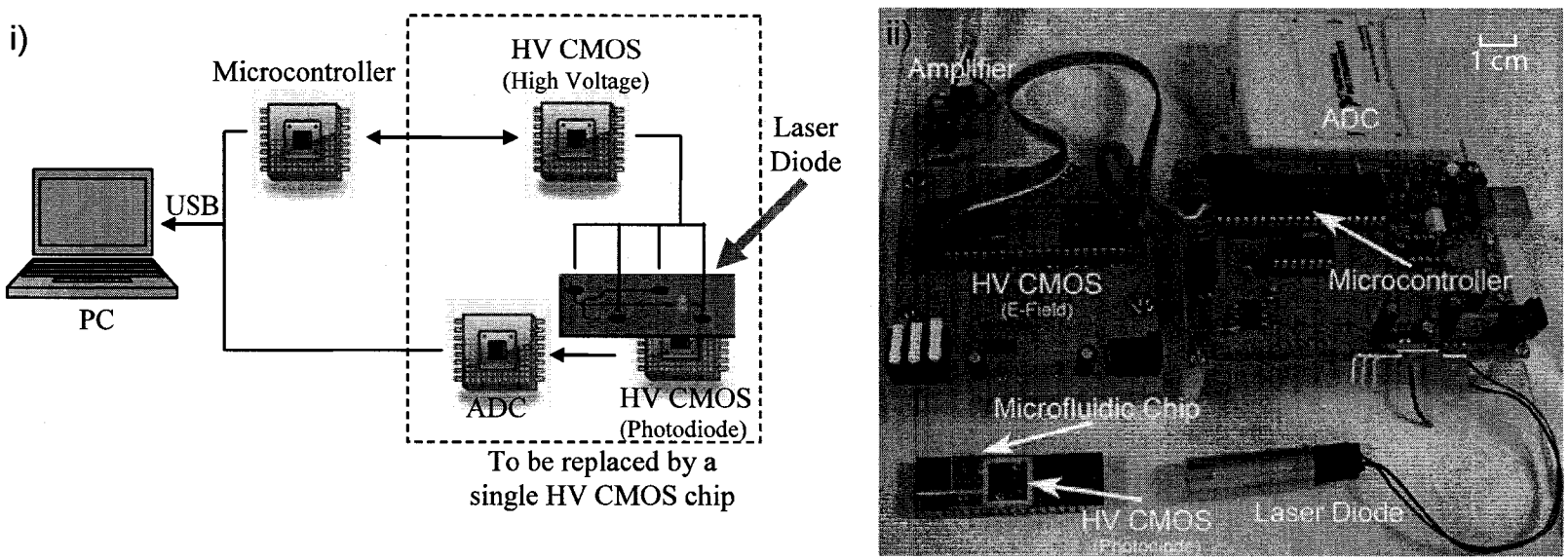

Figure 4.8: (i) A block diagram of the electronics used in microchip system C. (ii) A photograph of all of the components used to perform CE and LIF on microchip system C.

4.3 Results and Discussion

We demonstrate the electrophoretic separation and detection of BK virus DNA fragments amplified through PCR using end-labelled primers. This provides a means of comparing the sensitivity of the three systems described in Section 4.2 and also acts as a demonstration of the clinical relevance of this work. The results from 3 chip runs using each of the outlined detection configurations is compiled in Table 1 and a comparison of typical DNA fragment separations is shown in Fig. 4.9.

4.3.1 Preliminary Systems

As seen in Fig. 4.9, the primers and PCR products are clearly distinguishable in each system. As expected, microchip system A achieved the highest average SNR of 290. Though the excitation and detection optics remain the same (waveguide excitation, GRIN lens collection), a factor of ~4 decrease in average signal intensity is observed when switching between microchip system A and B. This is primarily a result of poor matching between the absorptive filter and the VIC-dye fluorescence spectrum (in comparison to the commercial interference filter) as seen in Fig. 4.6. Additionally, when the commercial external interference filter was replaced with the integrated absorptive filter on microchip B, an increase in the baseline was observed due to autofluorescence of the absorptive filter. The increased baseline results in a slight increase in shot noise at the detector. The mismatch in spectra between the filter and dye fluorescence and the slight increase in shot noise result in a reduction of the average SNR from 290 to 64 when microchip A was replaced with microchip B and the commercial interference filter was removed. However, both systems provide clearly distinguishably peaks and the results are comparable to our previous work using a commercial confocal system with similar microchips using the same DNA sample, concentration and fluorescent label [2].

		Baseline (volts)	Noise (volts)	Signal (volts)	SNR: Signal-to-noise ratio
Microchip A	Run 1	$3.8x10^{-2}$	$1.1x10^{-3}$	$5.5x10^{-1}$	478
	Run 2	$3.2x10^{-2}$	$1.5x10^{-3}$	$2.3x10^{-1}$	153
	Run 3	$3.3x10^{-2}$	$1.1x10^{-3}$	$2.7x10^{-1}$	240
	Average	$\mathbf{3.4x10^{-2}}$	$\mathbf{1.3x10^{-3}}$	$\mathbf{3.5x10^{-1}}$	290
	Std Dev (% of Avg)	**9.6%**	**17.4%**	**50.0%**	**58.1%**
Microchip B	Run 1	$7.7x10^{-2}$	$1.5x10^{-3}$	$1.6x10^{-1}$	103
	Run 2	$2.7x10^{-2}$	$1.6x10^{-3}$	$5.2x10^{-2}$	32
	Run 3	$1.3x10^{-1}$	$1.7x10^{-3}$	$9.8x10^{-2}$	57
	Average	$\mathbf{7.8x10^{-2}}$	$\mathbf{1.6x10^{-3}}$	$\mathbf{1.0x10^{-1}}$	64
	Std Dev (% of Avg)	**65.9%**	**5.7%**	**51.5%**	**56.2%**
Microchip C	Run 1[a]	$6.4x10^{-1}$	$9.0x10^{-4}$	$2.3x10^{-2}$	26
	Run 2[a]	$6.6x10^{-1}$	$8.6x10^{-4}$	$1.8x10^{-2}$	21
	Run 3[a]	$6.7x10^{-1}$	$9.7x10^{-4}$	$2.3x10^{-2}$	24
	Average	$\mathbf{6.6x10^{-1}}$	$\mathbf{9.1x10^{-4}}$	$\mathbf{2.1x10^{-2}}$	23
	Std Dev (% of Avg)	**1.9%**	**6.2%**	**12.8%**	**9.3%**

Table 4.1: Comparison of the baseline, noise, signal level and signal-to-noise ratio obtained from microchip CE runs using each of the microchip systems. The baseline and noise are calculated as the mean value and standard deviation of a 5 second region immediately prior to the arrival of the product peak. The signal is an average of the background-corrected primer and product peak heights, where background-correcting involves subtracting the baseline from the measured peak height. [a] the data from microchip system C was passed through a 5pt moving average filter.

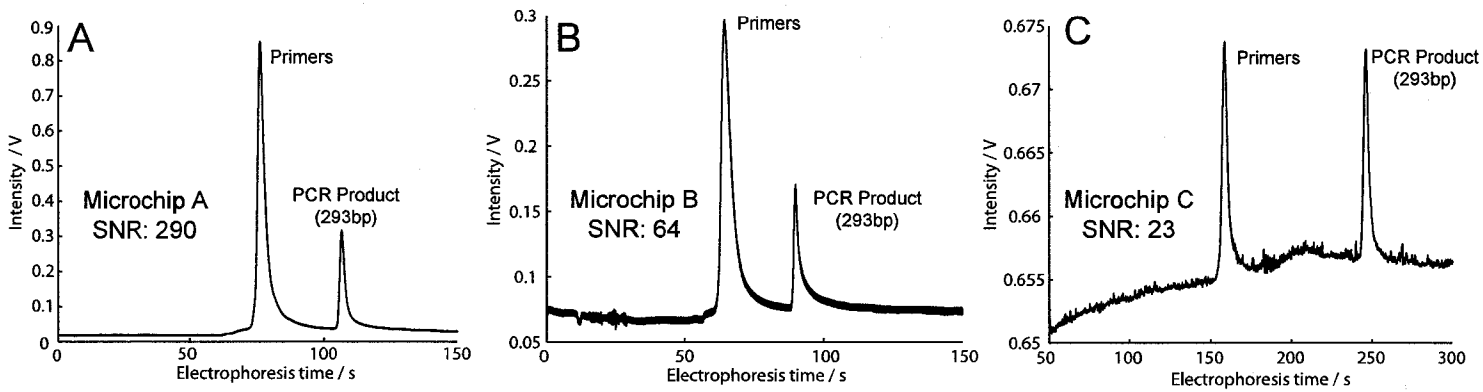

Figure 4.9: A series of electropherograms demonstrating the separation of BK virus PCR product using each detection configuration. (A) Microchip System A: A compact system containing integrated optical waveguides and a GRIN lens. This system achieves the highest sensitivity; however, it relies on a commercial dielectric interference filter. (B) Microchip System B: The requirement for a commercial interference filter is eliminated through the use of a pigmented photoresist, but at the cost of a slight decrease in sensitivity. (C) Microchip System C: A clear detection of the BK virus PCR product is demonstrated using our proof-of-concept for a pocket-sized microchip CE system. The slight differences in peak shape are thought to be a result of interaction between the sample and the channel wall. We are currently working to optimize our channel pre-treatment, sieving matrix chemistries and protocols to combat this problem.

4.3.2 Prototype Integrated System

Microchip system C is a proof-of-concept for a "pocket-sized" capillary electrophoresis system. Though the LCE was estimated to be significantly smaller than systems A and B, the average SNR was measured to be ~20 and the primer and product peaks are clearly distinguishable, as seen in Fig. 4.9C. However, the results from microchip system C cannot be directly compared to those of systems A and B since the sample concentration was larger (2μL was used vs. 0.3μL of BKV PCR product) and a moving average filter was applied to the collected electropherogram data to reduce the electronic noise.

While additional effort was required to produce results with microchip system C, we have demonstrated that this type of detection system is possible and we now provide a roadmap on how the performance could be significantly improved.

Though the estimated LCE is a factor of 40 times lower for microchip system C than when using the GRIN lens in systems A or B and a factor of 75 times lower than a confocal system [2], a result of the inverse square law is that the LCE can be dramatically increased by positioning the sensor closer to the sample (Fig. 4.10). Figure 4.10 provides an extrapolation of the LCE as the distance between the probe volume and the detector is varied for different detection configurations. For the 150 μm detector used in this work, we observe that a decrease in distance between the sample and detector from 1.8 mm to 200 μm would allow us to achieve a similar LCE to a confocal system with a NA of 0.55 and would increase the detected signal level by a factor of ~75 times. A reduction in spacing to 200 μm is entirely possible through the use of PDMS to encapsulate the die [10] or flip-chip bonding onto a thin glass substrate with patterned electrodes.

As the dimensions of the probe volume approach the distance between the sample and the photodetector, the simple point source approximation becomes less accurate due to increased variation between the solid angle subtended by the detector from each fluorophore in the probe volume. In this case, numerical or Monte Carlo methods may be required to accurately determine the average solid angle subtended by the detector [19].

Though it is difficult to predict the increase in detected scattered light (or aut-

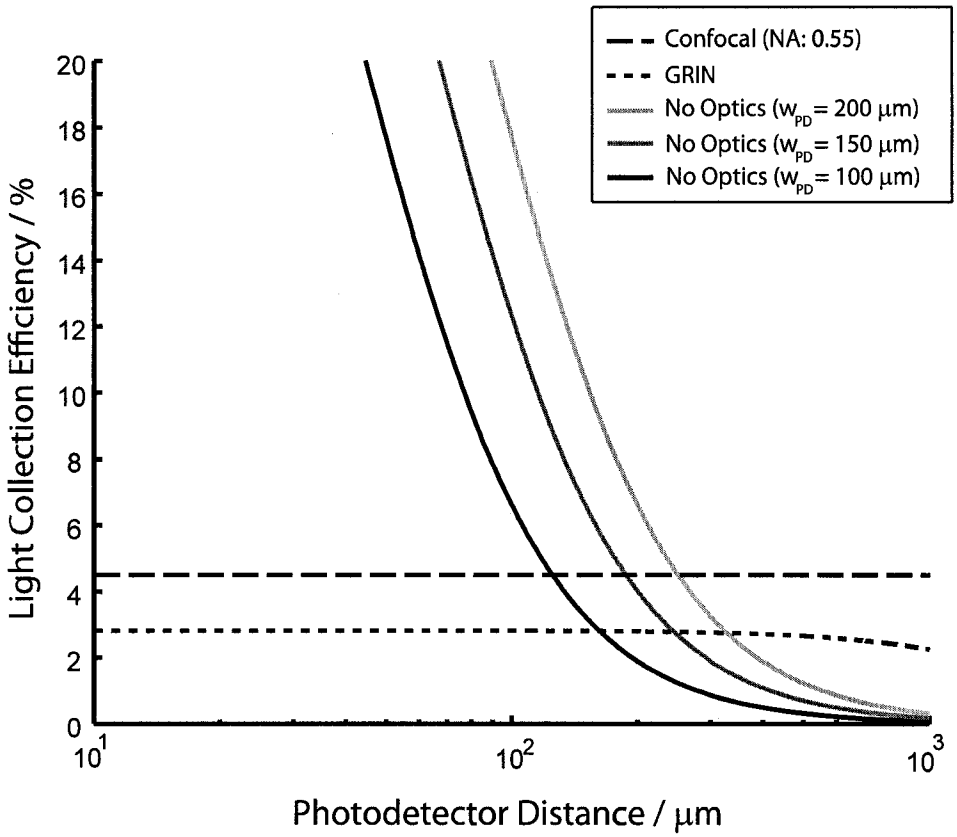

Figure 4.10: A comparison of the LCE of photodiodes with widths 100μm, 150μm and 200μm as a function of distance between the photodetector and the sample volume. For comparative purposes, the LCE of the GRIN lens and the confocal system used in our previous work are included [2]. The LCE of the confocal system is limited by the NA rather than the distance between the sample volume and the lens. With the 150x150μm^2 photodiodes used in this work, we could match the LCE of the confocal optical system if we could get within 200μm of the sample.

ofluorescence generated from scattered light), if we treat scattering centers as isotropic emitters it is conceivable that we would observe a similar factor of 75 increase in scattered light impinging on the detector. We are in the process of fully characterizing our electronics, but if the detector were shot noise limited, we estimate that the SNR would increase by a factor of 75/sqrt(75) = 8.7 since the shot noise scales as the square root of the background intensity [2]. If the noise in the system is not dominated by shot noise at the detector, the increase in SNR could be significantly greater than 8.7. A performance increase in SNR by a factor of ~9 would put the prototype integrated system on par with microchip systems A and B and would approach the sensitivity achievable using commercially available confocal systems [2].

We are working to integrate all of the electronics onto a single HV CMOS chip, which could then be operated and powered by a PC over a USB connection. As currently configured, two identical HV CMOS chips are required to operate as a photodetector and as a high voltage power supply. This configuration was convenient in our current prototype setup but only a single HV CMOS die is required to perform both functions. Additionally, we currently have prototype amplifier and ADC electronics on the HV CMOS die so these external components will not be required in future work. Control of the device by the PC over USB could also eliminate the requirement for a microcontroller on the μCE device itself. The entire system displayed in Fig. 4.8(i) could be replaced with a three-chip system. This system would consist of a microfluidic chip, a PSC-coated HV CMOS chip, a USB chip and a laser diode. If the laser diode were replaced with a surface mount LED butt-coupled to an integrated waveguide, the entire CE system could be fabricated into a device the size of a current USB memory stick. A removable PDMS microfluidic chip could be disposed of and replaced to avoid contamination or the entire system could be disposable due to its low cost.

4.4 Conclusions

We have demonstrated the use of integrated optics, miniature lenses and inexpensive photodetectors to build compact optical detection systems capable of detecting clinically relevant viral PCR product samples. In addition, we have demonstrated the feasibility of an inexpensive USB-key sized diagnostic systems composed of 2-3 chips which have the same functionality as conventional CE systems. Except for the inexpensive laser diode, we have integrated all of the "unconventional" components required for CE, such as the high-voltage generation and photodetector, onto a HV CMOS chip. Although we used an off-chip amplifier and ADC, the present HV CMOS chip already contains prototype ADC and amplifier circuitry that we expect to use in future designs. Though we were limited to a low LCE using our existing prototype setup, we were able to demonstrate the capability to repeatably detect an end-labelled PCR product using our novel system. In future work, a reduction in the microfluidic chip substrate thickness to 200 μm will allow us to achieve a comparable LCE to a conventional confocal system, with a concomitant increase in SNR. A further increase in sensitivity could be achieved through optimal matching of the fluorescence dye to the integrated filter. There is no longer any technical uncertainty as to the feasibility of extremely low-cost ("USB key" style) detection systems.

Bibliography

[1] D. J. Harrison, A. Manz, Z. H. Fan, H. Ludi, and H. M. Widmer, "Capillary electrophoresis and sample injection systems integrated on a planar glass chip," *Analytical Chemistry*, vol. 64, no. 17, pp. 1926–1932, 1992.

[2] C. Bliss, J. McMullin, and C. Backhouse, "Rapid fabrication of a microfluidic device with integrated optical waveguides for DNA fragment analysis," *Lab on a Chip*, 2007. DOI: 10.1039/b708485d.

[3] C. Bliss, J. McMullin, and C. Backhouse, "Integrated wavelength-selective optical waveguides for microfluidic-based laser induced fluorescence detection," *Lab on a Chip*, 2007. Submitted.

[4] M. Khorasani, Masters of Science Thesis, University of Alberta, 2007.

[5] M. Behnam, "Integration of high voltage CMOS and microfluidic technologies for genetic analysis systems," Masters of Science Thesis, University of Alberta, 2007.

[6] E. Verpoorte, "Chip vision - optics for microchips," *Lab on a Chip*, vol. 3, no. 3, pp. 42N–52N, 2003.

[7] M. Dandin, P. Abshire, and E. Smela, "Optical filtering technologies for integrated fluorescence sensors." *Lab on a Chip*, 2007. DOI:10.1039/b704008c.

[8] S. Gotz and U. Karst, "Recent developments in optical detection methods for microchip separations," *Analytical and Bioanalytical Chemistry*, vol. 387, no. 1, pp. 183–192, 2007.

[9] K. B. Mogensen, J. El-Ali, A. Wolff, and J. P. Kutter, "Integration of polymer waveguides for optical detection in microfabricated chemical analysis systems," *Applied Optics*, vol. 42, no. 19, pp. 4072–4079, 2003.

[10] M. L. Chabinyc, D. T. Chiu, J. C. McDonald, A. D. Stroock, J. F. Christian, A. M. Karger, and G. M. Whitesides, "An integrated fluorescence detection system in poly(dimethylsiloxane) for microfluidic applications," *Analytical Chemistry*, vol. 73, no. 18, pp. 4491–4498, 2001.

[11] M. A. Burns, B. N. Johnson, S. N. Brahmasandra, K. Handique, J. R. Webster, M. Krishnan, T. S. Sammarco, P. M. Man, D. Jones, D. Heldsinger, C. H. Mastrangelo, and D. T. Burke, "An integrated nanoliter DNA analysis device," *Science*, vol. 282, no. 5388, pp. 484–487, 1998.

[12] J. R. Webster, M. A. Burns, D. T. Burke, and C. H. Mastrangelo, "Monolithic capillary electrophoresis device with integrated fluorescence detector," *Analytical Chemistry*, vol. 73, no. 7, pp. 1622–1626, 2001.

[13] V. Namasivayam, R. S. Lin, B. Johnson, S. Brahmasandra, Z. Razzacki, D. T. Burke, and M. A. Burns, "Advances in on-chip photodetection for applications in miniaturized genetic analysis systems," *Journal of Micromechanics and Microengineering*, vol. 14, no. 1, pp. 81–90, 2004.

[14] T. Kamei and T. Wada, "Contact-lens type of micromachined hydrogenated amorphous Si fluorescence detector coupled with microfluidic electrophoresis devices," *Applied Physics Letters*, vol. 89, no. 11, 2006.

[15] V. J. Sieben and C. J. Backhouse, "Rapid on-chip postcolumn labeling and high-resolution separations of DNA," *Electrophoresis*, vol. 26, no. 24, pp. 4729–4742, 2005.

[16] E. Acosta, C. Gomezreino, and J. Linares, "Effective radius and numerical aperture of grin lenses with revolution symmetry," *Applied Optics*, vol. 26, no. 15, pp. 2952–2955, 1987.

[17] Applied Biosystems, *User Bulletin #5, ABI Prism 7700 Sequence Detection System.* Foster City, CA: Applied Biosystems, 1998.

[18] G. V. Kaigala, R. J. Huskins, J. Preiksaitis, X. L. Pang, L. M. Pilarski, and C. J. Backhouse, "Automated screening using microfluidic chip-based PCR and product detection to assess risk of BK virus-associated nephropathy in renal transplant recipients," *Electrophoresis*, vol. 27, no. 19, pp. 3753–3763, 2006.

[19] R. Whitcher, "Calculation of the average solid angle subtended by a detector to source in a parallel plane by a Monte Carlo method," *Radiation Protection Dosimetry*, vol. 102, no. 4, pp. 365–369, 2002.

Chapter 5

Conclusions

5.1 Summary of Work

The projects completed throughout the duration of the program have each contributed to the simplification and miniaturization of lab-on-a-chip systems through the integration of various optical components.

In Chapter 2, we presented an inexpensive technique to fabricate microfluidic devices with integrated liquid-core optical waveguides and compared their performance to a commercially available confocal fluorescence detection system. In Chapter 3, we added additional functionality to the liquid-core waveguides by creating built-in optical filters. The wavelength-selective waveguides are formed by allowing dye molecules to diffuse into the liquid core from the surrounding dye-doped PDMS. We are able to control the rate of dye diffusion by using either polar or non-polar liquid core materials.

In Chapter 4, we report the development of a novel fluorescence-based capillary electrophoresis system that has the capability to be integrated onto a pocket-sized platform. Through the use of high-voltage (HV) CMOS microelectronics we simultaneously eliminate the need for an external PMT photodetector and a bulky high voltage power supply to drive the electrophoresis. We demonstrate the ability of this system to perform clinically relevant assays (DNA fragment analysis of BK virus) and describe future plans to integrate the entire microchip CE system onto a pocket-sized platform that can be operated and powered over a USB connection to a laptop PC.

5.2 Future Work

There are several interesting paths and tasks that could not be explored due to time limitations.

System Calibration: The sensitivity of each of the detection systems is compared by computing the average SNR over a series of electrophoretic separations using nearly identical BKV PCR product samples under the same experimental conditions. While this is useful when comparing the systems developed in this work to each other, it is difficult to compare the LOD with other published results. In future work, the limit of detection should be determined for a constant flow of a commonly available dye, such as Rhodamine B.

Autofluorescence: Both the dye-doped waveguide system from Chapter 3 and the pigmented photoresist film in the prototype polymer / HV CMOS integrated system suffer from autofluorescence. In each case, the autofluorescence from the absorptive filter was found to limit the performance of the system since the autofluorescence contributed to the background at the detector. In future work, alternate absorptive materials should be investigated and characterized to find low autofluorescence alternatives. The addition of quenching species to absorb the autofluorescence generated by the color filter may be a solution provided the quencher does not absorb the fluorescence signal generated by the sample.

LED Excitation: Throughout this project we have integrated three of the four key components for a fluorescence sensing system, as mentioned in Sec. 1.3, into the miniaturised platform. The excitation source is the last remaining bulk optic that needs to be integrated, though we are currently using an inexpensive solid-state laser, which is a more compact solution than a large gas laser. Light emitting diodes (LEDs) should be investigated as an alternate excitation source. LEDs are inexpensive, power efficient and small and therefore seem suitable for this application. However LEDs are not optimal and the trade-offs include a wide spectral

content that may overlap with the fluorescence spectrum, low output power and a wide emission angle. These characteristics make the integration of LED excitation non-trivial, but highly desirable to achieve the end goal of an entirely integrated system.

HV CMOS Packaging: In Sec. 4.3, a discussion of the performance increase expected upon reducing the gap between the HV CMOS die and the microfluidic channel was provided. Currently, the HV CMOS die is wirebonded and packaged in a ceramic DIP package. However, this provides a limit on how close we can position the photodiode with respect to the microfluidic channel. New packaging techniques may allow this gap to be significantly reduced. This has been accomplished in previous work by other groups through PDMS encapsulation to achieve gaps sizes of 200μm [1] and even 20μm [2]. A more complex, but more robust, technique may be to flip-chip bond the HV CMOS die to a thin, metallized glass substrate. The glass substrate would then form the substrate for the microfluidic system. Glass substrates at least as thin as 170μm are available from FISHER Scientific. As discussed in Sec. 4.3, either of these two options would allow the light collection efficiency to be improved to provide equivalent performance to a confocal system.

Electronics Integration: Electronics such as a transimpedance amplifier and an ADC have been implemented in the CMOS microchip, though they were still being characterized during the work of Chapter 4. Future work should include optimizing these electronics to provide similar performance to the external components. This would allow the number of components in the prototype system to be reduced to four: a microfluidic chip, a PSC-coated HV CMOS chip, a USB chip and a laser diode.

Bibliography

[1] M. L. Chabinyc, D. T. Chiu, J. C. McDonald, A. D. Stroock, J. F. Christian, A. M. Karger, and G. M. Whitesides, "An integrated fluorescence detection system in poly(dimethylsiloxane) for microfluidic applications," *Analytical Chemistry*, vol. 73, no. 18, pp. 4491–4498, 2001.

[2] K. S. Shin, Y. H. Kim, J. A. Min, S. M. Kwak, S. K. Kim, E. G. Yang, J. H. Park, B. K. Ju, T. S. Kim, and J. Y. Kang, "Miniaturized fluorescence detection chip for capillary electrophoresis immunoassay of agricultural herbicide atrazine," *Analytica Chimica Acta*, vol. 573, pp. 164–171, 2006.

Appendix A

Fabrication Protocols

A.1 PDMS Microchip Fabrication

A.1.1 SU-8 Master Fabrication

SU-8 has become extremely popular in the last few years in applications involving microfluidics and MEMS. The epoxy-based material has excellent chemical and biological inertness and it can be used to form high aspect ratio patterns in film thicknesses between 1μm and 2mm, depending on the formulation and quality of photolithography equipment. Though SU-8 is a very useful material, the protocol is highly equipment-dependent and the standard process must be tuned to the available equipment. We achieved satisfactory results with the protocol below, which is a modified version of the protocol in Sanket Goel's thesis [1] and the standard protocol available from Microchem. Note that we used glass substrates due purely to convenience and compatibility with our PDMS casting equipment, however SU-8 tends to adhere better to silicon substrates.

A.1.1.1 Materials

- 10.16 x 10.16 x 0.11 cm^3 (LxWxH) borofloat substrate (Paragon Optical Company, PA, USA)
- Chrome mask created using a pattern generator (DWL 200, Heidelberg Instruments, CA, USA) in the University of Alberta Nanofab
- SU-8 2050 negative photoresist (MicroChem Corp., MA, USA)
- SU-8 Developer (MicroChem Corp., MA, USA)

A.1.1.2 Setup

1. Warm up three hotplates to 200°C, 65°C, 95°C

   * Placing a 1-cm thick aluminium plate on the hotplate seems to improve the temperature distribution and drastically improves the uniformity of the film. In this work, an aluminium plate was placed on each of the hotplates and was not moved off of the hotplate at any time during the processing. The UofA nanofab has since fabricated aluminium plates with built-in thermocouples to sit on the hotplates to improve temperature distribution and temperature read-out accuracy.

   * Covering the substrate with aluminium foil during softbake and PEB prevents particles from landing on substrate and may reduce premature exposure of the SU-8.

2. Line spinner with aluminium foil for ease of cleanup.

3. Turn on mask aligner (Oscar) to allow lamp to warm up for at least 30 minutes.

A.1.1.3 Process

1. **Wafer Preparation**

   The borofloat glass substrate should be cleaned in a fresh 3:1 (H_2SO_4:H_2O_2) Piranha for 30 minutes, rinsed in deionised water, dried with N_2 and dehydrated on the 200°C hotplate for 10 minutes. The substrate should be cooled by moving it down to the 95°C and 65°C hotplates for 1 minute each. Clean the substrate with N_2 to remove rogue particles prior to adding resist.

2. **SU-8 Spin-coating**

   Place substrate in the center of the chuck. Dispense SU-8 in the center of the substrate directly from the bottle. Keep the bottle very close to the wafer (1-2cm) to prevent the formation of bubbles. Dispense enough SU-8 such that 80% of the substrate is coated. Stop pouring by slowly rotating the bottle to prevent bubbles from forming. To achieve a film thickness of approximately 60μm, spin coat the SU-8 (with the lid on the spinner) as follows:

- 0 to 500 rpm @ 100 rpm/s
- 500 rpm, 10 seconds
- 500 to 2500 rpm @ 300 rpm/s
- 2500 rpm, 30 seconds
- 2500 to 0 rpm @ 125 rpm/s

Or adjust the spin parameters to achieve the desired thickness. Let the SU-8 reflow for 10 minutes without lifting the lid to increase the uniformity of the film. Longer resting periods (such as overnight) have been reported in the literature but an extension of the rest period has not been explored in this work.

* Since the nanofab does not have an edgebead removal system compatible with SU-8, edgebead remains a significant issue. Edgebead prevents the mask from making close contact with the SU-8. This is undesirable since the diffraction of UV rays as they pass between the mask and the surface of the SU-8 may result in resolution or exposure problems and therefore this distance should be minimized.

3. **Soft Bake**

The SU-8 film is soft baked to drive off solvent prior to exposure. A two-step soft bake at 65°C and 95°C is used. The substrate is baked at 65°C for 1 minute and transferred to the 95°C for 8 minutes. Cool the substrate to room temperature by turning off the 95°C hotplate and leaving for 30 minutes.

* While the 65°C bake step is thought to provide more controlled solvent evaporation, and thus better adhesion and film uniformity, we have found that extended time at the low temperature causes a skin to form on the surface of the film, causing uneven evaporation during the 95°C bake step. This results in the formation of craters/divots on the surface of the film. This may be more of an issue on thick (1.1mm), insulating glass substrates than on silicon.

4. **Exposure**

Align the substrate using a mask aligner (AB-M Inc., CA, USA). For a 60μm film, Microchem recommends an exposure dose of (150 to 215)*1.5 (glass)

= 225 to 323 mJ/cm^2. Choose 300 mJ/cm^2 and determine the exposure time by dividing the average power at 365 nm (in mW/cm^2) by 300 mJ/cm^2.

5. **Post Exposure Bake (PEB)**

   The exposed regions of the SU-8 become cross-linked during the PEB. The PEB should occur immediately after exposure to prevent diffusion of the photogenerated cross-linking acids. Bake the substrate at 65°C for 1 minute and 95°C for 7 minutes. Slow cooling is essential to minimize thermal stress. Cool the substrate to room temperature by turning off the 95°C hotplate and leaving for 30 minutes.

6. **Develop SU-8 Photoresist**

   Unexposed SU-8 is removed during development. The SU-8 film should be developed using the SU-8 developer (or other compatibly developers as suggested by Microchem). Fill a glass dish with enough developer to cover the substrate and have a second glass dish ready to rinse with IPA. Submerse the substrate in the developer and agitate vigorously for 5 minutes. Remove, rinse with IPA (NOT water!!) and lightly dry with N_2. If a white residue forms, the development is not yet complete.

   * If high aspect ratio features are not developing, try replacing the bath with fresh developer. Typical development times are 5-7 minutes.

7. **Hard Bake**

   Microchem suggests a hard bake if the SU-8 is to be left as part of the device or to anneal out any micro-cracks. A hard bake temperature of 150°C to 250°C for 5 to 30 minutes is suggested.

8. **Removal**

   We have successfully removed SU-8 by placing the substrate in a cold Piranha overnight and a 3:1 hot Piranha for 30 minutes. Placing a substrate with a large amount of SU-8 in a hot Piranha is extremely dangerous since the reaction is exothermic!! If a large amount of SU-8 is present after the cold Piranha treatment, place the substrate in a new cold Piranha for an additional

night.

* Talk to the Nanofab staff to obtain approval before placing SU-8 coated substrates in a Piranha bath.

A.1.2 PDMS Casting and Bonding

A.1.2.1 Materials

- soft lithography master (SU-8 coated glass or silicon, DRIE etched silicon)
- soft lithography substrate holder/mold
- Sygard 184 PDMS base/curing agent (Dow Corning, NC, USA)
- silanizing agent (tridecafluoro-1,1,2,2-tetrahydrooctyl-1-trichlorosilane) (United Chemical Technologies, PA, USA)
- toluene (optional)
- Sudan II dye (optional)

A.1.2.2 Process

1. **Master Silanization**

   Once the master has been fabricated, it should be silanized to prevent the adhesion of PDMS to the master so the PDMS replica can be easily removed. The silanizing agent is toxic and should be handled with care. In the fumehood, add 2-3 drops of silanizing agent to a glass vial using a disposable plastic eyedropper. Place the plastic eyedropper in a plastic bag with your name and the date and leave in the fumehood. The master is placed in a vacuum dessicator along with the glass vial. The dessicator is sealed and a vacuum is applied. The silanizing agent will form a monolayer on the surface of a master after 1-2 hours. Remove the glass vial and place in the plastic bag, along with the eyedropper. Seal the bag and place in the PDMS waste bin under the fumehood. Remove the silanized master and place in a storage container until step 3.

2. **PDMS Mixing and Degassing**

   The Sylgard 184 PDMS is a two-part base/curing agent and should be mixed

at 10:1 (v/v). For approximately 1 mm thick PDMS, mix 15g of PDMS base and 1.5g of PDMS curing agent. Mix vigorously with a disposable plastic eyedropper. Place the PDMS mixture into the top vacuum oven and degas at -25in·Hg at room temperature for 30 minutes or until bubbles are no longer visible.

* For larger quantities of PDMS, a gradual raise in vacuum to -25in·Hg is necessary to prevent PDMS from overflowing. This can be achieved by opening the vacuum in stages (i.e. closing the vacuum at -15in·Hg, wait for a few minutes, open the vacuum and close at -20in·Hg, etc.)

3. **Dye-doped PDMS** (Optional)

   To create dye-doped PDMS, dissolve Sudan II dye in a small amount of toluene and add to the PDMS mixture. The volume of toluene added should be less than 10% of the PDMS volume to ensure proper PDMS curing. For a dye concentration of 1200μg/mL, add 19.8mg of Sudan II dye to 1mL of toluene. Care should be taken when handling Sudan II dye (i.e. double gloves) since it may be carcinogenic. Ensure all of the dye is dissolved prior to mixing with the PDMS, this may require brief heating of the solution on a hotplate. Add the dye solution to 16.5g of the PDMS base/curing agent mixture and stir vigorously for several minutes to ensure the dye is completely distributed within the PDMS. Degas in the vacuum oven as in the previous step.

   * A complete study of the repeatability of the dye-doped PDMS protocol has not been carried out. It would be useful to perform such a study to assess the impact of run-to-run process variations on the optical transmission properties of the dye-doped PDMS. A sample study could involve producing several featureless dye-doped PDMS substrates. The optical transmission of each of these substrates would be characterized using the spectrophotometer to determine the impact any run-to-run variations have on the properties of the filter. The variation in the optical transmission within a single substrate should also be determined by characterizing several points on a single substrate. Training on the PerkinElmer Lambda 900 UV/VIS/NIR spec-

trophotometer (PerkinElmer, MA, USA) is available from staff at the U of A Nanofab.

4. **PDMS Curing**

The substrate holder/mold creates a seal along the master and contains the PDMS during curing. The substrate holder differs for a 4-inch square glass substrate and for a 4-inch round silicon substrate. In this work the substrate holder used was custom built by the Backhouse lab and was named Wilma. Load the substrate into the substrate holder and pour the uncured PDMS onto the substrate. Pop any bubbles using a gentle stream of N_2. Place the substrate holder in the bottom PDMS vacuum oven and adjust the screws in the levelling plate to ensure the substrate holder is level. Cure at 80°C for 2 hours for standard PDMS or 4 hours for dye-doped PDMS.

After the curing is complete, remove the substrate holder from the oven and let cool. Remove the PDMS by cutting around the edge of the PDMS and dismantling the substrate holder. Cover the feature side of the PDMS with blue tape available in the glass bonding area to prevent contamination. Holes must be punched in the PDMS to provide access to the microfluidic channels. Create the access wells using the 1.5mm PDMS hole punch.

5. **PDMS Bonding**

Repeat steps 1-3 with a blank borofloat glass substrate to create a featureless PDMS slab. Perform a clean sequence on the μEtch reactive ion etch (RIE) system according to the standard nanofab protocol (75% RF (225W), 80% O_2, 150mTorr, 10 minutes). Place the patterned and featureless PDMS slabs in the μEtch RIE chamber with the side to be bonded facing up. Expose to the oxygen plasma according to the standard nanofab PDMS bonding protocol (33.3% RF (100W), 25% O_2, 200mTorr, 30 seconds). Remove the PDMS and carefully place the two slabs in contact. Apply a slight pressure to remove air bubles. The sooner contact is made after exposure to the plasma, the stronger the bond. Leave the PDMS overnight to ensure complete bonding. Dice the slab into individual chips using a razor.

A.2 Fabrication of a Composite Microchip with PSC Optical Filter

This is a detailed protocol to assist in the fabrication of composite microchips with PSC optical filters. In brief, a single unbonded, PDMS slab containing microfeatures, fabricated as described in A.1.2, is diced and bonded to a PSC-coated glass substrate.

A.2.0.3 Materials

- 10.16 x 10.16 x 0.11 cm^3 (LxWxH) borofloat substrate (Paragon Optical Company, PA, USA)
- APX-K1 adhesion promoter (Brewer Science, MO, USA)
- PSC Red negative photoresist (Brewer Science, MO, USA)
- 0.23 normal TMAH developer (optional for photopatterning PSC Red)
- unbonded PDMS microchips

A.2.0.4 Process

1. **Wafer Preparation**

   The borofloat glass substrate should be cleaned in a fresh 3:1 (H_2SO_4:H_2O_2) Piranha for 30 minutes, rinsed in deionised water, dried with N_2.

2. **Adhesion Promoter**

   The APX-K1 adhesion promoter increases the bond strength of the PSC Red to the borofloat glass substrate. Pour ~3-5mL APX-K1 (or enough to coat 80% of the substrate) onto the center of the substrate and spin at 500rpm for 35 seconds. Bake the substrate on a contact hotplate at 150°C with vacuum hold engaged for 2 minutes. Remove from hotplate and let cool to room temperature.

3. **PSC Red Photoresist**

   Pour ~3-5mL PSC Red (or enough to coat 80% of the substrate) onto the center of the substrate, spread at 500 rpm for 5 seconds and spin at 1000 rpm

for 30 seconds. Bake the substrate on a contact hotplate at 100°C with vacuum hold engaged for 2 minutes. Remove the wafer and expose at 365nm (I-line) using the contact mask aligner for a total dose of 300mJ/cm^2. If desired, develop using TMAH. The 25% TMAH stocked by the nanofab must be diluted to 0.23 normal in order to achieve successful development. A final cure is required at 190°C for 1 hour in the convection oven.

A single photoresist layer deposited according to the manufacturers recommended process is $\sim$1.5μm thick. In order to achieve suitable optical filter strength for the work outlined in this thesis, several layers must be deposited. In this work, we deposited 6 resist layers for a total PSC Red thickness of 12μm. Repeat this step (including the final cure) for each PSC Red layer. The stress of a single or multiple PSC Red layers was not characterized in this work. However, a few micro-cracks were apparent in the 6 layer film. It was not determined what the overall impact of these micro-cracks was on the performance of the PSC film (i.e. light leakage). However, autofluorescence of the PSC Red film was found to be more significant than light leakage through the film.

4. **Substrate Dicing**

   Dice the PSC-coated borofloat substrate to achieve the desired chip size using the standard nanofab dicing protocol on the diamond touch dicing saw. Place in the chamber with the double-layer of blue tape on the PSC side to protect the film during dicing. In this work, we obtained twenty 21x16mm devices using a single 4-inch square wafer. While only one substrate was diced in this work, the PSC film was found to reliably pass the "Scotch tape test" since the film did not de-laminate upon removal of the two layers of blue tape.

5. **Microchip Bonding**

   Now the PDMS, which contains the microchannels, is bonded to the PSC-coated borofloat glass substrate using the same protocol as for PDMS-PDMS bonding. The PDMS should be diced using a razor into individual chips and

access holes should be punched in the PDMS prior to bonding. Place the patterned PDMS slabs in the μEtch RIE chamber with the side containing the features facing up. Also, place the PSC-coated glass in the chamber with the glass side facing up (the PSC resist should be on the bottom of the final device). Expose to the oxygen plasma according to the standard nanofab PDMS bonding protocol (33.3% RF (100W), 25% O_2, 200mTorr, 30 seconds). Remove the PDMS and carefully place the PDMS and glass in contact. Apply a slight pressure to remove air bubles. The sooner contact is made after exposure to the plasma, the stronger the bond. Leave the microchips overnight to ensure complete bonding.

A.3 Post-processing of a packaged HV CMOS chip to add a PSC Optical Filter

This protocol details the post-processing required to coat a HV CMOS die wire-bonded to a ceramic DIP package with PSC Red photoresist.

A.3.0.5 Materials

- HV CMOS die wire-bonded to a ceramic DIP package
- APX-K1 adhesion promoter (Brewer Science, MO, USA)
- PSC Red negative photoresist (Brewer Science, MO, USA)

A.3.0.6 Process

Unlike the PSC Red photoresist process described above, PSC Red is deposited on the HV CMOS die using an "eye-dropper" process. While spin-coating PSC Red on the unpackaged wafer would result in a film with greater uniformity, the photoresist over the bonding pads would need to be removed to allow for electrical connection. We wanted to ensure there were no paths for excitation light to reach the photodiode so we deposited PSC on the packaged die. This could not be done using a spin-coater, so a drop of PSC Red is placed on the packaged HV CMOS die. This ensured that the bonding pads and wires were coated with PSC Red.

1. **Adhesion Promoter**

   The APX-K1 adhesion promoter increases the bond strength of the PSC Red to the silicon / oxide substrate. Using a pipette, deposit 50 μL of APX-K1 onto the center of the HV CMOS die. Bake the packaged die in an oven at 200°C for 1 hour. Remove from oven and let cool to room temperature.

2. **PSC Red Photoresist**

   Using a pipette, deposit 50 μL PSC Red onto the center of the die. Bake the substrate in an oven at 100°C for 1 hour. Remove from oven and let cool to room temperature. Repeat a second time to add an additional layer of PSC Red photoresist.

For the work performed in chapter 4, the PSC Red film thickness was measured to be ~22 μm. In order to prevent additional stress on the film, we refrained from exposing and hardbaking the photoresist. The uniformity and repeatability achieved through this photoresist deposition technique has not been explored. Future work should focus on photoresist deposition by spin-coating at the wafer level, rather than using an "eye-dropper" technique, to enhance both the uniformity and repeatability.

Bibliography

[1] S. Goel, "Opto-biochips for microcytometry," Doctor of Philosophy Thesis, University of Alberta, 2006.

Appendix B

Experimental Protocols

B.1 DNA Fragment Analysis - Microchip Preparation

B.1.1 Channel Coating

Prior to performing electrophoresis in PDMS or glass microchips, a channel coating is applied to the microchannel to reduce the interaction between the sample and the channel walls. The channel coating has been found to improve the electrophoresis performance, possibly by reducing electroosmotic flow (EOF) or reducing sample adsorption to the channel wall. The channel coating technique described here was developed by Dr. Dammika Manage.

B.1.1.1 Materials

- linear polyacrylamide (LPA - MW 600k - 1,000k, 10% in water) (Polysciences Inc., PA, USA)
- Dynamic Coating (Dynamic coating, cat. DEH-100, The Gel Co., CA, USA)
- PDMS or glass microfluidic chip

B.1.1.2 Coating Preparation

1. Weigh 300 mg of 10% LPA into a 1 mL Eppendorf tube.
2. Add 200 μL of water and 100 μL of Dynamic coating.
3. Vortex until all of the LPA is dissolved. Store at 4^{o}C.

B.1.1.3 Coating Method

1. Rinse the chip with water and dry with N_2.
2. Fill the chip with the channel coating mixture. Top up each of the wells to prevent evaporation from the channel.
3. Cover the chip and wait 20-45 minutes.
4. Rinse wells with water. Force out channel coating solution. Rinse with water and dry with N_2.

B.1.2 Reagent Preparation

B.1.2.1 Materials

- Tris
- TAPS acid
- Na_2EDTA
- linear polyacrylamide (LPA - MW 600k - 1,000k, 10% in water) (Polysciences Inc., PA, USA)
- Filtered Autoclaved Milli-Q Water

B.1.2.2 Buffer Preparation

This recipe was originally in a publication by Applied Biosystem titled "ABI PRISM377 DNA Sequencer". The protocol was subsequently updated by Dr. Dammika Manage.

1. Combine the following reagents in a 50mL conical tube to create 10xTTE:

Component	Weight/Vol.	Final Amt./Conc.
Tris	3.027 g	0.5 mM
TAPS acid	6.082 g	0.5 mM
Na_2EDTA	0.186g	0.01 mM
Filtered Autoclaved Milli-Q Water	Fill	
Total	**50 mL**	

2. Mix well.

3. Check the pH of the 10X TTE. The pH should be 8.3±0.3. If the pH is not in this range, then discard the buffer. Due to contamination from use (i.e. insertion of pipettes), the buffer degrades over time. For this reason the buffer should be periodically replaced.

4. To dilute to 1xTTE, mix 100μL of 10xTTE with 900 μL of autoclaved milli-Q water and mix well using the vortex.

B.1.2.3 Sieving Matrix Preparation

This recipe describes the preparation of the 6% LPA polymer used as a sieving matrix in this work. The protocol was developed by Dr. Dammika Manage.

1. Weigh 300 mg of 10% LPA into a 1 mL Eppendorf tube.

2. Add 200 μL of water.

3. Vortex until all of the LPA is dissolved. Store at 4^{o}C.

B.1.3 Chip Loading

B.1.3.1 Materials

- 6% LPA
- 1xTTE
- VIC-labelled, unpurified BKV PCR Product
- Filtered autoclaved Milli-Q water

B.1.3.2 Procedure

The following chip loading procedure makes reference to the microfluidic channel and well configuration as labelled in Fig. 2.1.

1. Load the chip with 6% LPA by forcing the polymer in through the BW well using a syringe. Prior to removing the syringe from BW, use a microscope to inspect for bubbles within the injection and separation channels. Verify that the polymer begins to enter each of the wells. This ensures that electrical

contact will be made between the buffer and polymer. The polymer should just begin to bead into the well, excess polymer should be removed using a pipette.

2. Load BW, SW and B with 3 μL 1xTTE. Stir the solution in each well using the pipette tip. Verify that bubbles are not present between the buffer and the polymer in each well.

3. Load S with 0.3 μL 1xTTE, X μL BKV sample, 2.7-X μL water. Stir very well (20-30 seconds) to ensure the sample and buffer are mixed well. In this work, the standard sample volume is X=0.3 μL. However, this was increased for certain detection systems developed in Chapter 4. Enough water is added such that the entire volume is 3 μL. This results in a concentration of 0.1xTTE in the S well. A lower buffer concentration encourages the electrophoretic transport of the DNA from the S well instead of buffer ions.

4. Verify that no bubbles are present anywhere in the chip. The chip is ready to be inserted into the electrophoresis system.

B.2 Optical Detection Configuration

B.2.1 Waveguide-based Laser Induced Fluorescence Detection

This optical detection configuration was used throughout chapters 2 and 3.

B.2.1.1 Materials

- 5 mW, 532 nm green laser diode module (Holograms & Lasers Int., TX, USA)
- 10x microscope objective
- 62.5 μm core optical fiber (62.5/125 μm core/cladding buffered multimode fiber)
- X-Y-Z micropositioner x 2
- PDMS microfluidic chip
- 62.5 μm core optical fiber with a single SMA adapter (62.5/125 μm core/cladding buffered multimode fiber with SMA adapter)

- D590/55m bandpass optical filter (Chroma, VT, USA)
- PMT (H5784-20, Hamamatsu, Japan) with SMA adapter
- ADC (NI USB-6009, National Instruments, TX, USA)
- PC running Labview. The labview program is called PMT_utility_bliss_3_clean_trimmed.vi and is located on Gaea at: /home/Archive/Data/2007/cbliss/Labview/48kS_PMT_VIs/

B.2.1.2 Laser to Optical Fiber Coupling

The 5 mW, 532 nm green laser diode module (Holograms & Lasers Int., TX, USA) used in this work is collimated with a built-in lens and has a beam diameter of $\sim$1 mm. In order to interface with the microfluidic chip, the laser must be focused into an optical fiber, which is then inserted into a fiber-to-waveguide coupler.

1. Mount the laser diode on an optical table.
2. Mount the 10x objective on an X-Y-Z micropositioner and mount the positioner on the optical table in the path of the laser diode.
3. Using the micropositioners, position the 10x objective so the beam is centered on the lens. One way to achieve this is to remove the lens, mark the center of the laser spot on a target (ie. a wall or curtain) 6 feet away, add the lens to the optical path and adjust the micropositioners so the center of the beam spot matches the marked spot without the lens. Once the objective is aligned, do not adjust these micropositioners.
4. Cleave and clean (with IPA) both ends of a 62.5 μm optical fiber. The optical fiber can be cleaved using an optical fiber cleaver available in the McMullin lab. Mount one end on a X-Y-Z micropositioner and mount the positioner on the optical table in the path of the laser.
5. Using the micropositioners, slowly adjust the fiber position so that it is at the focus of the 10x objective. To maximize the coupling efficiency, monitor the output of the other end of the fiber with an optical power meter. For a 5 mW laser, it is possible to get 3 mW out of the opposite end of the optical fiber.

B.2.1.3 Optical Fiber to Waveguide Coupling

It is relatively simple to couple light into the integrated waveguides using the fiber-to-waveguide couplers developed in this work.

1. Load the waveguide channels with a high refractive index liquid (OE-43-Part-B PDMS pre-polymer, glycerol, n = 1.50 index matching fluid).

2. While looking through a microscope with a 5x objective, gently insert the optical fiber into the tapered region of the waveguide. Holding the optical fiber close to the tip allows the fiber to be inserted with greater force. The fiber should butt-up against the waveguide similar to as seen in Fig. 2.2B.

3. When removing the fiber, gently pull the fiber out of the coupler to prevent the formation of bubbles. If bubbles form the waveguide may need to be reloaded with liquid.

. ** Note: Do NOT add water to the waveguide channel. Water is generally not miscible with the waveguide core liquids and will be difficult to remove. It is best if the waveguide channel is loaded prior to adding the sieving matrix or other reagents.

For the excitation waveguide, an optical fiber with loose ends on each sides of the fiber is used. Light is coupled from the laser diode into one side of the fiber and the other side is inserted into the waveguide. The fiber used for the detection waveguide is loose on the side inserted into the waveguide and has an SMA connector on the opposite end for interfacing to the PMT.

B.2.1.4 PMT Detector

The PMT detector is configured as described in Fig. B.1. In configurations requiring the use of an external optical filter, the filter is positioned between the SMA adapter and the PMT. Black electrical tape is used to mechanically secure the simple system and to prevent background light from reaching the PMT window.

The PMT is powered using a +/- 15Vdc supply as described in Fig. B.1. The PMT output is connected to the first analog input of the ADC (AI 0). The white $V_{control}$ wire is connected to the first analog output of the ADC (AO 0) and is

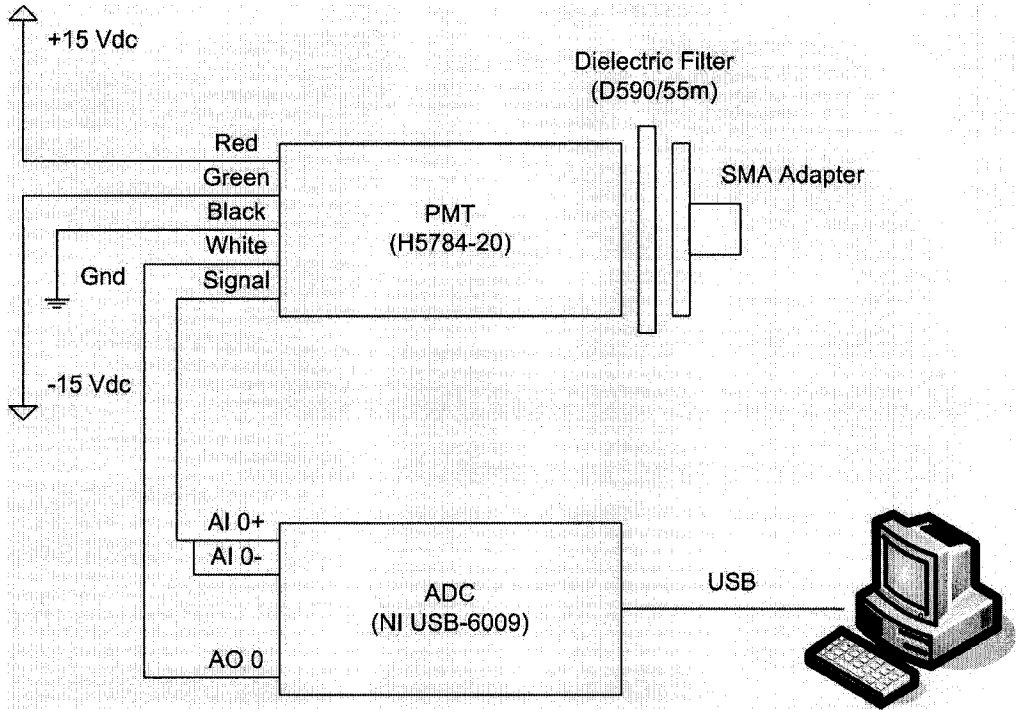

Figure B.1: PMT wiring diagram

driven between 0 and 0.9Vdc to adjust the PMT gain. The ADC is controlled using LabView on a PC. The ADC is sampled at 48 kS/s each 960 samples are averaged and written to a text file resulting in an effective sample rate of 50 S/s. This greatly reduces the noise in the acquired signal.

B.2.2 GRIN Lens-based Laser Induced Fluorescence Detection

This optical detection configuration was used through the initial portion of chapter 4.

B.2.2.1 Materials

- 5 mW, 532 nm green laser diode module (Holograms & Lasers Int., TX, USA)
- 10x microscope objective
- 62.5 μm core optical fiber (62.5/125 μm core/cladding buffered multimode fiber)
- X-Y-Z micropositioner x 2

- PDMS or PDMS/glass microfluidic chip
- GRIN Lens (LGI630-6, Newport, CA, USA)
- D590/55m bandpass optical filter (Chroma, VT, USA)
- Photodiode (P57-506, Edmund Optics, NJ, USA)
- Transimpedance amplifier (as described below)
- ADC (NI USB-6009, National Instruments, TX, USA)
- PC running Labview. The labview program is called PMT_utility_bliss_3_clean_trimmed.vi and is located on Gaea at: /home/Archive/Data/2007/cbliss/Labview/48kS_PMT_VIs/

B.2.2.2 Optical System

The optical detection system is setup as shown in Fig. 4.3A,B. The excitation light is delivered to the sample via waveguide through a fiber-coupled laser diode as described in Sec. B.2.1. The excited sample volume at the intersection between the waveguide and the separation channel is centered over the GRIN lens. The photodiode is positioned under the GRIN lens. In cases where an external optical filter is required, the filter is placed between the GRIN lens and the photodiode.

For the 0.29 pitch GRIN lens used in this work, the object (d_1) and image (d_2) distances are related through [1]

$$d_2 = \frac{1}{n_0\sqrt{A}} \times \frac{n_0\sqrt{A}d_1\cos\left(L\sqrt{A}\right) + \sin\left(L\sqrt{A}\right)}{n_0\sqrt{A}d_1\sin\left(L\sqrt{A}\right) - \cos\left(L\sqrt{A}\right)} \tag{B.1}$$

where n_0 is the refractive index of the center axis of the lens, $\sqrt{A}$ is the gradient-index constant and L is the length of the lens. The magnification of the lens is given by [1]

$$m = \frac{-1}{n_0\sqrt{A}\sin\left(L\sqrt{A}\right)\left[d_1 - \frac{\cot\left(L\sqrt{A}\right)}{n_0\sqrt{A}}\right]} \tag{B.2}$$

For the lens used in the work, n_0=1.608, $\sqrt{A}$=0.339 and L=5.37 mm. For an approximately 1 mm thick microfluidic chip substrate, the microfluidic channels are imaged at ~2 mm at a magnification of -1.3, neglecting refraction at the surface

of the chip. However, the distance between the photodiode and the glass window of the TO-18 can package is 0.087 inches or 2.21 mm. Also, the thickness of the interference filter adds ~1 mm to the distance between the photodiode and the surface of the GRIN lens. This means that the microfluidic channel will not be in perfect focus at the photodiode. This can be seen in Fig. 4.4. A ray trace of the optical path through the GRIN lens is given in Fig. B.2.

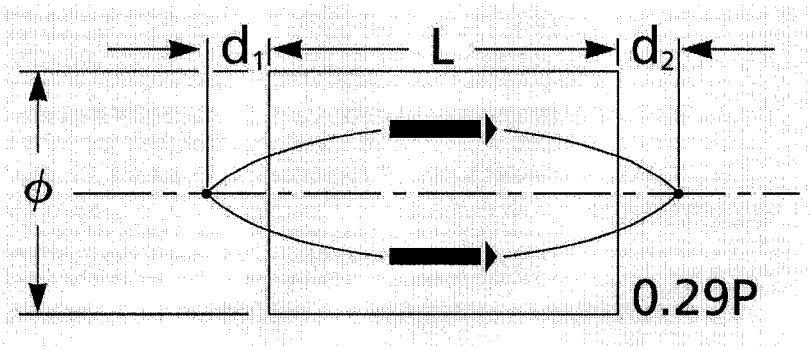

Figure B.2: A ray-trace schematic of a 0.29 pitch graded-index lens [1]. d_1 is the object distance, d_2 is the image distance, L is the length of the lens and ϕ is the diameter of the lens.

B.2.2.3 Photodiode Detector System

The photodiode is connected to a transimpedance amplifier to amplify the current generated by the photodiode. A schematic of the amplifier used in this work is provided in Fig. B.3. This amplifier system was designed by Alex Stickel. The 1 GΩ feedback resistor provides a gain of 1V/nA and the potentiometer provides the user with the ability to correct for the amplifier offset.

The amplifier output, V_{out}, is connected to the first analog input (AI 0) of the ADC. The ADC in controlled through a LabView interface using a PC. Using the same program with the PMT system, the ADC is sampled at 48 kS/s each 960 samples are averaged and written to a text file resulting in an effective sample rate of 50 S/s. This greatly reduces the noise in the acquired signal.

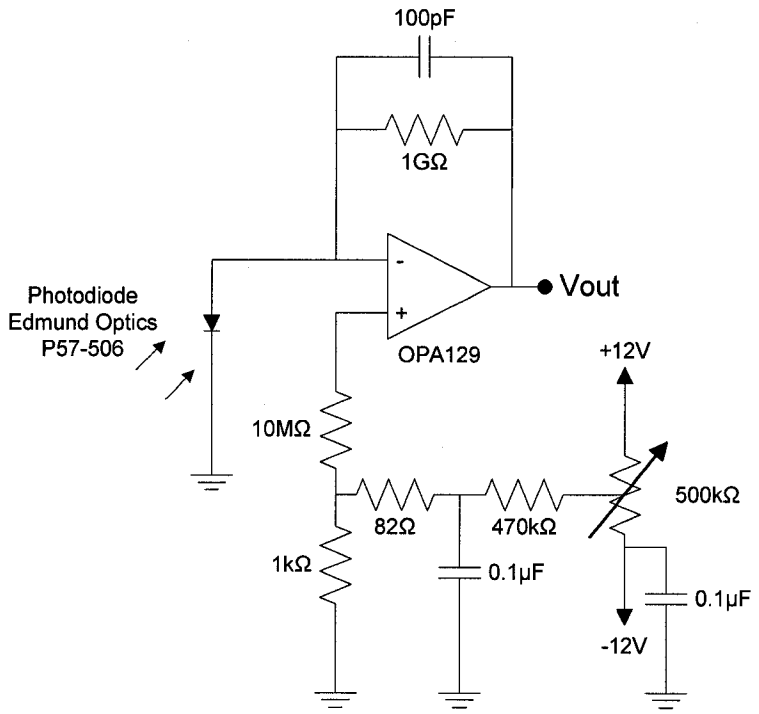

Figure B.3: A schematic of the transimpedance amplifier system used to amplify the photodiode current.

B.2.3 Laser Induced Fluorescence Detection using a compact "USB-key" prototype system

This optical detection configuration was used through the final portion of chapter 4.

B.2.3.1 Materials

- 5 mW, 532 nm green laser diode module (Holograms & Lasers Int., TX, USA)
- X-Y-Z micropositioner x 1
- PDMS microfluidic chip
- PSC-coated DALSA HV CMOS Chip (Chip version: ICKAATC1)
- Transimpedance amplifier (as described in Sec. B.2.2.3)
- ADC (NI USB-6009, National Instruments, TX, USA)
- PC running Labview. The labview program is called PMT_utility_bliss_3_clean_trimmed.vi and is located on Gaea at: /home/Archive/Data/2007/cbliss/Labview/48kS_PMT_VIs/

B.2.3.2 Optical System

The optical detection system is setup as shown in Fig. 4.3C. Included in the green laser diode module is a plastic collimating lens. To focus the collimated output, a compound lens was created by placing a second lens, removed from another laser module, in series with the collimating lens. The focal depth was adjusted to a few centimeters by adjusting the distance between the two lenses. The laser diode was mounted above the microfluidic chip and a set of micropositioners were used to adjust the beam position (Fig. B.4).

The PDMS microfluidic chip was positioned on top of a packaged HV CMOS chip coated in PSC Red photoresist. The diameter of the beam was estimated by comparing the spot size of the focused laser diode to the width of the photodiode. As seen in Fig. B.5, the diameter of the focused beam was approximately the same as the width of the photodiode (150 μm). The distance between the microfluidic channel and the photodiode was measured to be 1.8 mm, resulting in poor fluorescence light collection efficiency from the illuminated sample. In future work,

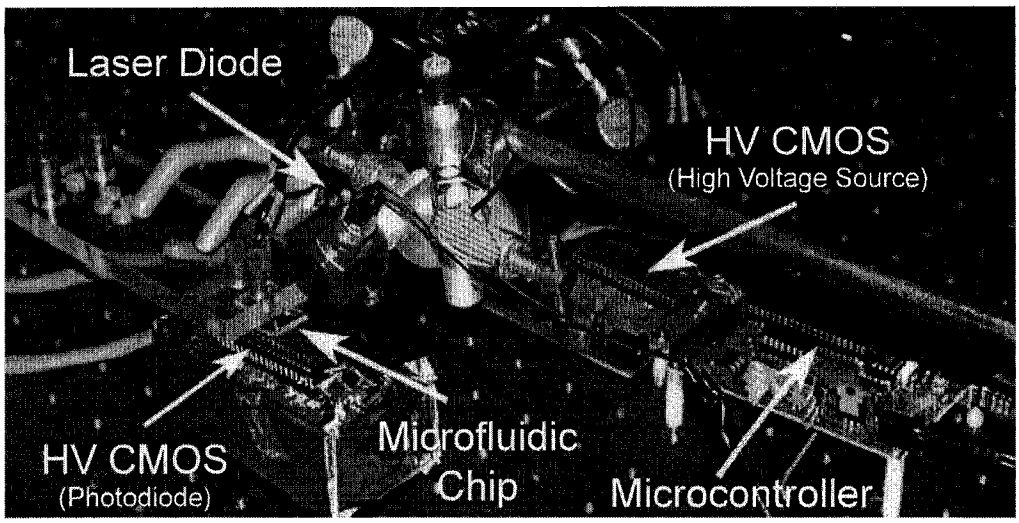

Figure B.4: A photograph of the prototype integrated system used to detect BK virus using a HV CMOS power supply and photodiode.

an increase in sensitivity could be achieved by packaging the HV CMOS die in a different manner to allow the photodiode to be positioned closer to the microfluidic channel. This is discussed in detail in Chapter 4.

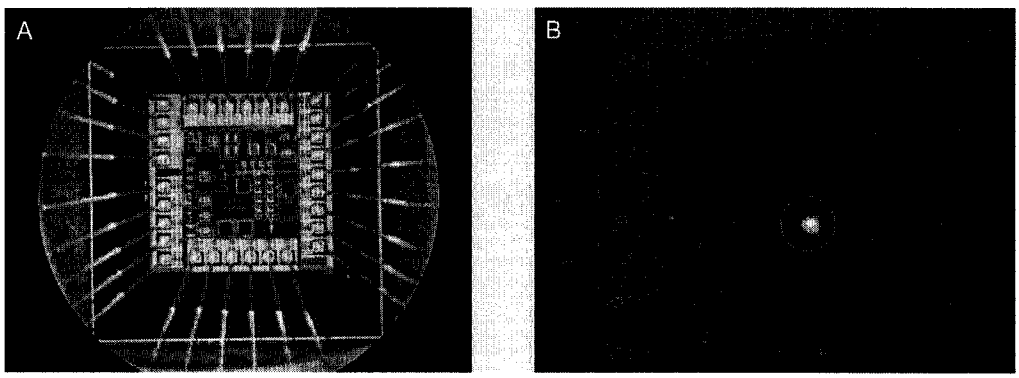

Figure B.5: (A) A photograph of the uncoated HV CMOS die. (B) A photograph of the focused laser spot on shining directly onto the HV CMOS photodiode to assist in assessing the diameter of the beam. The PDMS microfluidic chip is not present in either photograph.

B.2.3.3 Photodiode Detector System

The photodiode is connected to the same transimpedance amplifier system described in Sec. B.2.2.3. As seen in Fig. B.4, The amplifier was packaged in an aluminium foil coated box to reduce the electronic noise due to coupling from surrounding electronic equipment. Again, the output of the amplifier was connected to the ADC and subjected to similar signal processing as described in Sec. B.2.2.3.

B.2.3.4 High-Voltage Electrophoresis Electronics

The requirement for an external high-voltage power supply is eliminated by replacing the external HV source and switching with a HV CMOS-based chip fabricated by DALSA Semiconductor. The high voltage is generated using an inductive DC-DC boost converter. Details on the HV CMOS electronics are beyond the scope of this thesis. More information is available from the theses of Maziyar Khorasani [2] and Mohammad Behnam [3] from the Department of Electrical and Computer Engineering at the University of Alberta.

Bibliography

[1] Melles Griot, *The practical application of light (Product Catalog)*, vol. X, pp. 6.46–6.50 Carlsbad, CA, USA: Melles Griot, 2007.

[2] M. Khorasani, Masters of Science Thesis, University of Alberta, 2007.

[3] M. Behnam, "Integration of high voltage CMOS and microfluidic technologies for genetic analysis systems," Masters of Science Thesis, University of Alberta, 2007.

Appendix C

Optical Power Budget

This appendix provides a summary of the optical power budget for several of the systems described in this work. The optical power budget is used to quantify the optical power at various positions throughout the detection system. This tool was used to assess potential design configurations prior to implementation throughout the course of the project.

When possible, each of the optical elements used in this work have been characterized independently. The total optical loss can thus be determined by summing the losses for each individual component and at the interface between components.

Referring to Fig. 1.2, it can be seen that the optical path needs to be characterized for both excitation and fluorescence wavelengths since some components (i.e. optical filters) treat light at each wavelength (or set of wavelengths) differently. For this reason, the optical power budget traces both the fluorescence and scattered excitation light paths independently for the detection phase. The excitation efficiency is the percentage of light emitted from the laser that reaches the sample. The detection efficiency is a measure of the fraction of the total emitted fluorescence or scattered excitation light which reaches the detector.

A fraction of the excitation light is absorbed by the sample and re-emitted as fluorescence. The efficiency of this process, η, is a function of the sample concentration, the fluorophore quantum efficiency, the wavelength-dependent extinction coefficient of the fluorophore (i.e. the ability to absorb light) and the size of the probe volume. For this reason, η may vary between systems depending on the experimental setup. In addition, a fraction of the excitation light, γ, is scattered or reflected

by surfaces and surface roughness (or defects) within the microfluidic chip. This scattered emission light contributes to the background (and noise) at the detector. This number may also vary depending on the detection configuration, the microchip design and chip-to-chip fabrication variations. When calculating the fluorescence detection efficiency, it is assumed that the fluorescence is emitted isotropically (i.e. equally in all directions) and the effect of the lens light collection efficiency is factored into the power budget. Since the reflected / scattered excitation light is not necessarily isotropic, the light collection efficiency is not factored in to the optical path estimate and thus becomes factored into γ. Estimates for η and γ for the systems analyzed below are calculated using the results reported in the previous chapters.

Since the majority of the numbers provided below have been measured experimentally, these may vary with changes to the instrumentation (electrical or optical), detection setup (i.e. quality of alignment) or fabrication process. The numbers provided below should thus be used as a rough indicator of the optical power expected in these systems rather than an exact quantification.

C.1 Microfluidic Toolkit

The following optical power budget has been calculated using data found in Ref. [1] and through measurements performed during the work of Chapter 2. A schematic of the optics used in the μTK can be found in Fig. 2.5A.

C.1.1 Excitation Efficiency

Wavelength: 532 nm (Excitation)

Description	Value	Label	Source
Laser Power, 532 nm (W)	$4.0\text{x}10^{-3}$	A	μTK manual [1]
Dichroic/Lens Efficiency	43%	B	calculated: C/A
Excitation Power (W)	$1.7\text{x}10^{-3}$	C	measured: Sec. 2.3
Excitation Efficiency	**43%**	D	calculated: C/A

Result: 43% of the laser power reaches the sample.

C.1.2 Detection Efficiency

Wavelength: ~550-650 nm (Fluorescence)

Description	Value	Label	Source
Fluorescence Emission, ~550 nm (W)	$\eta \times C$	E	
Light Collection Efficiency	4.5%	F	calculated: Sec. 2.2.2
Dichroic Beamsplitter (570 nm)	80%	G	μTK manual [1]
550 nm Longpass Filter	86%	H	μTK manual [1]
Filter/Emission Spectra Overlap	73%	I	calculated: Sec. C.5
568.2 nm Bandpass Filter	80%	J	μTK manual [1]
Filter/Emission Spectra Overlap	11%	K	calculated: Sec. C.5
Fluorescence at Detector (W)	$0.2\% \times \eta \times C$	L	calculated: E×F×G×H×I×J×K
Detection Efficiency	**0.2%**	M	calculated: L/E

Result: 0.2% of the fluorescence emitted by the sample reaches the photodetector.

From Table 2.2, we see that the average fluorescence signal was 1.3 V. At a PMT sensitivity of 36 V/nW (Table 2.1), this corresponds to a detected fluorescence power of 36 pW. The total emitted fluorescence would be approximately 36pW / 0.2% or 18 nW. This leads to η = 18 nW / 1.7 mW = 0.001%.

Wavelength: 532 nm (Excitation)

Description	Value	Label	Source
Collected Excitation Light, 532 nm (W)	$\gamma \times C$	N	
Dichroic Beamsplitter (532 nm)	28%	O	μTK manual [1]
550 nm Longpass Filter	$10^{-2.7}$	P	μTK manual [1]
568.2 nm Bandpass Filter	$10^{-5.5}$	Q	μTK manual [1]
Scattered Light at Detector (W)	$1.8\text{x}10^{-9} \times \gamma \times C$	R	calculated: N×O×P×Q
Excitation Light Suppression	$\mathbf{1.8\text{x}10^{-9}}$	S	calculated: S/N

Result: Excitation light collected by the lens is attenuated by a factor of $1.8\text{x}10^{-9}$.

The amount of scattered excitation light collected by the μTK was determined by analyzing the electropherogram baseline after freshly loading the sample and reagents in a clean chip prior to the introduction of DNA into the detection region. The average measured signal at a sensitivity of 36 V/nW over three tests was 51 mV $\pm$ 1.8% or 1.4 pW. The electronic offset of the μTK PMT was measured to be 3.9 mV or 0.1 pW by running the system at a sensitivity of 36 V/nW with the laser source and lights off. This means that we have 1.3 pW of scattered excitation light reaching the detector.

The total amount of scattered excitation light collected by the lens is determined by dividing 1.3 pW by $1.8\text{x}10^{-9}$ which gives 0.7 mW. From this, γ = 0.7 mW / 1.7 mW = 40%. It seems extrodinarily high that 40% of the total excitation power is reflected or scattered back into the μTK lens. It is more probably, however, that the performance of the interference filters is reduced due to light entering the filter at off-normal incidence (see Fig. 4.5). This would result in a greater transmission of excitation light than the $1.8\text{x}10^{-9}$ estimated here.

C.2 Integrated Waveguide-based Fluorescence Detection

The following optical power budget has been calculated using measurements performed during the work of Chapter 2. A schematic of the optics used in the waveguide system can be found in Fig. 2.5B. The optical power budget for this waveguide system can be applied to the dye-doped waveguide system of Chapter 3 by removing the impact of the external optical filters and accounting for the wavelength-dependent attenuation of the dye-doped waveguides.

C.2.1 Excitation Efficiency

Wavelength: 532 nm (Excitation)

Description	Value	Label	Source
Laser Power, 532 nm (W)	$4.5\text{x}10^{-3}$	A	measured
Laser-to-fiber Efficiency	67%	B	calculated: D/A
Fiber Loss (dB)	$\sim$0	C	fiber loss is negligible
Fiber Output Power (W)	$3.0\text{x}10^{-3}$	D	measured: Sec. 2.3
Fiber-to-waveguide Coupling Efficiency (dB)	$\sim$3	E	measured: Sec. 2.2.2
Waveguide Loss (dB/cm)	1.9	F	measured: Sec. 2.2.2
Waveguide Length (cm)	0.5	G	designed
Excitation Power (W)	$1.2\text{x}10^{-3}$	H	calculated: $\text{A}\times\text{B}\times10^{-0.1\times(E+F\times G)}$
Excitation Efficiency	**27%**	I	calculated: H/A

Result: 27% of the laser power reaches the sample.

C.2.2 Detection Efficiency

Wavelength: ~550-650 nm (Fluorescence)

Description	Value	Label	Source
Fluorescence Emission, ~550 nm (W)	$\eta \times H$	J	
Light Collection Efficiency	0.8%	K	calculated: Sec. 2.2.2
Waveguide Loss (dB/cm)	1.0	L	measured: Sec. 2.2.2
Waveguide Length (cm)	0.5	M	designed
Waveguide-to-fiber Coupling Efficiency (dB)	~4.6	N	measured: Sec. 2.2.2
Fiber Loss (dB)	~0	O	fiber loss is negligible
D590/55m Bandpass Filter	81%	P	spec sheet
Filter/Emission Spectra Overlap	48%	Q	calculated: Sec. C.5
Fluorescence at Detector (W)	$0.1\% \times \eta \times H$	R	calculated: $J \times K \times 10^{-0.1 \times (L \times M + N)} \times P \times Q$
Detection Efficiency	**0.1%**	S	calculated: R/J

Result: 0.1% of the fluorescence emitted by the sample reaches the photodetector.

From Table 2.2, we see that the average fluorescence signal was 5.5 V. At a PMT sensitivity of 39 V/nW (Table 2.1), this corresponds to a detected fluorescence power of 141 pW. The total emitted fluorescence would be approximately 141pW / 0.1% or 141 nW. This leads to η = 141 nW / 1.2 mW = 0.012%.

A similar experiment was performed by replacing the PMT with a calibrated optical power meter. Fluorescence signals of between 15 and 80 pW were observed. This demonstrates the range of detected signals that could be expected due to run-to-run variability in the biology and detection system.

The same experiment (chip, sample concentration, buffer, polymer) was per-

formed in both the μTK and the waveguide system so we expect that η should be similar for both systems. However, we observe a factor of 10 increase in η for the waveguide system. This could be due to the larger absorbance length in the waveguide system (100 μm) as compared to the μTK (60 μm). Also, the higher optical flux in the μTK (5.4 $\mu W/\mu m^2$) as compared to the waveguide system (0.3 $\mu W/\mu m^2$) may result in photobleaching of some of the fluorophores, reducing the amount of fluorescence generated per mW of optical power.

Wavelength: 532 nm (Excitation)

Description	Value	Label	Source
Scattered Light, 532 nm (W)	$\gamma \times H$	T	
Waveguide Loss (dB/cm)	1.9	U	measured: Sec. 2.2.2
Waveguide Length (cm)	0.5	V	designed
Waveguide-to-fiber Coupling Efficiency (dB)	~4.6	W	measured: Sec. 2.2.2
Fiber Loss (dB)	~0	X	fiber loss is negligible
D590/55m Bandpass Filter	$10^{-6.7}$	Y	spec sheet
Scattered Light at Detector (W)	$5.6\text{x}10^{-8} \times \gamma \times H$	Z	calculated: $T \times 10^{-0.1 \times (U \times V + W)} \times Y$
Excitation Light Suppression	**$5.6\text{x}10^{-8}$**	AA	calculated: Z/T

Result: Excitation light collected by the lens is attenuated by a factor of $5.6\text{x}10^{-8}$.

The amount of scattered excitation light collected by the waveguide system was determined by analyzing the electropherogram baseline after freshly loading the sample and reagents in a clean chip prior to the introduction of DNA into the detection region. The average measured signal at a sensitivity of 39 V/nW over three tests was 6.7 mV $\pm$ 6.1% or 0.2 pW. The electronic offset of the μTK PMT was measured to be -0.8 mV or -0.02 pW by running the system at a sensitivity of 36 V/nW with the laser source and lights off. This means that we have ~0.22 pW of scattered excitation light reaching the detector.

The total amount of scattered excitation light collected by the lens is determined by dividing 0.22 pW by $5.6\text{x}10^{-8}$ which gives 3.9 μW. From this, γ = 3.9 μW / 1.2 mW = 0.3%. Similar to the μTK system, the performance of the interference filter was found to be reduced due to light entering the filter at off-normal incidence (see Fig. 4.5). This may result in a greater transmission of excitation light than the $5.6\text{x}10^{-8}$ estimated here.

C.3 Graded-index Lens / Photodiode-based Fluorescence Detection

The following optical power budget has been calculated using measurements performed during the work of Chapter 4. A schematic of the optics used in the GRIN lens system can be found in Fig. 4.3A. The optical power budget for this GRIN system can be applied to the absorptive-filter-based system of Fig. 4.3B by replacing the external optical filter with the integrated PSC Red filter.

C.3.1 Excitation Efficiency

Wavelength: 532 nm (Excitation)

Description	Value	Label	Source
Laser Power, 532 nm (W)	$4.5\text{x}10^{-3}$	A	measured
Laser-to-fiber Efficiency	67%	B	calculated: D/A
Fiber Loss (dB)	$\sim$0	C	fiber loss is negligible
Fiber Output Power (W)	$3.0\text{x}10^{-3}$	D	measured: Sec. 2.3
Fiber-to-waveguide Coupling Efficiency (dB)	$\sim$3	E	measured: Sec. 2.2.2
Waveguide Loss (dB/cm)	1.9	F	measured: Sec. 2.2.2
Waveguide Length (cm)	0.5	G	designed
Excitation Power (W)	$1.2\text{x}10^{-3}$	H	calculated: $\text{A}\times\text{B}\times10^{-0.1\times(E+F\times G)}$
Excitation Efficiency	**27%**	I	calculated: H/A

Result: 27% of the laser power reaches the sample.

The optical path for the excitation portion is identical to that of Sec. C.2.1.

C.3.2 Detection Efficiency

Wavelength: ~550-650 nm (Fluorescence)

Description	Value	Label	Source
Fluorescence Emission, ~550 nm (W)	$\eta \times H$	J	
Light Collection Efficiency	2.3%	K	calculated: Sec. 4.2.2.1
D590/55m Bandpass Filter	81%	L	spec sheet
Filter/Emission Spectra Overlap	48%	M	calculated: Sec. C.5
Fluorescence at Detector (W)	$0.9\% \times \eta \times H$	N	calculated: J×K×L×M
Detection Efficiency	**0.9%**	O	calculated: N/J

Result: 0.9% of the fluorescence emitted by the sample reaches the photodetector.

From Table 4.1, we see that the average fluorescence signal was 0.35 V. At a photodiode responsivity of 0.22 A/W (interpolated from data provided in Sec. 4.2.2.1) and a transimpedance gain of 1V/nA, this corresponds to a detected fluorescence power of 1.6 nW. The total emitted fluorescence would be approximately 1.6 nW / 0.9% or 177 nW. This leads to η = 177 nW / 1.2 mW = 0.015%. As expected, the fluorescence efficiency is very comparable to the waveguide system of Sec. C.2.

Wavelength: 532 nm (Excitation)

Description	Value	Label	Source
Scattered Light, 532 nm (W)	$\gamma \times H$	P	
D590/55m Bandpass Filter	$10^{-6.7}$	Q	spec sheet
Scattered Light at Detector (W)	$2.0 \times 10^{-7} \times \gamma \times H$	R	calculated: P×Q
Excitation Light Suppression	$\mathbf{2.0 \times 10^{-7}}$	S	calculated: R/P

Result: Excitation light collected by the lens is attenuated by a factor of 2.0×10^{-7}.

The amount of scattered excitation light that reaches the photodiode was determined in Sec. 4.2.2.1 to be 0.72±0.02 nW with a dark reading of 60 pW (corresponding to the electronic offset). The total amount of scattered excitation light collected by the GRIN lens is determined by dividing 0.72 nW by 2.0×10^{-7} which gives 3.6 mW. From this, γ = 3.6 mW / 1.2 mW = 300%. Since the scattered light cannot be greater than the excitation light, we know this is incorrect. However, we know from Sec. 4.2.2.1 that the performance of the interference filter was found to be reduced to OD3 due to light entering the filter at off-normal incidence (see Fig. 4.5). From the measurements performed in Sec. 4.2.2.1, we expect γ to be closer to 0.67 μW / 1.2 mW = 0.06%.

C.4 Photodiode-based Fluorescence Detection via HV CMOS Device

The following optical power budget has been calculated using measurements performed during the work of Chapter 4. A schematic of the optics used in the GRIN lens system can be found in Fig. 4.3C. As discussed in Chapter 4, the fluorescence detection efficiency could be increased by decreasing the gap between the microfluidic chip and the photodetector.

C.4.1 Excitation Efficiency

Wavelength: 532 nm (Excitation)

Description	Value	Label	Source
Laser Power, 532 nm (W)	4.5×10^{-3}	A	measured
Excitation Efficiency	~75%	B	estimate
Excitation Power (W)	3.4×10^{-3}	C	calculated: A×B
Excitation Efficiency	**75%**	D	calculated: C/A

Result: 75% of the laser power reaches the sample.

The excitation efficiency for this system is a rough estimate and is highly dependent on the accuracy of the alignment. The laser is focused to a spot size of 150 μm onto a channel with a width of 100μm. With perfect alignment, the excitation efficiency would be $\sim(100 \times 150)/(\pi(150/2)^2) = 85\%$. To account for some misalignment, the efficiency is this calculation was reduced to 75%.

C.4.2 Detection Efficiency

Wavelength: ~550-650 nm (Fluorescence)

Description	Value	Label	Source
Fluorescence Emission, ~550 nm (W)	$\eta \times D$	E	
Light Collection Efficiency	0.06%	F	calculated: Sec. 4.2.2.3
PSC Filter (22 μm)	22%	G	measured: Sec. 4.2.2.3
Filter/Emission Spectra Overlap	18%	H	calculated: Sec. C.5
Fluorescence at Detector (W)	$0.002\% \times \eta \times D$	I	calculated: E×F×G×H
Detection Efficiency	**0.002%**	J	calculated: I/E

Result: 0.002% of the fluorescence emitted by the sample reaches the photodetector.

From Table 4.1, we see that the average fluorescence signal was 0.02 V. At a photodiode responsivity of 0.16 A/W (as measured in Sec. 4.2.2.3) and a transimpedance gain of 1V/nA, this corresponds to a detected fluorescence power of 125 pW. The total emitted fluorescence would be approximately 125 pW / 0.002% or 6.3 μW. This leads to η = 6.3 μW / 3.4 mW = 0.19%. We expect η to be larger than the previous systems since the sample concentration was increased by a factor of 7 from 0.3 μL to 2 μL. In comparison to the system of Sec. C.3, η is a factor of 13 times higher. The additional factor of 2 may be due to the increased probe volume in the HV CMOS system (900 pL) as compared to the GRIN system (420 pL).

Wavelength: 532 nm (Excitation)

Description	Value	Label	Source
Scattered Light, 532 nm (W)	$\gamma \times D$	K	
PSC Filter (22 μm)	$10^{-4.7}$	L	measured: Sec. 4.2.2.3
Scattered Light at Detector (W)	$2.0 \times 10^{-5} \times \gamma \times D$	M	calculated: K×L
Excitation Light Suppression	$\mathbf{2.0 \times 10^{-5}}$	N	calculated: M/K

Result: Excitation light collected by the lens is attenuated by a factor of 2.0×10^{-5}.

The amount of scattered excitation light that reaches the photodiode was determined in Sec. 4.2.2.3 to be ~3.5 nW after accounting for the dark reading (electronic offset) of 0.098 V or 0.6 nW. The total amount of scattered excitation light collected by the proximity setup is determined by dividing 3.5 nW by 2.0×10^{-5} which gives 0.2 mW. From this, γ = 0.2 mW / 3.4 mW = 5%. The generation of autofluorescence from the pigmented filter has not been accounted for in this optical budget. Autofluorescence will reduce the expected performance of the optical filter and will reduce the estimated value of γ.

C.5 Filter Overlap

The emission spectra of the VIC fluorophore can be found in Fig. 4.6. To determine the amount of fluorescence that will pass through the optical filter, it is necessary to know the fraction of the fluorescence emission that is located within the passband of the optical filter. This is calculated by dividing the area under the emission spectra curve between the passband wavelengths of the filter by the total area under the emission spectra. For instance, the passband of the D590/55m filter is between 562.5 nm and 617.5 nm so the area of under the VIC emission spectra curve between these wavelengths divided by the total area under the emission curve is 48%. Thus, the fraction of fluorescence that passes through the filter will be 48% multiplied by 81%, the transmission of the fiter passband collection. Below is a table of the filter/emission spectra overlap for the optical filters used in this work.

Optical Filter	Wavelengths Transmitted (nm)	Filter/emission spectra overlap	Ref.
550 nm Longpass (μTK)	$\lambda \geq 550$	73%	Fig. 2.5
568 nm Bandpass (μTK)	$563 \leq \lambda \leq 573$	11%	Fig. 2.5
D590/55m	$562.5 \leq \lambda \leq 617.5$	48%	Fig. 4.6
Sudan II Dye	$\lambda \geq 550$	73%	Fig. 3.2
PSC Red Photoresist	$\lambda \geq 600$	18%	Fig. 4.6

Bibliography

[1] Micralyne, *Microfluidic Tool Kit Operating Manual*, v3.30.00 ed. Edmonton, Alberta, Canada: Micralyne Inc., 2002.